A NOVEL COIL DESIGN FOR MAGNETIC NERVE STIMULATION

BY

NAFIA AL-MUTAWALY

A NOVEL COIL DESIGN FOR MAGNETIC NERVE STIMULATION

By
Nafia Al-Mutawaly

A Thesis
Submitted to the School of Graduate Studies
in Partial Fulfilment of the Requirements
for the Degree
Master of Engineering

McMaster University
September 1998

Master of Electrical Engineering (1998)

McMaster University
Electrical and Computer
Engineering
Hamilton, Ontario

TITLE: A Novel Coil Design for Magnetic Nerve Stimulation

AUTHOR: Nafia Al-Mutawaly, B.Sc.E., (University of Mosul)

SUPERVISOR: Professor Raymond D. Findlay

NUMBER OF PAGES: xiii and 138

Abstract

Magnetic nerve stimulation is a non-invasive method of exciting a neural tissue which can be achieved by exposing the body to a transient magnetic field. This field is generated by passing a high current through a coil over a short period of time. By positioning this coil in a specific orientation over the targeted nerve, the time variation of the magnetic field will create an electric field in the conductive milieu of the body. Induced currents will result from that electric field. If those currents reach a certain amplitude within a specific time period this will cause a neural depolarization. This depolarization will enable us to test and examine the excited nerve which will provide us with the necessary data for an effective treatment.

In my thesis I will analyse the benefits of magnetic nerve stimulation with the objective of designing a coil that provides a focussed magnetic field. This field will excite the targeted nerve with minimal or to no excitation to the surrounding nerves. This means that we can effectively apply or measure the excitation of the targeted nerve without involving the surrounding nerves.

It is my intention to bring this application to a practical platform where a simple circuit with lower power requirements can be used. This will enable some patients requiring physiotherapy to safely administer magnetic nerve stimulation to themselves without the help of a therapist.

Acknowledgements

I would like to take this opportunity to thank my supervisor, Dr. Raymond Findlay for his guidance and support through out the course of this thesis. Dr. Findlay always took time out of his busy schedule to help me; "For you Nafia, I always have time". Dr. Findlay not only provided me with technical knowledge, but also with his experience which can not be found in any book.

Like that of an older brother, Dr. Joseph Dableh's enthusiasm and encouragement perceived throughout this project. His advice when I faced a road block was greatly appreciated; "Whenever you have a problem put a bag of ice on your head, be patient, and work hard until you solve the problem".

A personal thank you to Dr. Szabodas for the valuable tools that he provided me with through his course despite working early Sunday mornings.

A special thanks to Dr. H. de Bruin for his valuable help in guiding through the biological aspect of my thesis. He was always patient and generous with his time in answering all of my questions and clarifying my concerns.

Thank you to Steve Spencer who provided me with computer programming support, as well as, answering all my "quick questions". Thank you to Adam who was very helpful in providing the necessary data books and addresses for suppliers and manufactures.

Finally, thank you to a very special person, Tracey, my wife. Her patience, understanding and sacrifices have not gone unnoticed. Without her support this work would not be possible. We have taken each step together.

List of Figures

Symbols

B	Magnetic flux density	
C	Capacitor bank	
C_m	Membrane capacitance	
c_m	Nodal membrane capacitance per unit area	
C_n	Nodal capacitance	$2.5\mu F\ cm^{-2}$
D	Electric flux density	
d	Axon inside diameter	
d_i/d_o	Ratio of inner to outer axon diameter	0.6
dl'	Vector representing a small length of the coil	
E_{cl}	Chloride ion potential	
E_K	Potassium ion potential	
E_L	Leakage Nernst potential @ 37°C	-80.01 mV
E_{na}	Sodium ion potential	
E_{Na}	Sodium Nernst potential @ 37°C	35 - 35 mV
f	RCL Circuit operating frequency	
g_{Cl},	Chloride conductances	
g_K	Potassium conductances	
g_L	Leakage conductance	$128mS\ cm^{-2}$
g_{Na}	Sodium conductance	$1445\ mS\ cm^{-2}$
g_{Na}	Sodium conductances	
H	Magnetic field strength	
$I_{c,n}$	Capacitor C_m current	
$I_{i,n}$	Total ionic current	
$I_{i,n}$	Sum of individual ionic currents	
i_1	Current in the stimulating coil (the primary)	
i_2	Current in the nerve (the secondary)	
J	Electric current density	
J_K	Potassium current densities	
J_L	Leakage current densities	
J_{NA}	Sodium current densities	
K	dielectric constant of myelin	7
K_g	A constant which depends on the shape of the coil and the position of the point at which A is calculated	
k_1	Coupling coefficient between L_c and L_n.	
k_2	Ratio of the linkage field relative to the total field	
L_c	Inductance of the stimulating coil	
L_n	Nerve inductance	
ℓ	Length	
M	Mutual inductance between the nerve and the stimulating coil	
N	Node of Ranvier	

N	Number of turns	
n	Number assigned to each node of Ranvier.	
Q	Total charge	
R	Equivalent resistance for the coil wires, leads, connectors and the cables that link the capacitor bank to the coil	
r_i	Inter nodal resistance	
r_{in}	Longitudinal axon resistance	
r_m	Membrane radial resistance	
r_{out}	External resistance for the surrounding fibres per unit length	
T	Period of one complete cycle	
T_p	The circuit time constant (C_nR_n.)	
V	Voltage at any point along the axon	
V_a	Initial action potential voltage	
V_e	Membrane external voltage	
$V_{e,n}$	External nodal voltage	
V_i	Membrane internal voltage	
$V_{i,n}$	Internal nodal voltage	
V_m	Membrane potential	
V_m	Membrane resting potential	
V_T	Threshold voltage	
x	Distance along the axon	
Δx	Internodal length	
δ	Electrical skin depth	
ϵ_0	permitivity of a vacuum	8.85×10^{-8} μF cm^{-1}
ϵ_r	Tissue dielectric constant	
$\nabla.$	Divergence	
$\nabla\times$	Curl	
$-\nabla\Phi$	Electrostatic potential (electric scalar potential)	
λ	Length or space constant	
λ_{mye}	Space constant for the myelinated axon	
λ	Length or space constant	
μ_c	Relative permeability of the core	
μ_o	Permeability of free space	
$-\partial A/\partial t$	Contribution of the electric field from magnetic induction	
ϕ	Magnetic flux	
ρ	Electric charge density	
ρ_a	Resistivity of axoplasm	5.47×10^{-2} kΩ cm
ρ_i	Axoplasmic (intercellular) resistivity	
ρ_{mye}	Resistivity of myelin	7.4×10^{5} kΩ cm
σ	Tissue conductance	
τ_d	Ratio of the current pulse duration	
τ_m	Time constant	
τ_{mye}	Time constant for the myelinated axon	

ζ	Electric field intensity
ζ_A	Induced electric field
ζ_i	Electric field inside the fiber
ζ_i (x,t)	Induced electric field parallel to the fiber
ζ_ϕ	Air/tissue interface
ζ_n	Induced voltage in the nerve
ζ_x	Electric field intensity

Table of Contents

Chapter 1

Introduction

1.1 Historical Review

By the end of the eighteenth century, the notion that animal tissue responded to electricity was reasonably well established. Galvani and Volta's experiments in the 1790s showed that an electric current could provoke a muscle contraction. In 1831 Michael Faraday described the magnetically induced current. Faraday wound two coils on an iron ring and found that whenever the coil on one side was connected or disconnected from a battery, an electrical current passed through the coil on the other side. His theory was that the iron ring acted as a channel linking the magnetic field of both coils such that any change in the magnetic field of the first coil would result in an induced current in the second. In1896 d'Arsonval showed that such a current could stimulate a tissue. Placing a large coil carrying substantial alternating current near the head of a human volunteer, d'Arsonval stated that the subject perceived bright spots, or "phosphenes" in the visual field. At the beginning of the 20th century and with the rapid development of more sensitive instruments it was possible to measure the transmitted information through the nerve fibre. The measured signals were called "action potentials". In the decade from 1940 to 1950 new techniques and creative models were developed by Huxley and Hodgkin[1]. Their models helped researchers to understand and measure the potential across a membrane.

Selective stimulation of peripheral nerves was reported in 1959 by Kolin et al [2]. Kolin achieved these stimulations by wrapping a frog sciatic nerve around an electrical pole.

In 1965 Bickford and Fremming [3] introduced the technique of nerve stimulation by

discharging a capacitor into a skin-surface coil. They applied this method to the peripheral nerves of humans and animals.

The first practical application of magnetic nerve stimulation to test deep nerves was done by Barker et al in 1982 [4]. By this event the modern era of magnetic stimulation started. Other pioneers such as McRobbie [5] designed and built a magnetic stimulator in 1985. Since then, magnetic nerve stimulation has gained popularity. More researchers have now entered into this field with the aim of improving this technique.

The concept of the induced current in Faraday's experiment is the same as the concept of magnetic nerve stimulation. The stimulating coil represents the first coil connected to a power supply. The targeted nerve represents the second coil while the tissues that separate the two coils represent the medium linking the magnetic field between both coils. Establishing an alternating current in the stimulating coil produces an alternating magnetic field that links the two coils. This field results in an induced current in the nerve. If the induced current reaches a certain threshold, nerve stimulation becomes evident.

1.2 Magnetic nerve stimulation:

Magnetic nerve stimulation has proven to be useful to excite the nervous system in a non-invasive method. Both the peripheral and central nervous systems can be activated by this technique. In the early years of magnetic stimulation development, researchers concentrated on proving the feasibility of using such a technique to achieve effective nerve stimulation. Over the past twelve years, magnetic stimulation has grown tremendously and moved from diagnoses usage to surgery monitoring and physiotherapy applications. This was the reward for researchers

who spent years improving the quality and efficiency of this technique. To improve the quality of magnetic stimulation, researchers had to solve the problem of the "unfocussed" field, which is the main drawback of magnetic stimulation. Their efforts resulted in the creation of different coils with many shapes and sizes. To improve the efficiency of the system, several coil designs were used in conjunction with many circuits. The aim in each design was to improve the coil output and reduce losses.

This technique has progressed rapidly over the last few years: it has moved from a simple experimental coil used in 1985 (Sheffield Hospital, UK) [6,7,8] to a highly sophisticated system with different monitors and sensors that can be used in an operating room to monitor delicate neural surgery [1]. Also, this technique has proved to be effective in testing and treating complicated cases of neural injury where electrical nerve stimulation has failed [1].

1.3 Thesis Problem

The main drawback in magnetic nerve stimulation is the "unfocussed" field. When applying a magnetic field to a non-magnetic material (such as biological tissue), the magnetic field diffuses throughout the material. This diffusion makes controlling the field inside the body extremely difficult and produces a weak field which is inefficient for exciting deep nerves. As well, this diffusion reduces the energy transferred from the stimulating coil to the targeted nerve (reduces the volumetric energy density in the targeted nerve). To overcome this drawback we need to generate a field that is strong enough to excite the targeted nerve without affecting the surrounding nerves. This could be achieved by improving the source magnetic field and the associated stimulating coil.

The effort in this thesis is concentrated on addressing the problem of the unfocussed field. The main objective is to design and evaluate a stimulating coil that can provide a focussed field in a very limited space. A secondary objective is to gather and summarize information that is most relevant for understanding the magnetic nerve stimulation and its practical clinical applications. This will assist in providing a better awareness of the most influential parameters and critical issues that play an important role in the general magnetic stimulation process.

1.4 Advantage of Using Magnetic Nerve Stimulation

The main alternative to magnetic nerve stimulation is the technique of "electrical nerve stimulation". In order to appreciate the benefits of magnetic nerve stimulation, let us first look at the drawbacks of the electrical nerve stimulation which can be summarized as follows:

1. Due to the high resistivity of the bones, an electrical field can not penetrate certain parts of the body, ie: skull and spine. As a result, electrical nerve stimulation has a limited effect on the nerves embedded in these areas. This is by far the biggest limitation of electrical nerve stimulation[1] .
2. Electrical nerve stimulation can be very painful. The pain is generated by the pain sensors, which are close to the surface of the body, and are triggered by the high electric fields generated by currents in the range of 10-40 mA. The pain occurs immediately underneath the stimulating electrodes [6].
3. In order to overcome the skin resistance problem, electrical nerve stimulation requires cleaning the skin and applying a conductive paste when attaching the electrodes. This process is time consuming and may irritate some patients [6].

4. An alternative technique is to use an electrode that penetrates the skin. However, this type of electrode can cause discomfort at insertion and pain when the stimulation begins. This pain is due to the high current density generated by the electrode positioned close to the nerve [6].
5. There is the possibility of undesirable side effects to the skin where the electrodes are attached, ie: burns or rashes.
6. Changing an electrode position to achieve maximum nerve stimulation is not an easy task. This change means consumption of time, more pain to the patient and wasted resources [2].

None of the above disadvantages is present when using magnetic nerve stimulation. Moreover, magnetic nerve stimulation provides the following key advantages:

1. Magnetic nerve stimulation allows for penetration through the skull or the spine, which enables us to safely investigate the nerves in these regions [2].
2. Magnetic nerve stimulation does not invoke severe muscle contractions or trigger pain sensors which makes it much more preferable compared to electrical nerve stimulation.
3. Magnetic nerve stimulation is done on or above the surface of the skin, which means no surface preparation or internal penetration is needed [2].
4. Magnetic nerve stimulation does not require the use of electrodes. This feature eliminates the undesirable side effects of skin irritation and helps to reduce costs.
5. Magnetic nerve stimulation will allow us to easily change the coil position until the maximum stimulation is reached.

1.5 Limitations of Magnetic Nerve Stimulation

The main drawback of magnetic nerve stimulation is the lack of a focussed field. An unfocussed magnetic field that stimulates the targeted nerve might undesirably stimulate other nerves. This is evident when we are stimulating a bundle of unmyelinated nerves (which are pre-dominant in the central nervous system). However, this disadvantage is compensated for by the fact that magnetic stimulation is more effective when applied to the central nervous system than electrical stimulation.

Another limitation for magnetic stimulation is the low efficiency of energy utilization when compared to electrical nerve stimulation. While the energy cost is not a major concern, in view of the short period of energization, the capital cost of the system to generate and handle the higher energy is much more than that of electrical stimulation.

1.6 Clinical Applications for Magnetic Stimulation

Since the first commercial machine became available in 1986, magnetic stimulation has been widely used in testing deep inaccessible nerves. It has also aided in the diagnosis of central nerve system diseases [9]. Such diseases, like multiple sclerosis, can be detected by stimulating the motor cortex and measuring the increased time taken for the impulse to reach the peripheral nerves.

Another application is localizing speech centres using rapid repetition rate stimuli so that the speech centres can be avoided during brain surgery. This will also apply for cortical operations to monitor the integrity of spinal cord during surgery [1]. Figure 1.1 shows different clinical applications for magnetic nerve stimulation.

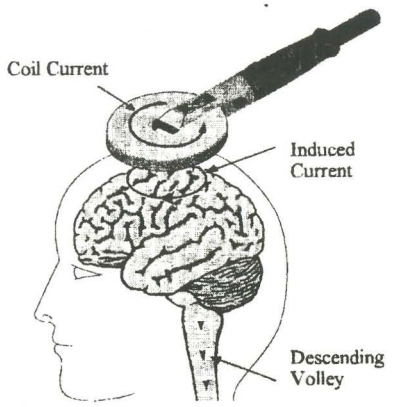

Application of circular coil
(a)

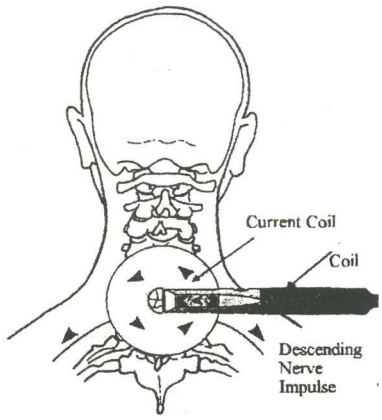

Application of circular coil
(b)

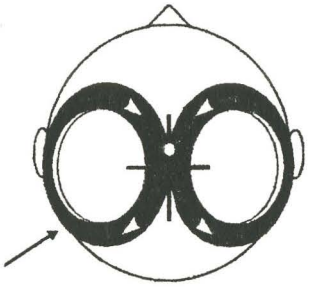

Application of figure "eight" coil
(c)

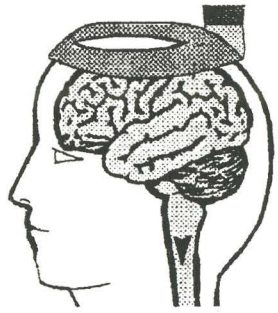

Application of figure "eight" coil
(d)

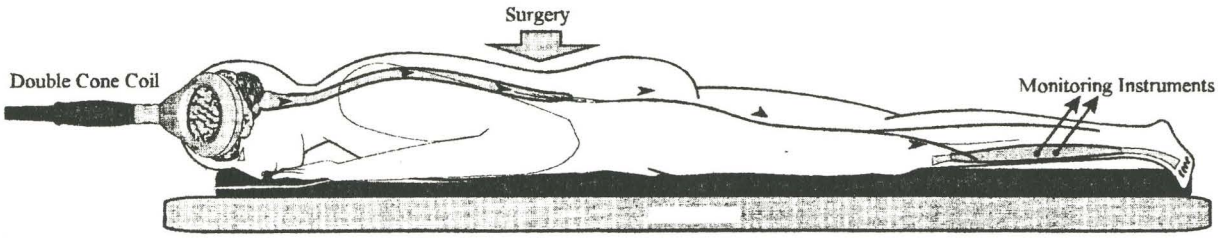

The use of a double cone coil in operating room monitoring
(e)

Figure 1.1
Different clinical applications for magnetic nerve stimulation (taken from [1]).

Other clinical applications are respiratory pacing by stimulating the phrenic nerve, stroke rehabilitation, and restoring function to neurologically impaired individuals.

Magnetic stimulation can also aid in the process of healing cuts and broken bones [7,10,11]. Two techniques for this application have been used. The first technique involves implanting two or more electrodes close to the wound or the fracture and passing a low direct current through those electrodes. The second technique involves exposing the wound or fractured bone to a magnetic field generated by a coil placed outside the targeted area. The latter is more favourable as it avoids the need for implanted electrodes. It is now possible to buy or rent commercial equipment for healing purposes especially for deep wounds or fractured bones that are slow to heal.

1.7 Previous Coil Designs

Over the last decade several coils have been developed for magnetic nerve stimulation. The first practical coil was developed by Barker and et al [7] at the University of Sheffield in 1985. The shape of this coil was circular (see figure 1.2). This coil was then modified by researchers for various reasons; some aimed to have a more focussed field to aid in central nerve stimulation (ie: cortical stimulation), while others sought to have a stronger field which could be used for organ stimulation (ie: heart stimulation).

With the intention of using a coil for cortical stimulation, Ueno and Hiwaki [12] were the first to join a pair of circular coils creating what is called an"eight"shaped coil (figure 1.3). The currents in these coils pass in opposite directions at the edges and in the same direction at the joint, which results in a maximum value for the tangential magnetic field intensity under the

joint. By positioning the coil joint over the targeted nerve, effective stimulation occurs.

Stimulating the heart is more difficult than stimulating the nerves because of the differences in excitability properties of cardiac and neural tissue. Also, as the primary component in the heart is blood which is an excellent conductor, any currents induced in the heart will dissipate rapidly. Therefore, the energy required for cardiac stimulation is larger than that required for nerve stimulation. Nevertheless, Hosono et al [13] and Geddes et al. [14] increased the magnetic field density to a level adequate for heart stimulation. These researchers implemented larger "eight" shape coils which had the capacity to store and release more energy (several kilojoules per pulse). Other researchers decided to proceed with a "Butterfly" shape coil which has the same concept of "eight" shaped coil [15] (see figure 1.4). Weyh et al modified the "butterfly" coil by decentralizing the coil turns [16]. This resulted in an "Eccentric Coil" . This modification increased the magnetic field intensity at the joint of the coil while minimizing it for the rest of the coil. Over the last few years there have been other designs and modifications for the stimulating coil [17,18,19,20].

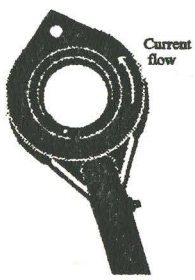

Focal point coil manufactured by Cadwell (taken from [20])
(b)

Basic circular coil
(a)

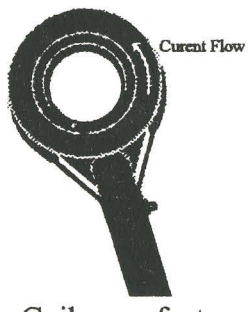

Circular Coil manufactured by Cadwell (taken from [20])
(c)

Figure 1.2

Basic and commercial circular coils.

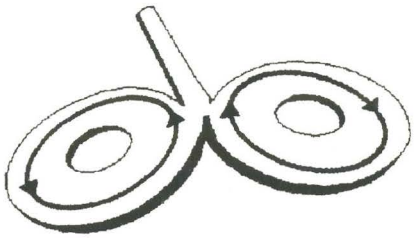

Figure "eight" coil
(a)

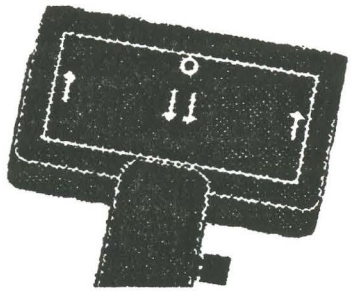

Corticoil manufactured by Cadwell
(taken from [20]) (b)

Figure 1.3
Basic and commercial figure "eight" coils.

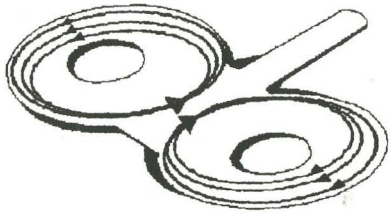

Butterfly coil
(a)

Butterfly coil manufactured by Magstim
(taken from [1]) (b)

Figure 1.4
Basic and commercial butterfly coils.

1.8 The Proposed Coil

The stimulating coil represents the main component in magnetic nerve stimulation as it determines the field shape and distribution. The design of the coil is not an easy task as the created magnetic field should be at its peak value in the small targeted area (the nerve) for a

short period of time. (See Appendix A for more details about the proposed coil design.) Creation of such a field requires either a high pulsating current ($50x10^6$ A/s) or an enormous number of turns. A high pulsating current involves several complications related to circuit design and safety issues. On the other hand, the high number of turns is not practical for the stimulating coil because of the requirements it imposes on the pulse forming circuit. (See Appendix B for further details regarding the stimulating circuit.) Therefore, to achieve such a field (especially within a biological region) is a challenge. Previous researchers have attempted to solve this problem by modifying either the conductor layout and orientation or varying the pulse shape and rise time. The outcome of those solutions only strengthened the magnetic field, with minor improvements to the field shape.

In this thesis we propose two types of coils with the objective of obtaining a focussed magnetic field. The theory behind the design of the proposed coils consists of two parts. The first type involves modifying the layout of the conductors from previous designs, and the introduction of a third set of windings (see figure 1.5). The second type involves the introduction of a ferromagnetic material (see figure 1.6). We have considered the past work in this field as a milestone and built upon it. By decentralizing the turns of a figure "eight" coil, the resultant coil resembles the shape of a child's "slinky" toy. The field for this coil will be concentrated at the junction and weakened in other areas. Next, we introduced a third set of windings positioned perpendicular to the joint of the "slinky" coil (figure 1.5). The combination of the three coils enhances the magnetic field close to the targeted nerve. The field shape and its degree of penetration can be controlled by independently varying the amount of current supplied to the three coils. For example, if the targeted nerve is close to the skin, then we will increase the

amount of current in the perpendicular set and reduce it in the other two.

The second type of coil design involves the introduction of a ferromagnetic material. (See Appendix A for more details.) The ferromagnetic material (having relative permeability much higher than that of air) will channel the field outside the body. This results in controlling the magnetic field in the region external to the body and minimizes its diffusion inside the body.

The core for the first type is an ultra high density polyethylene material while the core for the second type is a Cobalt alloy (Cobalt 50). Other than the difference in the core material, both coils are similar in shape, size, number of turns, and type of conductors. The key difference between our air core coil and commercial coils is the third set of windings. The addition of the third coil was deduced on the basis of work by previous researchers involving the impact of coil orientation [21,22]. As will be outlined in this thesis, the simulations that we ran using a software package called "Magnet", clearly indicated an improvement in the field shape and strength after the introduction of the third set. The amount of energy used to supply the coil during the simulations is the same amount of energy used in other coil designs. However, the resultant field was higher and sharper across the targeted nerve. The third set of windings improved the field shape and strength, thus producing more effective stimulation.

In the second coil type, the introduction of a ferromagnetic core results in a dramatic improvement in the field control and consequently a more effective stimulation. Also, the magnetic core will transfer the energy from the coil to the targeted nerve more efficiently than an air core.

The main issues and construction guidelines, that have to be carefully considered in assembling these coils, are summarized in Appendix A. It should be noted that a sample coil for

each type was constructed; but the facilities to subject these coils to an experimental testing program could not be obtained. Therefore, the presented information is for reference purpose for potential future work.

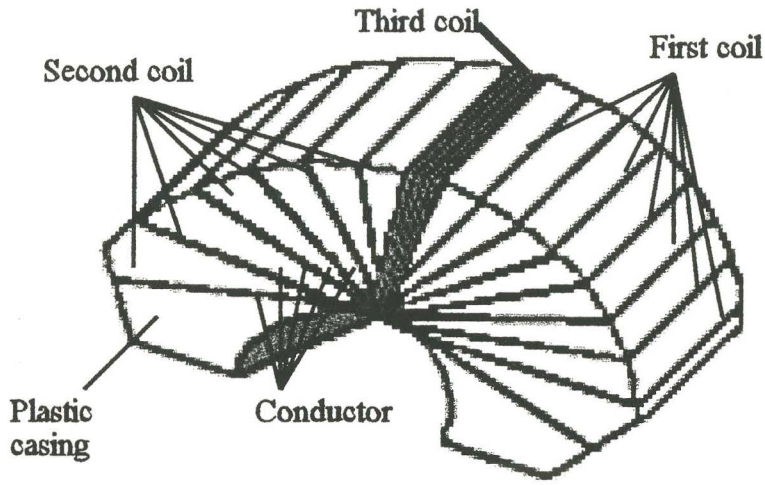

Figure 1.5
The proposed air core coil

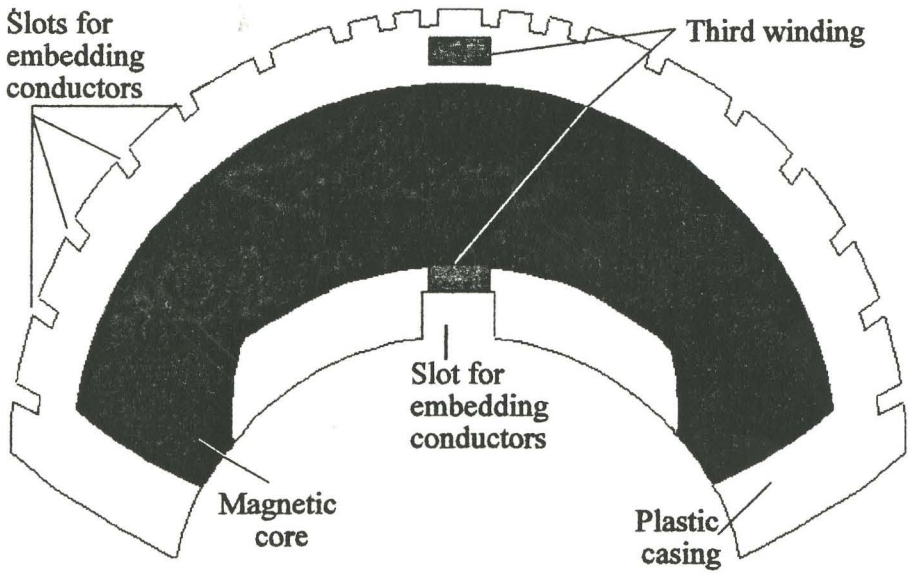

Figure 1.6
The proposed magnetic core coil.

1.10 Thesis Outline

The history and general concept of magnetic nerve stimulation, its benefits and advantages over electrical nerve stimulation, the state-of-the-art, the main limitation and the problem addressed in this thesis have been summarized in Chapter 1.

Chapter 2 covers the biological aspects of magnetic nerve stimulation including a brief description of the neural system. The physical behaviour of the nerve during the stimulation is discussed. A model that represents a stimulated peripheral nerve as an electric circuit is described and analysed mathematically.

Chapter 3 describes the numerical simulation performed on the previous coil designs as well as the proposed coil designs. The software package used to perform this simulation and the basic theory of applying the finite element technique are also presented. Key results from these simulations and the advantages of the proposed coil designs are also summarised in Chapter 3.

Chapter 4 covers conclusions, recommendations and an outline for possible future work in this area.

Chapter 2

Representation Of The Neural System

Before approaching the technical side of magnetic stimulation it is important to outline some of the fundamental aspects of the neural system. This chapter covers an overview of the nerves and the theories describing their response during magnetic stimulation. The most accepted models used to represent the nerves are presented. Finally, a detailed mathematical analysis for a myelinated nerve combined with a stimulating circuit is outlined. The primary goal of this chapter is to provide the reader with a basic background about the nervous system and its behavior. This will facilitate a better understanding about the nerves interaction with external magnetic field. Also, the concepts covered in this chapter will be used when defining the computer model that represents the nerve in the following chapter.

In general, nerves in the body are made up of individual cells or fibres. They conduct, generate messages and integrate various inputs for many human functions. The human nervous system is a collection of about $10^{11\pm1}$ neurons arranged in a highly structured manner. The nervous system can be divided into two portions: the central nervous system (CNS) and the peripheral nervous system (PNS). The central nervous system consists of the brain and the spinal cord while the peripheral nervous system consists of all the neurons that are not in the central nervous system[23]. Another categorization of the nervous system is in terms of the direction of information flow. The *afferent* nervous system takes information from the peripheral nervous system toward the central nervous system. The *efferent* nervous system takes information from the central nervous system toward the peripheral nervous system [2].

2.1 Nerve Cell (Neuron)

The nerve cell (neuron) is the basic element for the nervous system. The neurons are responsible for coding, transmitting, transforming, and decoding information. The morphology of neurons varies greatly, however, they have certain common features. Figure 2.1 shows different types of neuron [2].

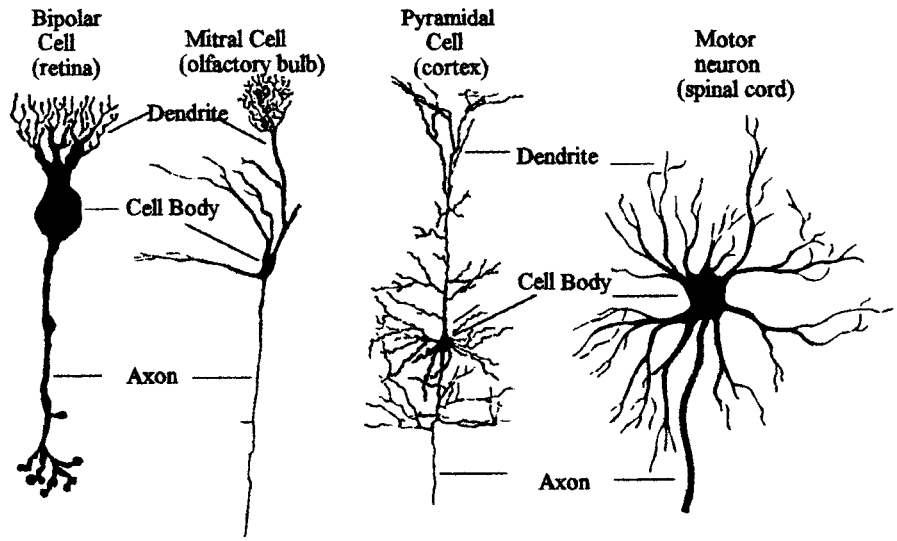

Figure 2.1
Different types of neuron (taken from [2]).

A typical neuron consists of a cell body containing a nucleus and a long thread-like fibre called the axon. The axon is about 10 μm in diameter and can be one metre in length. The axon boundary or the "membrane" separates the cytoplasm intracellular fluid from the interstitial fluid. Figure 2.2 shows a schematic diagram for the cell membrane.

There are two major categories of axons: myelinated and unmyelinated axons. If the axon is surrounded with a layer of myelin sheath then, the nerves are called myelinated nerves.

However, if the axon is bare, then the nerves are called unmyelinated nerves. Myelinated axons are found predominately in vertebrates, whereas unmyelinated axons are found in both vertebrates and invertebrates. The two types of axons differ not only in their structures, but also in their action potential modes of conduction.

As the targeted nerve is a peripheral myelinated nerve, the focus for the remainder of this thesis is on the myelinated nerves. Figure 2.3 shows a typical myelinated neuron. Figure 2.4 shows an electron micrograph for the node of Ranvier and the cross and longitudinal section of a myelinated nerve.

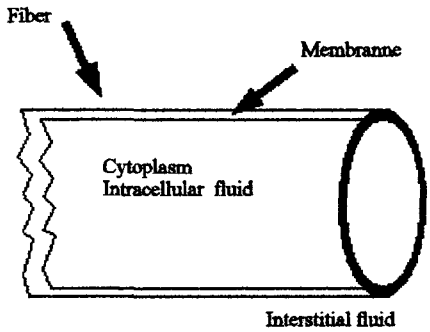

Figure 2.2
A cell membrane (after [2]).

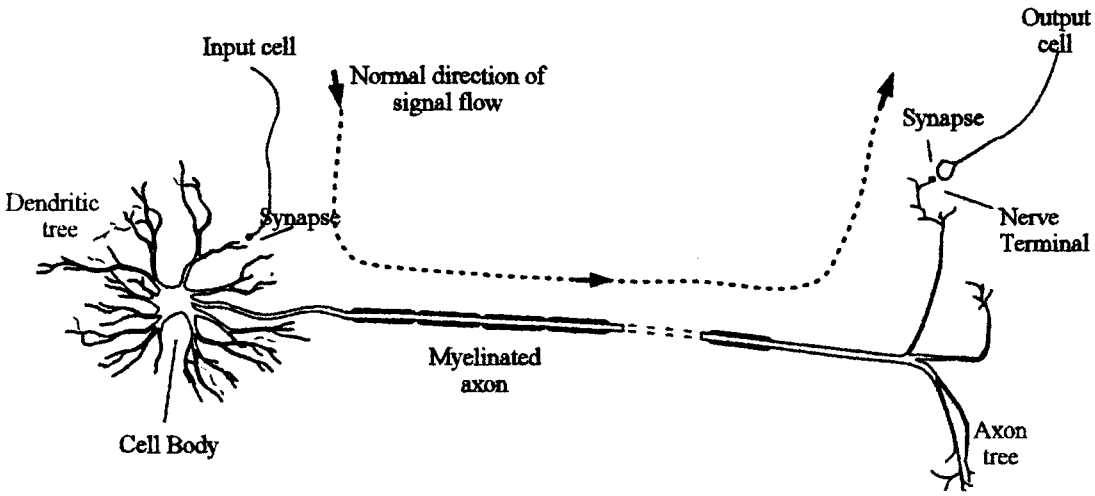

Figure 2.3
A typical myelinated neuron (after [23]).

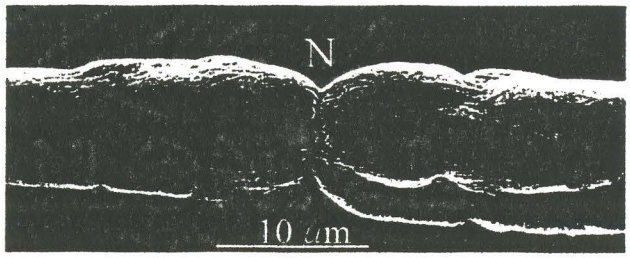

Longitudinal view of a myelinated nerve.
(a)

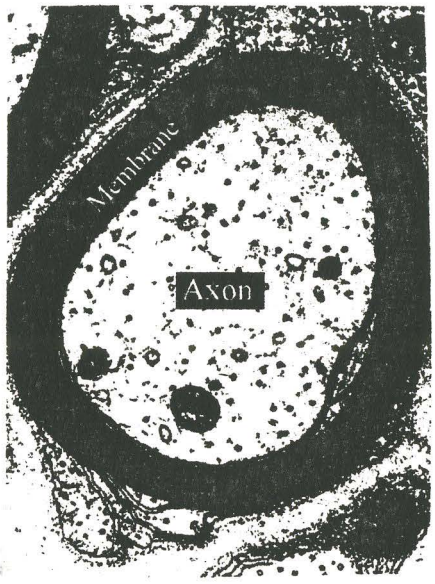

Cross section for myelinated
nerve (the internode region).
(b)

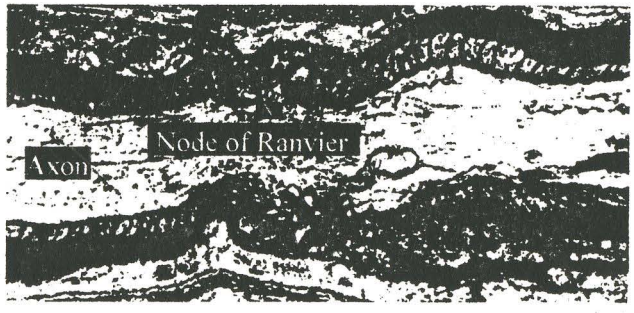

Longitudinal view through a node of Ranvier.
(c)

Figure 2.4
Various views of myelinated nerve (taken from [2]).

2.2 Structure of Myelinated Nerve Fibre

A myelinated fibre consists of an axon ensheathed by myelin. The myelin sheath is a cylindrical sleeve around the axon, segmented approximately every millimetre. The segments of myelin are called internodal segments or internodes. These segments are separated by narrow gaps called nodes of Ranvier which control the interstitial fluid that contacts the nerve cell.

The internodes are not part of the neuron, but are formed by supporting cells. Supporting cells are found both in the central and in the peripheral nervous system. In the PNS, the supporting cell associated with neurons is called the Schwann cell. A single Schwann cell supplies the myelin for a single internode. Thus, a peripheral myelinated nerve consists of an axon wrapped in a sequence of Schwann cells, one at each internode. Figure 2.5 shows a schematic diagram for a Schwann cell.

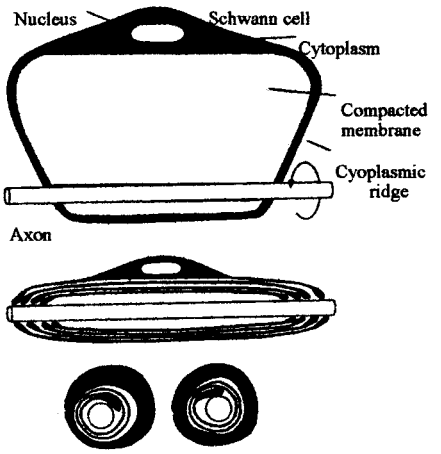

Figure 2.5
Schematic diagram for a Schwann cell (after [2]).

A variety of functions are ascribed to the supporting cells, including providing mechanical support for neurons, buffering extracellular solution composition, guiding the migration of neurons during development of the nervous system, nourishing neurons, participating in the formation of the blood-brain barrier, and disposing of cellular waste.

2.3 Action Potential

Nerves generate and transmit electrical signals called action potentials to convey information. The action potentials are the link between the nerves themselves as well as between the nerves and muscles. The time period for the action potentials and their rate of repetition represent the information type generated and transmitted by the nerves. When the action potentials that are transmitted along the axon reach the axon terminals they form the input signals for the next neurons or muscle fibre. This is applicable for both myelinated and unmyelinated nerves.

Inputs to a neuron from the axons of other neurons occur at synaptic sites which are scattered over the surfaces of the dendrites, the cell body, and the axonal tree. A neuron may contain one synaptic input or many thousands of synaptic inputs.

Action potentials that enter a nerve cell produce local potentials in the neuron which then spread to the cell body. If the nerve depolarization due to the action potential is large enough while its threshold for eliciting is low, an action potential sequence may be produced. Such output action potentials propagate from the cell body via the axon into the axonal terminals.

2.4 The Mechanism of the Nervous System

Many theories and models have been developed over the last 50 years to analyse the nervous system and its physiological activities. The majority of researchers agree that any activity within the nervous system is a sequence of chemical diffusions between the neurons and its surroundings through the cell membrane. Therefore, they considered the membrane as the centre of the nervous system activities. Consequently, we will start with the cell membrane and its components as a first step of our analysis.

The most effective model for a cell membrane is an electrical circuit that represents the variance in potential difference.[1] This can be justified for two main reasons: first, the action potentials (which are transmitted or received by the neurons) can be represented as electrical signals. Secondly, the chemical diffusion across the membrane results in a potential difference which varies in value and polarity according to the neuron activities.

2.5 Electrical Equivalent Circuit for a Cell Membrane

The membrane can be represented by a circuit which depicts neuron activities through its elements. Figure 2.6 shows this circuit where E_{Na}, E_K, E_{Cl}, represent the Sodium, Potassium and Chloride ion potentials ("Nernst Potentials"[2]) respectively. g_{Na}, g_K, g_{Cl}, represent the

---

[1]The membrane potential is the result of the difference in the density for the principle inorganic ions (Na^+ K^+ Cl^-). This difference and the ion variance within the cell function as an energy source much like a battery. This source is maintained by a complex metabolic driven process known as the Sodium-Potassium pump. In this pump the effects of the chloride current is neglected as it is insignificant.

[2]When the membrane reaches electrochemical equilibrium it approaches the Nernst Potential for K^+ which varies between -60 to -90 mV with the inside of the cell negative relative to the outside.

Sodium, Potassium and Chloride conductances respectively. C_m, r_m, and V_m are the membrane capacitance, resistance and potential respectively.

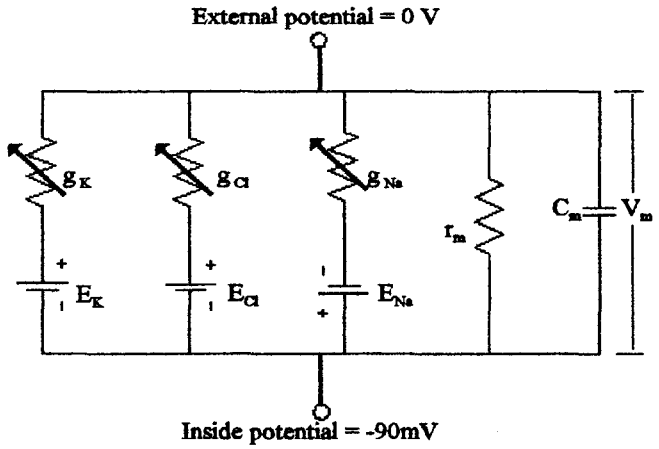

Figure 2.6
An equivalent circuit for a cell membrane (after [2])

The membrane behaves as a leaky capacitor with a time constant τ_m determined by r_m and C_m. Chemical and electric changes affect the trans membrane potential. The electrical potential difference across the membrane balances the tendency of the ions to diffuse in the direction of its concentration gradient. If one of the ion conductances predominates, V_m, the trans membrane potential, will be closer to the potential of that channel (E_{Na}, E_K, E_{Cl}). If, for example, the sodium conductance (g_{Na}) is increased by Δg_{Na}, a current increase,$((E_{Na}-V_m)\,\Delta g_{Na})$ will be initiated.

When nerve depolarization occurs, changes in the membrane potential will be dominated by the Na^+ ion. This happens when a negative stimulus at the surface is applied or a positive current is injected into the cell. This causes g_{Na} to increase, resulting in more Na^+ ion entering. When V_m changes by approximately +30 mV, further depolarization (which is self driven) will

occur resulting in a spike or "action potential".

During relaxation a similar movement by the potassium ions in the opposite direction will occur. The return to resting potential (re-polarization) is due to the increased conductance of the K^+ ion. The Sodium-Potassium pump maintains the resting ion balance, since K^+ would tend to leak out of the cell and Na^+ would tend to leak in at the resting potential. Figure 2.7 shows the change in Sodium and Potassium during the course of an action potential [23]. It also shows the resulting action potential.

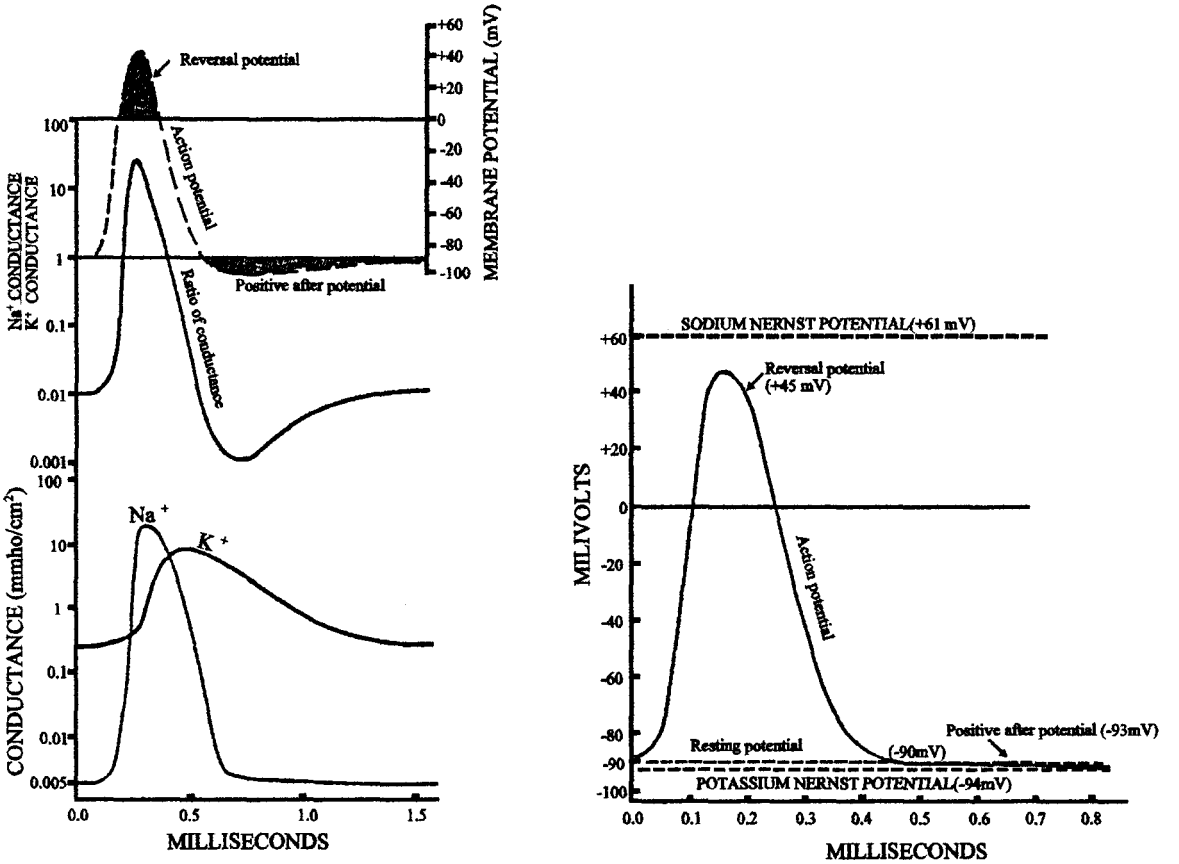

Figure 2.7
Changes in the Sodium and Potassium during action potential (taken from [23]).

2.6 Propagation of action potential

The transmission of information or the transfer of action potential along a nerve cell occurs as one of two mechanisms: the cable properties of the fibre and the active regeneration of the action potential in the surrounding membrane. The resulting equivalent circuit for an axon resembles an equivalent circuit for a "cable". (More details regarding the "cable equation" will be discussed later in this chapter.)

The movement of external currents in the interstitial fluid is crucial for the propagation of the action potential along a myelinated nerve fibre. An experiment outlined by Weiss [2] demonstrates the transfer of the action potential. The figure below shows the experiment set-up for a myelinated nerve model.

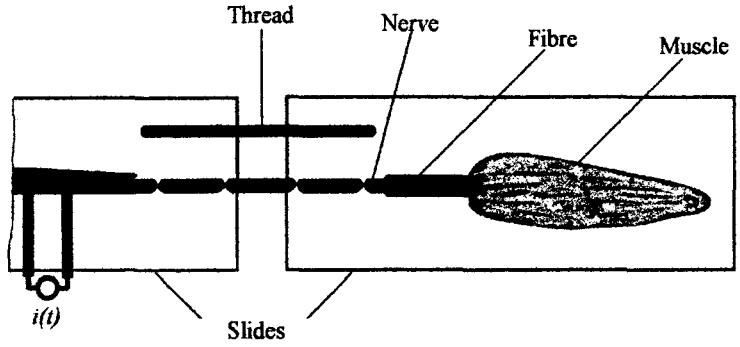

Figure 2.8
Experiment set-up for a myelinated nerve model (after [2]).

Figure 2.8 shows a nerve that is attached to a muscle and dissected so that a single fibre connects the central branch of the nerve with the muscle. An inter nodal region spans an insulated region between two microscope slides. With the two microscope slides insulated from each other, electrical stimulation of the nerve causes no muscle contraction. If a saline-soaked

thread is used to electrically connect the two microscope slides, nerve stimulation is evident as it causes muscle contraction. Thus, nerve conduction from the node to the left of the insulated gap causes excitation to the node at the right only if an extracellular path for the electric current is present. This experiment explains the role of nodes of Ranvier in the transfer of action potential. It also proves that the myelinated sheath is an insulator that isolates the axon from surrounding fibres. Figure 2.9 shows the equivalent circuit for the previous model.

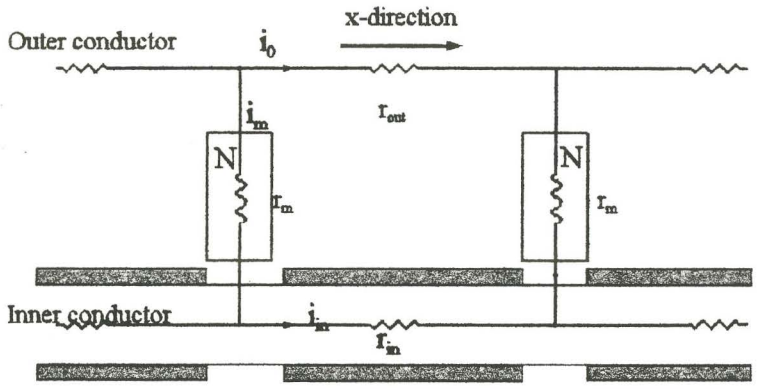

Figure 2.9
Equivalent circuit for the previous model (after [2]).

From the figure above, r_m represents the membrane radial resistance (Ω.m) at the node of Ranvier (N), r_{in} , is the longitudinal axon resistance (Ω/m), r_{out}, represents the external resistance for the surrounding fibres per unit length and x represents the distance along the axon. The voltage (V) at any point along the axon can be expressed with the following equation [23].

$$V = V_a \exp\left(\frac{-x}{\sqrt{r_m/r_{in}}}\right) \qquad (2.1)$$

where V_a represents the initial action potential voltage. The above equation shows that the

voltage along the membrane falls exponentially and the action potential travels from node to node according to the cable property. Another factor that affects the propagation of the action potential is the regeneration of the action potential by the excited nodes that lay sequently on the action potential path. In order for the action potential to be transmitted from one node to another V should remain above the threshold value of V_m (membrane trans potential) to re-excite the new node. The result of the excitation is a rapid conduction of the action potential down the length of the axon (50 m/s for motor neurons in man).

2.7 Membrane behavior during Action Potential

Figure 2.10 represents a myelinated nerve with its main components: the membrane, the node of Ranvier and the myelin sheath. Its also shows the combination of the internode and the node of Ranvier.

Figure 2.11 shows an electrical model for the previous figure as originally formulated by McNeal [2]. It is evident from this figure that the node of Ranvier represents the main components affected during the transfer of action potentials [3]. Also, from figure 2.11 we can conclude that the current passes through the internode only in a longitudinal direction as the internode cross section resistance is very high. This high resistance is due to the myelin sheath. However, at the node of Ranvier the currents will be divided into two components: longitudinal and cross sectional. The equivalent circuit in figure 2.11 illustrates the above.

---

[3] Although figure 2.9 and 2.11 represent an equivalent circuit for a myelinated axon, the former demonstrates the concept of action potential propagation, while the latter will be used to calculate the transfer of the action potential along the axon. Also, r_{out} has been eliminated as its value is very small (or its cross section area is very large) relative to r_{in}.

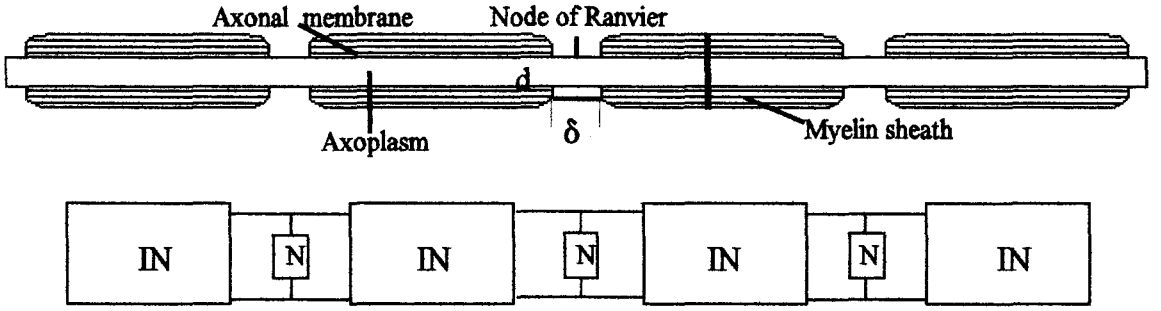

IN = Internode ; N = Node of Ranvier

Figure 2.10
A myelinated nerve with its main components (after [2]).

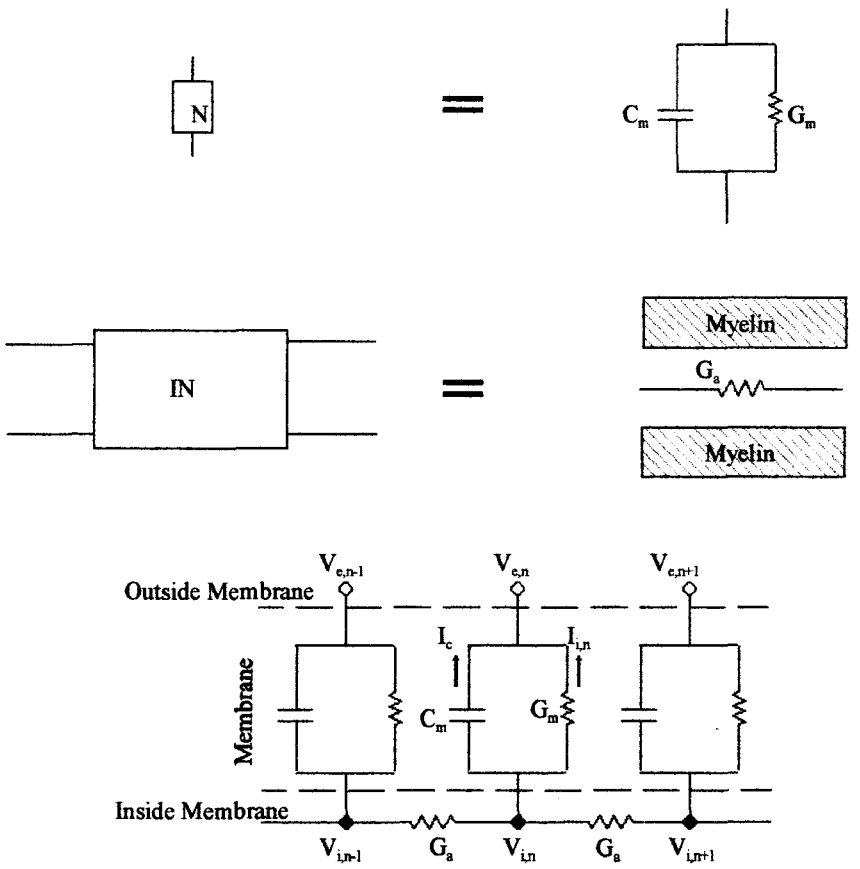

Figure 2.11
An electrical model for the previous figure (after [2]).

where V_i and V_e are the membrane internal and external voltages respectively at longitudinal position x, n is the number assigned to each node of Ranvier. C_m is the membrane capacitance, G_m is the membrane conductance (across the node of Ranvier), V_m is the trans membrane potential (which is considered to be relative to the resting potential, and is equal to 0 when the potential across the membrane is equal to the resting potential). $I_{i,n}$ is the total ionic current, $I_{c,n}$ is the capacitor C_m current (both at node n).

The current emanating from the *nth* node of Ranvier can be described as [2,23,24,25]:

$$C_m \frac{\partial V_{m,n}}{\partial t} + I_{i,n} = G_m(V_{i,n-1} - 2V_{i,n} + V_{i,n+1}) \qquad (2.2)$$

In this expression the ionic current $I_{i,n}$ is the sum of individual ionic currents:

$$I_{i,n} = \pi d\ \delta\ (J_{Na} + J_K + J_L) \qquad (2.3)$$

where the J_{NA}, J_K , and J_L terms are the Sodium, Potassium and leakage current densities respectively [24,25], d represents the axon inside diameter, and δ is the width for the node of Ranvier (N).[4]

---

[4] We notice that the chloride current I_{Cl} has been eliminated from this circuit as it has a minute effect relative to the other currents. Instead we will introduce a new term, J_L , which represents the total leakage current.

From figure 2.11 we can express the inter nodal resistance r_i with the equation

$$r_i = 4\rho_i \Delta x / \pi d^2 \qquad (2.4)$$

where ρ_i is the axoplasmic (intercellular) resistivity, Δx is the internodal length, and d is the axon diameter. The nodal membrane capacitance C_m is given by

$$C_m = c_m \pi d\ \delta \qquad (2.5)$$

where c_m is the nodal membrane capacitance per unit area and δ is the nodal gap width.

By applying Kirchhoff's law for voltage, we can represent the voltage across the membrane as:

$$V_{m,n} = V_{i,n} - V_{e,n} \qquad (2.6)$$

where $V_{i,n}$ and $V_{e,n}$ are the internal and external nodal voltages for the axon with reference to a point in the conducting medium outside the axon.

Substituting equation (2.6) into (2.2) results in:

$$\frac{\partial V_{m,n}}{\partial t} = \frac{1}{C_m} [G_m(V_{m,n-1} - 2V_{m,n} + V_{m,n+1} + V_{e,n} - 2V_{e,n} + V_{e,n+1}) - I_{i,n}] \qquad (2.7)$$

Equation (2.7) can be analogously expressed in continuous form as:

$$\tau_m \frac{\partial V_m}{\partial t} - \lambda^2 \frac{\partial^2 V_m}{\partial x^2} + V_m = \lambda^2 \frac{\partial^2 V_e}{\partial x^2} \qquad (2.8)$$

where λ (length or space constant (m)) and τ_m (time constant (s)) are:

$$\lambda = \sqrt{\frac{r_m}{r_i}} \quad ; \quad \tau_m = C_m r_m \qquad (2.9)$$

Notice that equation (2.8) connects continuous and discrete special derivatives together for the membrane voltages and external voltages respectively. Equation (2.8) is a form of the cable equation[5].

The cable equation represents a general formula for the transfer of the action potential along the axon. This equation can be used to calculate the threshold of the external voltage needed to elicit excitation or action potential from the targeted nerve.

One conclusion that can be drawn from equation (2.7) and (2.8) is that a second spatial derivative of voltage or equivalently a first derivative of the electric field must exist along the axis of an excitable nerve in order to support excitation. Nevertheless, excitation is possible in a locally constant electric field where the fiber is terminated or where it bends. The orientation change or the termination creates the equivalent of a spatial derivative of the applied field.

---

[5]This equation is called the "cable equation" due to its similarities with that solved first by William Thomas (also known as Lord Kelvin) in 1855. The original model was in connection with the laying of the Atlantic submarine cable to be used for intercontinental telegraphy. The equations for that model describe the potential along a leaky submarine cable. The similarity here is the leaky jacket for that model relative to the leaky membrane. [2,28]

2.8 Calculating the Strength of the Threshold Voltage

Basser and Roth [24,25] modified the cable equation in order to calculate the threshold of the electromagnetic field needed to obtain stimulation. They defined the trans membrane potential (which is governed by the cable equation) and linked it with the applied electric field (that results from the transient magnetic field) through the following equation [24]:

$$\tau_m \frac{\partial V_m}{\partial t} - \lambda^2 \frac{\partial^2 V_m}{\partial x^2} - (V_i - V_m) = \lambda^2 \frac{\partial \zeta_x(x,t)}{\partial x} \qquad (2.10)$$

where V_m is the membrane resting potential, V_i is the internodal internal voltage and ζ_x is the electric field intensity (V/m) induced in the nerve (due to the transient magnetic field).

For a myelinated nerve, equation (2.10) will be expressed as follows:

$$\tau_{mye} \frac{\partial V_m}{\partial t} - \lambda_{mye}^2 \frac{\partial^2 V_m}{\partial x^2} - (V_i - V_m) = \lambda_{mye}^2 \frac{\partial \zeta_x(x,t)}{\partial x} \qquad (2.11)$$

where λ_{mye} and τ_{mye} are the space and time constants for the myelinated axon, and can be represented as [24]:

$$\lambda_{mye} = di \sqrt{\frac{\rho_{mye}}{8\rho_a} \ln\left(\frac{d_o}{d_i}\right)} \qquad (2.12)$$

and

$$\tau_{mye} = \epsilon_o K \rho_{mye} \qquad (2.13)$$

Table 2.1 lists and describes the variables shown in equations (2.13), (2.14) and (2.15). Substituting the related variables from the table, the threshold voltage and the electric field needed to achieve nerve stimulation can be calculated [24,25].

Axon model Variables

E_{Na}	sodium nernst potential @ 37°C	35 - 35 mV
E_L	leakage nernst potential @ 37°C	-80.01 mV
g_{Na}	sodium conductance	1445 mS cm^{-2}
g_L	leakage conductance	128mS cm^{-2}
C_n	nodal capacitance	2.5μF cm^{-2}
ρ_a	resistivity of axoplasm	5.47 x 10^{-2} kΩ cm
ρ_{mye}	resistivity of myelin	7.4 x 10^5 kΩ cm
K	dielectric constant of myelin	7
ϵ_0	permitivity of a vacuum	8.85 x 10^{-8} μF cm^{-1}
δ	width of node ranvier	1.5 x 10^{-4} cm
d_i/d_o	ratio of inner to outer axon diameter	0.6

Table 2.1 [2,24,27,28]

2.9 Induced Electric Field in a Myelinated Nerve and The Effect of Charge Distribution

During magnetic stimulation, the electric field intensity ζ induced in a myelinated nerve depends on the coil current, the coil geometry, and the coil orientation with respect to the nerve. All of these factors must be considered when calculating the electric field intensity induced in the nerve. Also, it is important to consider the form and complexity of a myelinated nerve fiber when calculating the electric field intensity. The most accurate representation possible would incorporate the cable structure of a myelinated nerve along with a complete representation of nodal membrane and axoplasmic connections.

To calculate the electric field within a myelinated nerve, we have to consider the contribution of the intracellular electric field (that arises from the charge distribution on the membrane surface) and the charge accumulation on the tissue surface. Once the electric field within the nerve is known its effect on axon trans membrane potential must be ascertained.

To illustrate the above Roth et al., [26], computed the electric field intensity by adding the effect of the induced electric field ζ_A to the effect resulted from the induced charge distribution at the air/tissue interface ζ_ϕ. The former effect was calculated by approximating the circular stimulating coil as a polygon and then summing the induced electric field produced by each line segment. The latter was found by solving Poisson's equation in a homogeneous, cylindrical volume conductor, using a finite-difference technique [26].

2.10 Modifying the Cable Equation

In order to accommodate the effect of the charge accumulation and the induced voltage, we must modify equation (2.11). We will start by equating the axial components of the electric field inside the fiber ζ_x with the negative gradient of the intracellular potential

$$\zeta_x = -\frac{\partial V}{\partial x} \qquad (2.14)$$

However, in magnetic stimulation the time-varying magnetic field gives rise to an additional source of electric field through electromagnetic induction. Therefore, equation (2.14) must be amended to include the component of the induced electric field parallel to the fiber ζ_i (x,t)

$$\zeta_T = \zeta_x + \zeta_i (x,t) \qquad (2.15)$$

Where ζ_T is the total induced electric field, ζ_x is the electric field due to voltage gradient, and ζ_i is electric field due to the induced voltage that results from the rate of change of the magnetic flux ϕ. The term ζi can be represented as:

$$\zeta_i = -\frac{\partial A}{\partial t} \qquad (2.16)$$

Where A is the magnetic vector potential (see Chapter 3 for more details).

It is important to realize that the induced electric field can not be expressed with the gradient of the voltage only, but also must be related to the rate of change in magnetic field ϕ [26]. Both the field rate of change and induced electric field are determined by the coil current and geometry. We also note that it is the component of the electric field parallel to the fiber (in the axial direction) that enters the nerve and ultimately results in stimulation (from currents being induced inside the internodal). This is consistent with the conclusion that electric fields oriented parallel to nerve fibers cause stimulation more readily than electric fields oriented transverse to fibers[26,28]. Also, the strength of the electric field (ζ_ϕ) on the membrane due to charge on its surface is higher than the electric field strength (ζ_A) induced in the tissue [13][6]. Nevertheless, the contribution of ζ_ϕ to stimulation is less than the contribution of ζ_A as the charge movement (current) at the surface of the tissue is less than that induced in the tissue.

---

[6]The charge accumulation is due to the myelin dielectric characteristic (see Table 2.1).

2.11 Representing the Cell Membrane by a Resistor, Capacitor and an Inductor

The most common equivalent circuit representing the cell membrane is a combination of a resistor and a capacitor in parallel. To confirm the validity of this model, early experiments were conducted by Cole and Curtis (1939) and documented by Weiss [2]. In these experiments a giant axon of a squid was placed between two electrodes that were attached to two arms of a Wheatstone bridge. This arrangement allowed the electrical impedance between the electrodes to be measured over a range of frequencies. Cole and Curtis found that during action potential, the membrane capacitance was essentially constant, but that the membrane conductance showed a large transient increase. The conductance increase lags behind the increase in membrane potential and decays somewhat more slowly than does membrane potential. The wave shapes of the membrane potential and the conductance are shown in figure 2.12 (adopted from [2]).

From these results and the waveforms we conclude that the change in the conductance is due to a reactive element that charges at the beginning of the action potential and discharges when the potential drops in the circuit. By examining the waveform carefully we realize that this element behaves like an inductance! [2]. This means that the cell membrane might be represented by a resistor, a capacitor and an inductor. Figure 2.13 shows the equivalent circuit for the membrane according to the above assumption. The validity of this circuit is still questionable as all researchers believe that the membrane characteristics should involve only resistor and capacitor elements. They explain the waveform in figure 2.12 as being a nonlinear complex characteristic of the membrane conductance and capacitance. However, in this thesis I will apply an inductor (L_m) to my circuit model as my main goal is the analysis and the calculation of the induced current in the nerve.

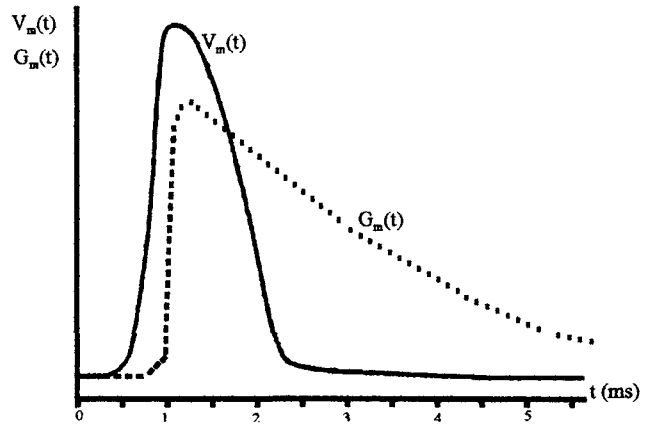

Figure 2.12
The waveforms for the membrane potential and conductance (after [2]).

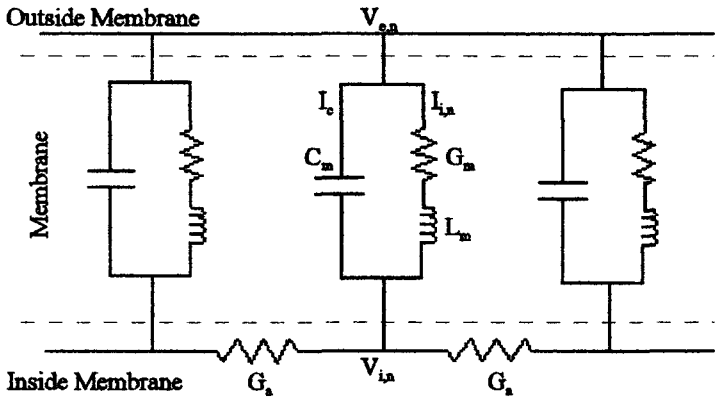

Figure 2.13
The membrane equivalent circuit including an inductance (after [2]).

2.12 An Electrical Model for the Nerve and the Stimulating Circuit

Magnetic stimulators employ two major components: a pulse generator; and a coil system that couples the energy from the pulse generator to the target nerve via a magnetic field. A typical stimulating circuit is a combination of a switching circuit and a capacitor bank. The capacitor is charged from a high voltage power supply and then its energy is discharged into the stimulating coil. Figure 2.14 shows a diagram that illustrates the stimulating circuit concept.

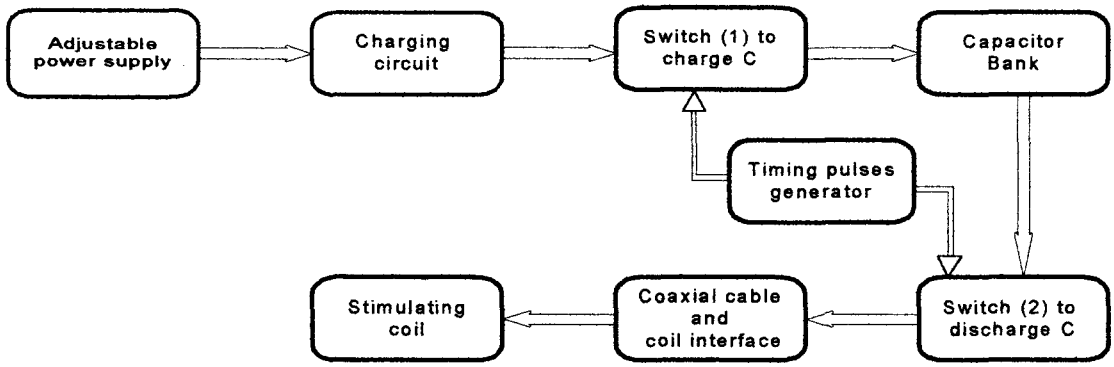

Figure 2.14
A block diagram for the stimulating circuit.

As the main components of this circuit are the capacitor bank and the stimulating coil, we will consider the equivalent circuit shown below for the previous diagram. Figure 2.15 shows a simple schematic diagram for a stimulating circuit. C represents the capacitor bank , R is the equivalent resistance for the coil wires, leads, connectors and the cables that link the capacitor bank to the coil. L_c is the inductance of the stimulating coil. S_1 and S_2 are the charge and discharge switches respectively. The circuit operates on the concept of charging and discharging of the capacitor bank. At the beginning S_2 is open while S_1 is closed allowing the capacitor to

charge from the power supply. Once the capacitor has reached its required voltage, S_1 will be opened and S_2 will be closed to allow the capacitor to discharge into the stimulating coil. The switching time of this process depends primarily on the type of stimulation required: repetitive or single stimulation. More details about the stimulating circuit and its components are outlined in Appendix B.

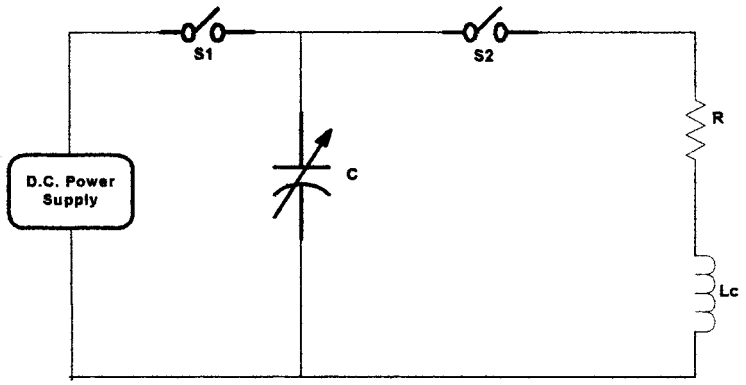

Figure 2.15
Schematic diagram for a basic stimulating circuit.

The stimulating circuit generates a pulsating current. This current results in a magnetic flux that links the coil and the nerve and can be represented by the following diagram.

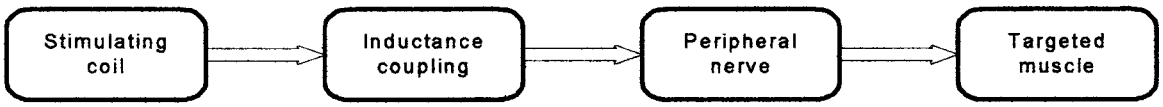

Figure 2.16
A diagram represents the linkage between the stimulating coil and the nerve.

Figure 2.16 can be substituted with an electrical circuit where the stimulating circuit can be represented by figure 2.15 and the peripheral nerve can be exchanged with the myelinated axon model (figure 2.13). These two circuits are linked together by a transformer which denotes the field linkage between the stimulating coil and the targeted nerve. Figure 2.17 shows the combination of equivalent circuit for a myelinated nerve and the stimulating circuit.

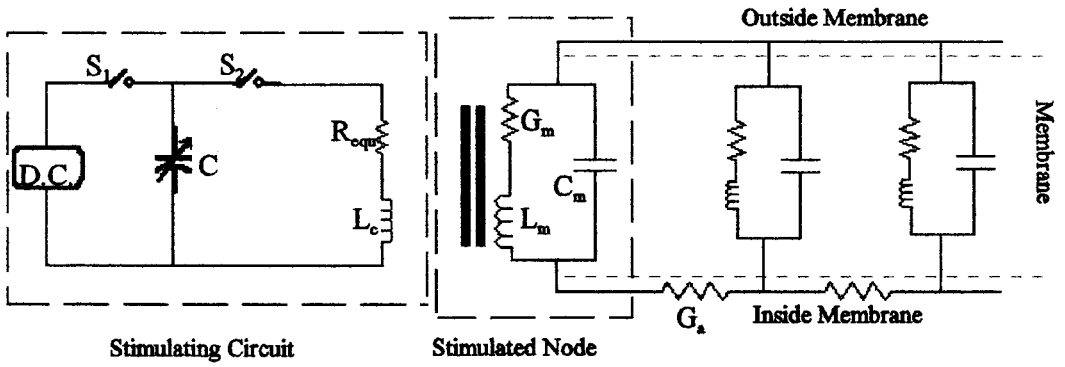

Figure 2.17
An equivalent circuit representing the combination of a stimulating circuit and a targeted nerve.

To calculate the induced voltage in the targeted nerve, we must calculate the electromagnetic linkage between the coil and the nerve. In the previous model we assumed that there is no electrical link between the stimulating coil and the nerve. This is true as the coil is electrically insulated from the tissue. This leaves us with only the magnetic field that links the coil and the nerve. In other words, the only source of excitation to the nerve will be the magnetic field created by the coil. The linkage between the coil and the nerve can be expressed as a transformer where the stimulating coil is the primary coil and the nerve is the secondary

coil. As the current passes through the primary, and according to Faraday's law, there will be an induced voltage in the nerve (the secondary coil) that can be given by:

$$v_e = M \frac{di_1}{dt} + L_n \frac{di_2}{dt} \qquad (2.17)$$

Where v_e is the induced voltage in the nerve, M is the mutual inductance between the nerve and the stimulating coil, L_n is the nerve inductance, i_1 is the current in the stimulating coil (the primary), i_2 is the current in the nerve (the secondary). The current i_1 will produce the magnetic flux that links the two coils. In the above equation the second term becomes negligible as its value is very minute relative to the rest of the equation. This will leave us with the effect of M only, where M can be represented as:

$$M = k_1 (L_n L_c)^{1/2} \qquad (2.18)$$

Where L_c is the stimulating coil inductance, k_1 is the coupling coefficient between L_c and L_n. The coefficient k_1 depends on the stimulating coil orientation, size and angle relative to the body. It also depends on the nerve depth, size, type and shape.

The next step is to estimate the value of the induced voltage. First the inductance of the nerve can be represented as a self inductance of a thin wire. From Appendix C the inductance for the nerve can be represented as:

$$L_n = \frac{\mu_o \ell}{8 \pi} \qquad (2.19)$$

where L_n is the inductance of a wire (nerve), ℓ is the nerve length, and μ_o is the permeability of

free space ($4\pi x10^{-7}$ $H.m^{-1}$). Also from Appendix C, the inductance for the coil is :

$$L_c = \frac{\mu_o \mu_c N^2 A}{d + k_2 \mu_c g} \qquad (2.20)$$

where L_c is the inductance of the coil, μ_o is the permeability of free space, μ_c is the relative permeability of the core, d is the core length, g is the air gap length, N is the number of turns, A is the cross section of the core and k_2 is a ratio of the linkage field relative to the total field. The value of k_2 is assumed to be piecewise (varies within certain range) in order for equation 2.20 to be valid for the case μ_c not equal to μ_o. The value of k_2 depends primarily on the length of the air gap, the coil shape, core length, core cross section area, and core material. Substituting L_c and L_n to calculate M we will get:

$$M = k_1 \left(\frac{\mu_o \mu_c N^2 A}{d + k_2 \mu_c g} * \frac{\mu_o \ell}{8 \pi}\right)^{\frac{1}{2}} \qquad (2.21)$$

The final equation is:

$$M = \frac{k_1 \mu_o N}{\sqrt{8 \pi}} \left(\frac{\mu_c A \ell}{d + k_2 \mu_c g}\right)^{\frac{1}{2}} \qquad (2.22)$$

To estimate e_n (the stimulus voltage applied to the trans membrane) we substitute equation (2.22) into equation (2.17) to get:

$$e_n = \frac{k_1 \mu_o N}{\sqrt{8 \pi}} \left(\frac{\mu_c A \ell}{d + k_2 \mu_c g}\right)^{\frac{1}{2}} \left(\frac{di_{coil}}{dt}\right) \qquad (2.23)$$

Now we have a voltage source and an excited nerve which is ready to move this voltage as an Action Potential to the designated target (i.e. muscle). According to Lenz's law this induced voltage will create a charge that will be transferred by the nerve. This transfer will occur due to the nerve conductance characteristics. In order for the target to respond, the total charge that is injected in the nerve should be equal to or higher than the threshold value of Resting Potential. This means that if the nerve maintains this charge (after all the losses due to leakages) then stimulation will be achieved.

Equation (2.23) is a linear equation that yields an imprecise value for the estimated induced voltage in the nerve. However, this equation is helpful when designing or analysing a stimulating coil as it outlines the main parameters that affect the induced voltage in the targeted nerve.

The final stage in nerve stimulation is the detection of the tissue action potential. This detection is done by measuring the signal from the targeted muscle. This part can be represented by the equivalent circuit shown below.

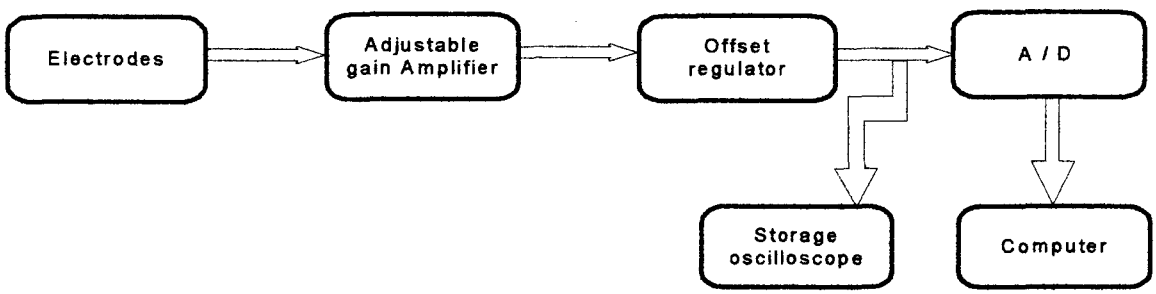

Figure 2.18
A block diagram for a detection circuit.

Chapter 3

Analysis of the Electric Field Induced in the Stimulated Nerve

3.1. Historical Review for Calculating the Electric Field in a Human Body

In magnetic stimulation, an analysis of the electric field induced in the tissue is important as it determines the stimulation area, the level of excitation in the targeted nerve, and the degree of improvement when using different types of coils. In general, to analyse an electric field we can either physically measure its related variables or calculate them from a simulated model. To measure the electric field variables in a human body is a difficult task primarily due to the measuring devices inaccessibility. Alternatively, we can model the stimulated nerve and calculate the required field variables using computer simulations.

Over the past few decades many studies have been conducted to calculate the electric field induced in the body. These studies concentrated on both low and high frequency applications. The low frequency studies [29-32] examined the impact of a 60 Hz field on the body, while the high frequency studies [33,34] examined the impact of a radio frequency field (during MRI and hyperthermia treatment for cancer) on the body.

For magnetic nerve stimulation the calculation of the electric field was done by several researchers [35-46]. These studies were applied to different parts of the body (limbs, cortical) and different model shapes (cylindrical, spherical).

3.2 Approximation for Calculating the Electric Field

When calculating an electric field induced in the tissue during magnetic stimulation, we will introduce four approximations.

In the first approximation we will ignore the effect of the applied field wavelength. As the frequency varies from 1-10 kHz for magnetic stimulation, the corresponding wave lengths will be much longer than any distance associated with the human body. This means that the instantaneous value of the field is approximately the same across the entire stimulated region.

In the second approximation we will neglect the skin depth which represents the distance inside the tissue at which the magnetic field is approximately one-third of the external field. This is because the induced currents in the tissue produce their own magnetic field that tends to cancel out the applied field. However, the magnetic field produced by the induced current in the tissue is smaller than that produced by the coil current.

In the third approximation we will neglect the nerve capacitive effect. As shown in Chapter 2, the impedance of a multi-cellular tissue can be modeled by a combination of resistors and capacitors. These circuit elements can be combined to yield an overall tissue impedance with a resistive to reactance ratio of:

$$\frac{R}{X_c} = \frac{2\pi f \epsilon_0 \epsilon_r}{\sigma} \qquad (3.1)$$

where ϵ_0 is a constant, 8.85×10^{-12} F/m, ϵ_r is the tissue dielectric constant, and σ is the tissue conductance S/m. At a frequency of 10 kHz, the dielectric constant of many tissues is on the order of 10^4 and the conductivity is about 1 S/m [2,26], implying that the ratio of resistive to

capacitive parts of the tissue impedance is 0.005. The contribution of the large capacitive reactance to the tissue impedance (which is a combination of parallel capacitors and resistors) can be neglected and the tissue can be considered to be purely resistive. This is equivalent to saying that any delays between the application of an electric field and the appearance of a charge distribution on the tissue surface are ignored. This approximation is weaker than the previous one and may break down for higher frequencies and tissues with unusually small conductivities or large permitivities. However, we can apply this approximation as the operating frequency will not exceed 10 kHz and the conductivities of the tissues involved are less than 1 S/m.

Finally, in the fourth approximation we will assume that the tissues of interest are homogeneous, isotropic and have a volume conductor with a simple geometry. This is clearly the least valid assumption, since all biological tissues are quite inhomogeneous and many are anisotropic. The only justification for this assumption is that these calculations are only a first step towards more accurate models.

3.3 General Formulation for Estimating the Electric Field

It is well known that the behaviour of the electromagnetic field in any current carrying device is governed by Maxwell's equations [27,47,48]:

$$\nabla \times \overline{\zeta} = -\frac{\partial \overline{B}}{\partial t} \qquad (3.2)$$

$$\nabla \times \overline{H} = \overline{J} + \frac{\partial \overline{D}}{\partial t} \qquad (3.3)$$

$$\nabla \cdot \overline{D} = \rho \qquad (3.4)$$

$$\nabla \cdot \overline{B} = 0 \qquad (3.5)$$

where ζ is the electric field, B is the magnetic flux density, H is the magnetic field, J is the electric current density, D is the electric flux density, and ρ is the electric charge density. The symbols $\nabla\cdot$ and $\nabla\times$ are called the divergence and curl which are the differentiation with respect to vector positions. The previous equations are applicable to a field diffused in a single medium. However, when two materials are used with either different magnetic permeability (μ), electrical permittivity (ϵ) or electrical conductivity (σ), the following continuity conditions (for the normal and the tangential components) should be satisfied.

$$\overline{n} \times (\overline{\zeta_1} - \overline{\zeta_2}) = 0 \qquad (3.6)$$
$$\overline{n} \times (\overline{H_1} - \overline{H_2}) = \overline{J_S} \qquad (3.7)$$
$$\overline{n} \cdot (\overline{D_1} - \overline{D_2}) = \sigma_S \qquad (3.8)$$
$$\overline{n} \cdot (\overline{B_1} - \overline{B_2}) = 0 \qquad (3.9)$$

To complete the above system of equations we must add another three equations to the previous eight. The additional equations are:

$$\overline{D} = \epsilon\overline{\zeta} \qquad (3.10)$$
$$\overline{B} = \mu\overline{H} \qquad (3.11)$$
$$\overline{J} = \sigma\overline{\zeta} \qquad (3.12)$$

Now we have a set of equations (11) that can be used to solve electromagnetic field problems in any material. Yet solving the above equations directly to determine the field vector is not an efficient technique either in effort or in time.

In order to render the numerical calculations more manageable, it is customary to represent the magnetic field by a vector potential which minimizes the number of unknown variables.

3.4 Specific formulation for the Electric Field in Magnetic Nerve Stimulation

To derive the required equation that represents the transient electric field during magnetic stimulation we will start by representing the magnetic field with a vector potential. We will choose our vector potential (A) such that :

$$\overline{B} = \nabla \times \overline{A} \qquad (3.13)$$

Equation (3.13) does not fully define $\bar{A}$, because a vector is uniquely defined if and only if both its curl and divergence are known, as well as its value at one space point (Helmholtz theorem). The specification of the divergence of $\bar{A}$ and the value of $\bar{A}$ at one point will be presented, subsequent to the derivation of the equation for the electric field.

Substituting equation (3.13) into equation (3.2) results in:

$$\nabla \times (\overline{\zeta} + \frac{\partial \overline{A}}{\partial t}) = 0 \qquad (3.14)$$

Applying the vector theory (*the curl of any gradient vanishes*) to equation (3.14) results in:

$$\nabla \times \nabla \Phi = 0 \qquad (3.15)$$

From equation (3.14) we conclude that ζ differs from the rate of change of $\bar{A}$ with respect to time by some static vector $\nabla \Phi$ where:

$$\overline{\zeta} = - \nabla \Phi - \frac{\partial \overline{A}}{\partial t} \qquad (3.16)$$

Equation (3.16) presents a formula for the electric field during magnetic stimulation. It shows that the electric field consists of two sources: a charge distribution and a time-varying magnetic field. The first source ($-\nabla \Phi$) is the electrostatic potential (electric scalar potential) that arises from fixed electric charge, while the second source($-\partial \bar{A}/\partial t$) represents the contribution of the electric field from magnetic induction due to the coil transient current.To physically demonstrate the above equation, when a stimulating coil (circular) is placed close to tissue an electric field will be produced due to the magnetic induction of the transient current. The shape of this field results in closed loops with the coil. These loops move charged ions in the tissue along the electric lines. Since air is an insulator the charge accumulates on the surface of the skin producing the second component of the electric field in equation (3.16).

The time required for this charge to accumulate is small compared to the rise time of the coil current. As the skin conductivity is low there will be no current to move these charges away from the tissue surface. Therefore, these charges will accumulate and create the static component of the electric field. Hence, the time derivative of $\bar{A}$ can be expressed by:

$$\bar{\zeta} + \frac{\partial \bar{A}}{\partial t} = 0 \qquad (3.17)$$

Figure 3.1 shows the distribution of the electric field within a tissue where the component for the induced electric field ζ_A (top section) is created due to the transient current by the coil. While ζ_ϕ (bottom section) the electric field, is generated by the accumulated charge on the surface of the skin. (This plot is for illustration purposes only and not meant to be quantitatively correct.)

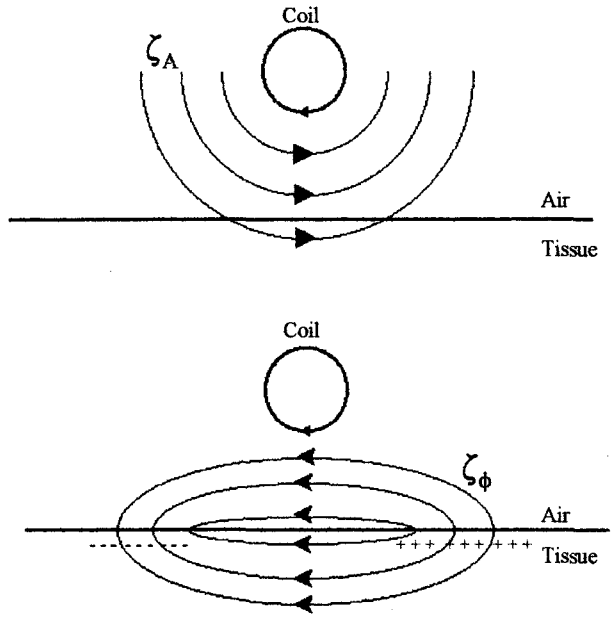

Figure 3.1
Electric field distribution within a tissue

As for calculating the vector potential Ā at one point in space we can use the coil geometry in conjunction with Amperes' law that defines Ā as follows [26]:

$$A = \frac{\mu_0 N\, i}{4\pi} \int \frac{dl'}{R} \qquad (3.18)$$

where N is the number of turns in the coil, I is the coil current, dl′ is a vector representing a small length of the coil (pointing in the direction of the current), and R is the distance from dl′ to the position where Ā is calculated. Equation (3.18) is valid for the case of free space, it is also valid for magnetic nerve stimulation since the relative permeability of nerve and tissues is identical to that of free space [27].

The previous equation can be solved as:

$$\bar{A} = Ni(t)K_g \qquad (3.19)$$

where K_g is a constant which depends on the shape of the coil and the position of the point at which $\bar{A}$ is calculated. Combining equation (3.17) and (3.19) the result will be:

$$\zeta = -N\frac{\partial i(t)}{\partial t} K_g \qquad (3.20)$$

For a circular coil, we can substitute equation (3.18) into equation (3.17) and the resultant equation will be:

$$\zeta_A = -\frac{\partial \bar{A}}{\partial t} = -\frac{\mu_0 N}{4\pi}\frac{\partial i}{\partial t}\int\frac{dl'}{R} \qquad (3.21)$$

Since dl′ and R both have dimensions of length, the integral in equation (3.21) is dimensionless. For distances from the coil similar to its size, the integral in equation (3.21) is approximately equal to one. Therefore, a rule of thumb for determining the order of magnitude of ζ_A is

$$|\zeta_A| = 0.1N\frac{\partial i}{\partial t} \qquad (3.22)$$

where $\partial i/\partial t$ has units of A/μs and ζ_A is in V/m. The integral over the coil geometry is the only difficult part in determining $\bar{A}$ (equation 3.18) and ζ_A (equation 3.21). This integral is very important as it defines the spatial distribution of the electric field, however, it is difficult to find analytic solutions to this integral. The alternative method is to evaluate it numerically [26].

3.5 Calculation of the scalar potential

The primary origin of $\nabla \Phi$ in magnetic stimulation is the electrical charges that accumulate at the interfaces between regions of different tissue conductivity and the air-skin interface. The charges at the interface can then be calculated as the normal component of the current density should be continuous at an interface between different conductors.

However, the second term in the expression for the electric field in equation (3.16) ($-\nabla \Phi$) is difficult to calculate because the source of Φ (the accumulated charge) is not known. One way to determine Φ is to assume that the tissue scalar potential obeys Poisson's equation

$$\nabla^2 \Phi = 0 \qquad (3.23)$$

To find a solution, boundary conditions on the tissue surface must be given [49,50]. We can then apply a suitable numerical method (ie: finite difference) to solve Poisson's equation [51]. Once Φ has been found, its contribution to the electric field, ζ_Φ is

$$\zeta_\Phi = -\nabla \Phi \qquad (3.24)$$

As I have mentioned in Chapter 2, the effect of ζ_Φ due to the accumulated charge Φ is relatively small compared to ζ_A [24]. Therefore, when calculating the electric field for our coil we will add another approximation to the previous one. We will assume that the effect of Φ is minimum and can be neglected.

In conclusion, to calculate the electric field in our coil, we will only calculate the component ζ_A or in other words, we will only calculate the vector potential $\bar{A}$.

3.6 The technique of calculating the induced electric field generated by our coil

To calculate the field produced by our model is not an easy task. This is due to the model geometrical complexity, the transient state of the supply and the various non linear mediums with different conductivities. Considering the above factors, it becomes impossible to solve this problem by an analytic method with precise results. Instead, a numerical method is needed. There are various numerical methods available, the most commonly used are: finite difference, integral formulation, circuit models, and finite elements.

The finite difference method can be used to solve electromagnetic problems. However, this technique is not the best if complex geometry is involved or if a fine grid is required. In this problem, the coil geometry is very complex, which makes it difficult to define a suitable grid. To accommodate the coil complex geometry the required grid must be extremely fine to minimize the error embedded in the solution during calculations. Also, the area of interest (the nerve) is small relative to the entire region. In conclusion, we need a grid that is large enough to satisfy the coil geometry and the size of the nerve. To solve a problem with a large grid size requires many computational hours. Furthermore, any grid refinements to improve the solution means a tremendous increase in the computational time.

The integral formulation method is commonly applied to steady state problems and very seldom to a transient field problem with complex geometry. Also, this method solves the problem for the entire region and not just the area of interest. This problem does have a transient field with complex geometry, and the area of interest is small (the nerve) thus, this method would not be suitable.

The circuit models method involves the subdivision of the conductive components in the

particular configuration to a number of segments where we can formulate an impedance matrix that relates the input voltage and current in each one of these segments. However, this method can not be applied to our problem as the value of the various parameters inolved is not easy to estimate for the type of media involved (nerve, tissues).

The final approach is the finite element method. This is the most appropriate method to solve this problem as it has the flexibility to handle complex geometry for various regions with different types of boundaries.

3.7 Advantages of using the Finite Element Method

The advantages of using a finite element method can be summarized as follows :

1. This method can be applied to a problem that consists of different materials adjacent to one another, as is applicable to this problem.
2. This method can be applied to a problem with complex geometry which has various types of boundaries. This holds true for our coil which has a complex shape and is defined within various boundaries.
3. In this method we can refine the mesh (grid) according to the solution requirements. This is compatible with our problem as the area of interest (the nerve) is very small relative to the remainder of the region.
4. In this method the concept of symmetry can be applied, which translates to a saving in computational time.

From the benefits mentioned above, we concluded that the Finite Element Method is a very powerful tool that can be used to solve this problem. Ideally, a time marching scheme, such

as the Crank-Nicholson scheme, can be used to handle the transient nature of the stimulating source currents [52]. This involves discretizing the input current (forcing function) in the time domain and applying the finite element technique for each time step, using the results of the previous step as an initial value bounded problem. For the purpose of this study, it was decided that we did not have to go through this procedure and to settle for magnetostatic solution for two fundamental reasons:

1. Our main interest is to evaluate the proposed coil designs, as outlined in Chapter1, in comparison to existing coils. For this purpose a single step solution (static condition) will provide a proper frame of reference for relative comparison of electric field focussing.
2. We did not have available for our use at McMaster university a transient finite element solver or other experimental resources to check transient findings.

3.8 Application of the Finite Element Method

The finite element method (FEM) is used to solve mathematical or physical problems which are usually defined in a continuous domain either by local differential equations or by equivalent global statements. This method allows us to solve various kinds of large-scale complex problems, for example; heat transfer, electromagnetic field and mechanics stress and strain, etc. Basically, this method transforms the solution of complicated partial differential equations (PDE) into solving a large set of algebraic equations. For this reason, it is one of today's best-accepted methods for numerical analysis. In electrical engineering the finite element method did not make its first appearance until 1968 [53]. Since then it has been used

for a wide range of applications [54,55]. Interestingly, despite its generality, the concepts that underlie the FEM method are more mathematically elegant in their simplicity.

The basic theory of the finite element method and the details of its mechanical application to solve PDE are well described in the literature [53,54,55]. The commercially available software package "Magnet"[56] was used to apply this technique to solve our problem.

3.9 Applicable Boundary Conditions

To reduce the computational time, an appropriately defined boundary is needed to solve this problem without introducing significant error to the solution particularly at the points of interest. The defined boundary reduces the solution region and consequently, minimizes the computational time.

Both the Dirichlet and homogenous Neumann boundary conditions can be applied to the finite element method. These boundary conditions are used almost universally to solve various classes of electromagnetic field problems.

For this problem I applied Dirichlet boundary conditions where the boundary will be defined at three times the diameter of the arm. This will ensure a minimum error for the field as its value will be negligible at that distance from the coil.

3.10 Modelling of the Stimulating Coil and the Targeted Nerve:

In order to evaluate the merits of the proposed coil designs, as compared to existing coils, the finite element technique had to be applied to a region that includes the stimulating coil as well as the targeted nerve and its environment.

The magnetic field density produced by each coil configuration, at the centre of the targeted nerve, is used as a basis for comparison. The design features of the proposed coil (with either magnetic or non-magnetic cores) have been outlined in Chapter 1 and Appendix A. The solution region is a two dimensional area that represents a cross-sectional view that is perpendicular to the targeted nerve path. The physical characteristics of the stimulation coil are captured by the geometry of the mesh. The electric and magnetic properties are also specified as required by Magnet.

As for presenting the targeted nerve, previous researchers [6,16,28,57-59] have represented the human body with a uniform conductivity. This simplistic model minimizes the computational effort. However, in order to achieve more accurate results, it was decided in this study to represent the main components of the arm with their various electric characteristics.

Grant's Atlas of Anatomy and Gray's Anatomy [60,61] were used as the basis for modelling the arm. The targeted nerve in this model is the Median Nerve as it is close to the skin surface, which makes it easier to stimulate. Figure 3.2 shows the target nerve (Median nerve) along the arm. Figure 3.3, 3.4 and 3.5 show the cross-sections for the upper limb. Figure 3.6 shows the approximated cross-section of the arm for the purposes of this analysis [7].

---

[7]After construction of my models, I had a discussion with Dr. Grooves, Head of Anatomy Department at McMaster Hospital. Dr. Grooves was helpful with her suggestions in modifying my models to accurately reflect the human arm.

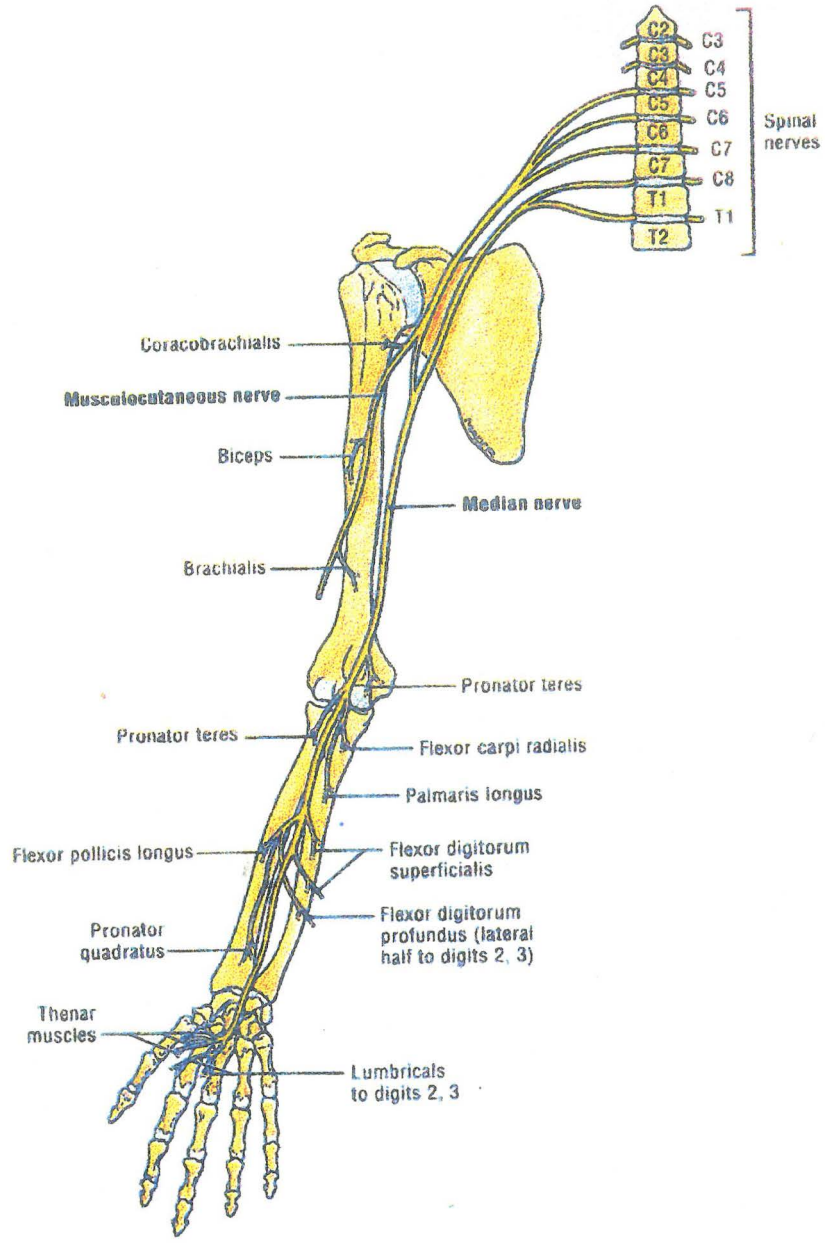

A. Median and musculocutaneous nerves.

Figure 3.2
Median nerve pathway (taken from [60])

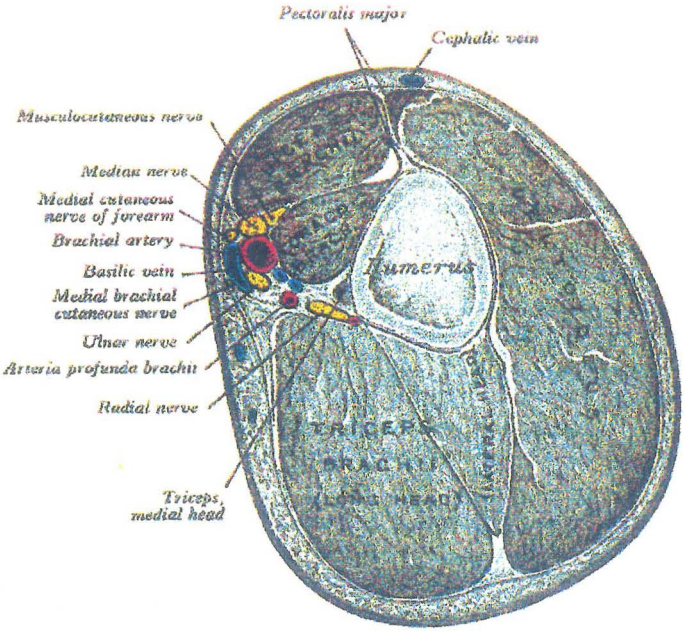

A transverse section through the right arm at the junction of the proximal and middle thirds of the humerus. Proximal aspect.

Figure 3.3
(taken from [61])

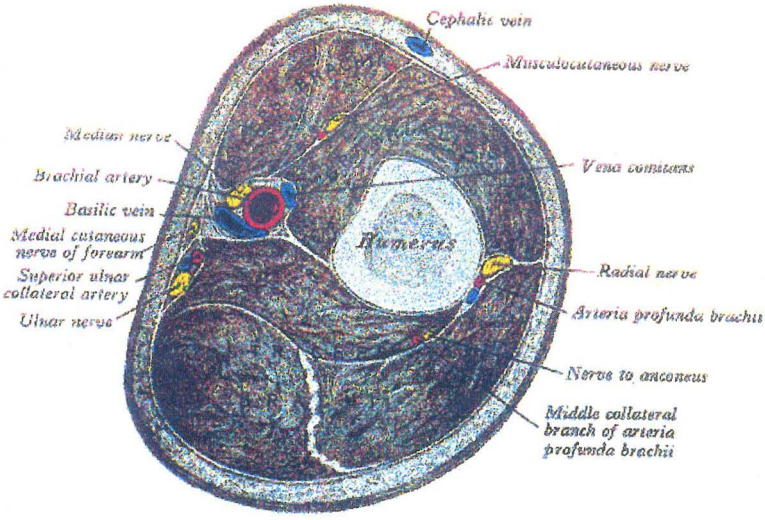

A transverse section through the right arm, a little below the middle of the shaft of the humerus. Proximal aspect.

Figure 3.4
(taken from [61])

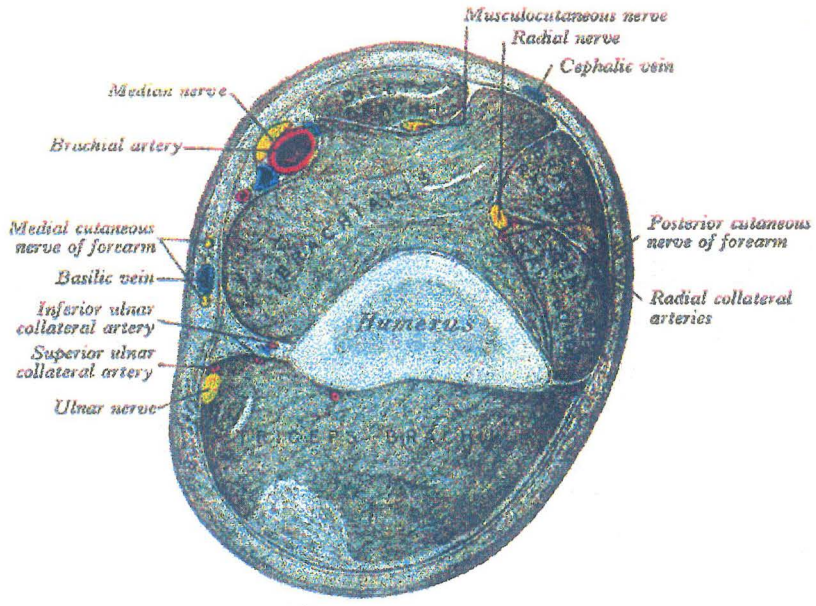

A transverse section through the right arm, 2 cm above the medial epicondyle of the humerus. Proximal aspect.

Figure 3.5
(taken from [61])

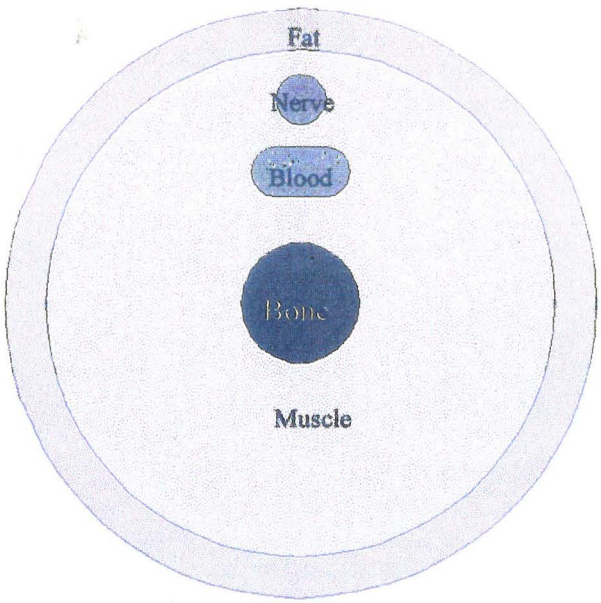

Figure3.6
A model representing a cross section for the arm

3.11 Simulations and Calculations

Eight different coil designs were analyzed using Magnet. Five of these coils were taken from the literature (they are the most commonly used for magnet stimulation). The last three coils, as listed below, are those that were proposed in this study to increase the magnetic field intensity and focus it better on the stimulated nerve. Comparison of the results obtained from the simulations were considered to be broad enough to allow proper evaluation of the improvement generated by each of the proposed coils. The coil designs that have been simulated are as follows:

1. The "eight" shape coil with uniform distributed windings, used by Uneo, and Amassian [3,12].
2. "Butterfly" coil with decentralized windings used by Weyh et al [16].
3. "Butterfly"coil modified to accommodate the curvature of the arm by Weyh et al [16].
4. "Butterfly" coil with decentralized windings and modified to accommodate the curvature of the arm by Weyh et al [16].
5. "Slinky" coil with two sets of windings by Tarjan et al [18].
6. "Slinky" coil with the third winding perpendicular to the other two windings (our air core coil).
7. "Slinky" coil with the third winding perpendicular to the other two windings and a ferromagnetic core (our ferromagnetic core coil).
8. The ferromagnetic core coil (our coil) with concentrated windings.

3.12 Problem Definition When Using the Software Package Magnet

Solving problems using the software package Magnet involves three main stages: the pre-processing of the input data, solving the problem, and the post processing of the output data.. The pre-processor requires that the problem be divided into two sections. The first section involves defining the problem geometry, the number of nodes/elements that creates a suitable mesh and the applicable boundary conditions [56]. The second section involves defining the material properties for each component in the overall mesh region, and the forcing function (current or voltage supply). The solving stage involves defining a suitable solver (ie: time harmonic or magnetostatic) and saving the solution. The post processor stages consists of presenting the results the unknown variables (presented in the main PDE ie: $\bar{A}$), and calculating the values of other parameters that are of interest, ie: flux density, current density, etc.

3.12.1 Problem Geometry, Generating a suitable Mesh, and Applying Boundary Conditions

For each of the simulated coils, the diameter of the arm was assumed to 10 cm. The diameter of the nerve, blood vessels, fat, muscle, and bone were obtained from figure 3.3, 3.4 , and 3.5 [61] by substituting the dimensions of these figures proportionally to the assumed size of the arm diameter. Square copper wire of gauge 12 was used for the coils. The total number of nodes used for the selected region was approximately 5,000 (the maximum limit that Magnet can handle). The majority of these nodes were concentrated in the area of interest, the nerve, and the interface between the coil and the arm. The remainder of the nodes were uniformly distributed in the remaining area. Also, these nodes were carefully defined to ensure that the

shape of the elements are equilateral triangles. This will minimize the extrapolation error in the value of the magnetic vector potential at the centre of the triangular element as a function of its values of the vertices of the triangle. For the boundary conditions, the boundary of the solution region was set as a circumference with a diameter of three times the diameter of the arm. Its centre was placed on the centre of the bone. Dirichlet boundary conditions were assumed for the outer circumference.

3.12.2 The Materials Properties and the Forcing Function

The material for the problem components are defined according to their conductance/ permeability characteristic curves. The conductances for the arm components were applied according to Table 3.1 [27,62]. The permeability is considered to be that of free space. For all the cases of the coil with magnetic core the conductivity and permeability for the Cobalt material were defined according to the supplier data sheets and B-H curves (Appendix B). As the characteristics of the materials involved in this problem (tissues and Cobalt) are not available in the "Magnet" material library, they were built and added to it.

The coil in this problem was defined as having nine turns of solid wire, thus, the skin effect is taken into consideration. A current source was defined as the forcing function (supply). For the magnetostatic solver, the peak value was 5,000 A while for the time harmonic solver, the current RMS value was 5,000 A and the assumed frequency was 2.5 kHz. The current density in the three coils depends upon the current supplied to each coil relative to the total current. Assuming that the total current was equally divided between the three coils, the current density for each coil was 4.1 kA/cm^2.

Tissue	Transverse Conductivity σ_z S/m	Longitudinal Conductivity σ_z S/m
Air	0	0
Skin	0.5	0.5
Fat	0.05	0.05
Muscle	0.08	0.5
Bone	0.013	0.013
Nerve	0.05	0.5
Blood	0.7	0.7

Table 3.1

Table of Tissue Conductivity (after [27,62])

3.12.3 Definition of the Forcing Function and Selection of the Solver

It should be noted that the version of Magnet (Magnet 5.1a) used in this study allows two choices of solvers: magnetostatic (direct current), and time harmonic (alternating current). As stated earlier, the current used in magnetic stimulation is of a transient nature (exponentially decaying sinusoidal function). During this study, a compromise had to be made to solve the transient case as a time harmonic or to simply look at it as a fixed value (magnetostatic case) representing the maximum peak of the transient waveform. Both of these approaches were attempted and the results were compared for all of the eight coil designs considered. It was determined that the effect of varying the frequency was minimal (3-5% variation). Therefore, for the purpose of required comparative analysis, the results of magnetostatic analysis were used. Only these results are presented in this study.

3.12.4 Post Processing and Results of the Analysis

We solved for magnetic vector potential $\bar{A}$. Following that we calculated the magnetic flux density B for both the nerve and the bone (region of interest). The magnetic flux density in the nerve centre represents the area of interest, while the magnetic flux density in the bone centre depicts the penetration level for the field. The value of the magnetic flux density B at the center of the nerve and the bone as well as the profile of the magnetic flux density distribution were used as the basis for assessing the merit of each coil design. The results of analysing the various coil designs listed previously are represented in graphical forms in figures 3.7 - 3.14. These results, the main observations that can be made, and the key features that should be pointed out are summarized as follows:

1. Figure 3.7 presents the magnetic flux lines and values of the flux density as the reference points for the "eight"shape coil with uniform distributed windings. As indicated earlier this coil which was reported in the literature was chosen for our analysis because it represented a marked improvement in the field concentration over the previous generation of circular coils. Also, this coil design served as a platform for further improvement in the design of butterfly shaped coils. The magnetic field density generated by this coil at the centre of the nerve was found to be 0.0393 Tesla while the value of the field density at the centre of the bone was 0.0113 Tesla. These values provided us with a first reference against which the improvements in other reported coils, as well as the coils in the studies, can be measured.
2. Figure 3.8 shows the same data using the "butterfly" shape coil with decentralized

windings (the coil windings are concentrated at the centre on one side and distributed on the other side). This coil was developed by Weyh et al. [16] for the purpose of central nerve stimulations where deeper penetration for the magnetic field is needed to overcome the presence of the bones and higher field concentration is required for effective stimulation. The results of analysing this coil show that the achieved magnetic flux density at the centre of the nerve is 0.0509 Tesla. This is about 30% higher than the flux density achieved using the figure "eight" coil. Another important indication that illustrates how effective this coil is in achieving higher field penetration is the value of the field at the centre of the bone (0.0960 Tesla). This is about 8.5 times higher then the value achieved with the previous figure "eight" shaped coil.

3. Figure 3.9 shows the results for a "butterfly" coil that was modified to accommodate the curvature of the arm. This modification was suggested by Weyh et al. to investigate the benefits of geometrical shaping of the butterfly coil. Analysis of the field distribution generated by this coil indicated that the magnetic flux density at the centre of the nerve was slightly reduced to 0.0496 Tesla from the value of 0.0509 Tesla achieved with the straight butterfly coil. However, the value of the magnetic flux density at the centre of the bone was increased to 0.1136 Tesla from 0.0960 Tesla achieved with butterfly straight coil. These results indicated that the maximum magnetic flux density can be shifted by changing the curvature of the coil. However, one has to be careful not to shift away from the desired target.

4. Figure 3.10 presents the results obtained by a "butterfly" coil with decentralized windings and modified to accommodate the curvature of the arm. It should be noted that the curvature of this coil is the same as the curvature of the coil presented in figure 3.9. Weyh et al. suggested this variation to assist the influence of changing the winding density distribution for this generation of coils. Results of our analysis showed that the magnetic flux density at the centre of the nerve is 0.0616 Tesla. This is about 21% higher then the maximum value (0.0509 Tesla) obtained by the straight butterfly coil with uniform winding density distribution. For this coil design, the magnetic flux density at the centre of the bone was reduced significantly to 0.0085 Tesla. This shows that this coil is best suited for concentrating the magnetic field on the targeted nerve.

5. Figure 3.11 shows the magnetic flux lines and values of the flux density at the reference points for a "slinky" coil with two sets of windings. This coil design was suggested by Tarjan et al. [18] in their attempt to improve the performance of the figure "eight" coil. Interestingly, the results of this study were published at about the same time when the work of Weyh et al. on the coil of figure 3.10 was published. Our finite element analysis for this coil showed that the magnetic flux density at the centre of the nerve is 0.0568 Tesla and the centre of the bone is 0.0088 Tesla. These results are quite comparable to those discussed in figure 3.10 (albeit a little smaller at the centre of the nerve). Therefore, the results presented in figure 3.9, 3.10, 3.11 represented the state of the art for the design of coils used in magnetic nerve stimulation. These results will be used as a bench

mark to evaluate the benefits of the coil designs proposed in this work.

6. Figure 3.12 shows results related to the proposed air core coil. The main modifications that were introduced in this coil design over the design of the slinky coil were:

a) the splitting of the figure "eight" coil into two coils that are connected in parallel and the re-distribution of the outer portion of the winding.

b) the introduction of a new coil in the plane perpendicular to the centre of the horizontal coil.

This design was investigated with a non-magnetic core (figure 3.12) and with a special magnetic core (figure 3.13 below). For the coil with a non-magnetic core, the magnetic flux density at the centre of the nerve was found to be 0.0554 Tesla. This is quite comparable to the value of 0.0568 Tesla obtained with the coil of figure 3.11. However, the magnetic flux density at the centre of the bone increased to 0.0156 Tesla from 0.0088 Tesla obtained with the slinky coil. The results mentioned above were obtained by dividing the total electric current equally among the three windings.

The results of Finite Element Analysis applied on this coil, assuming the current in the perpendicular coil was different than the current in the horizontal coil, showed that the magnetic flux density at the centre of the nerve can be made to vary from 0.055 to 0.065 Tesla. This range of variation is similar to the variation obtained when changing the curvature of the butterfly coil (figure 3.8, 3.9, 3.10). Therefore, the main advantage of this coil design resides in providing the

capability of changing the magnetic field intensity at the targeted nerve using the same coil rather then having to use several coils having different degrees of curvature.

7. Figure 3.13 shows the results of the finite element analysis for the coil design mentioned above but with the ferromagnetic core. As can been seen from these results, a tremendous improvement in the magnetic flux density was realized. The value of the magnetic flux density at the centre of the nerve was increased to 0.1445 Tesla: (2.6 times) the value obtained with the coil having a non-magnetic core and (2.3 times) the value obtained with the coil having the best results (figure 3.10).

8. Figure 3.14 shows the results for a ferromagnetic core coil with concentrated windings. This design variation over the one presented in figure 3.14 involves changing the winding distribution density of the horizontal coils. The comparison of this coil to the one presented in figure 3.13 is analogous to the comparison of the results obtained with the coil in figure 3.10 to those obtained with the coil in figure 3.9. The results presented in figure 3.14 showed that the magnetic flux density at the centre of the nerve and the centre of the bone were the same as that shown in figure 3.13. This clearly demonstrates that the presence of the core has the dominant effect in this coil.

Based on the above results, it can be concluded that the introduction of the magnetic core offers an advantage in increasing the strength of the magnetic flux density in the stimulated nerve.

It should be noted that in all of the figures mentioned above, the same current forcing function value (direct current source) was applied for each of the eight coils. To ensure consistent comparison the current was divided equally if the coil has two sets of windings. Similarly, when the model has three windings, the current was divided equally in the three coils. The results of comparative analysis indicated that the coils with three sets of windings are the most suitable for magnetic stimulation because they provide the ability of focussing the field in a controlled manner. This feature couldn't be achieved with coils that have a single or double set of windings. This demonstrates the key benefits of the coil design proposed in this thesis.

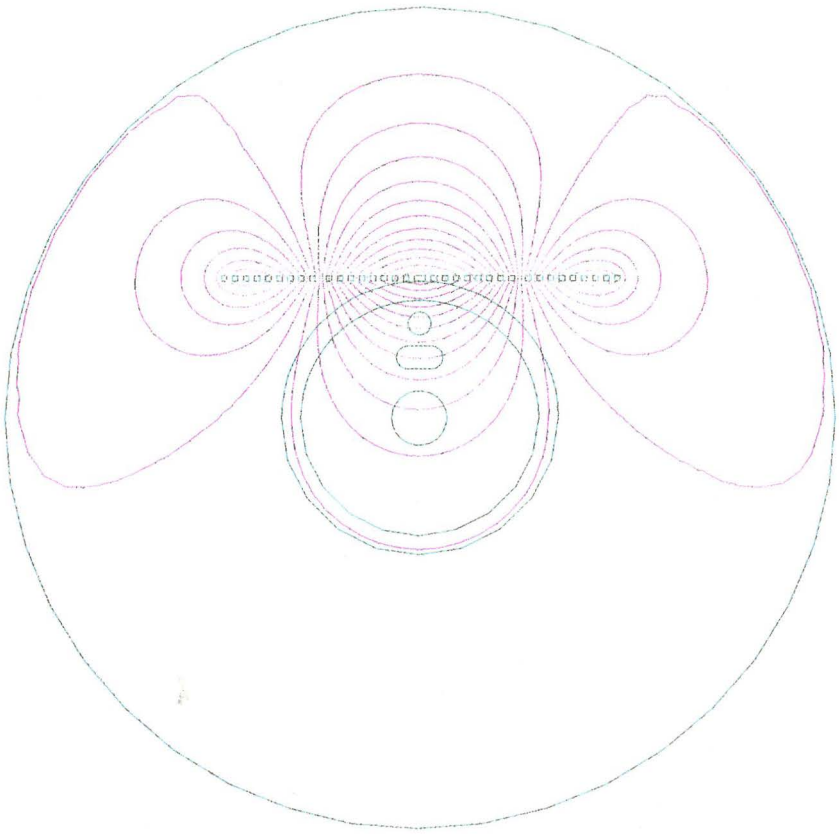

B at the centre of the nerve is =0.039297 Tesla

B at the centre of the bone is =0.01127 Tesla

Figure 3.7
The field lines for an "eight" shape coil with uniform distributed windings

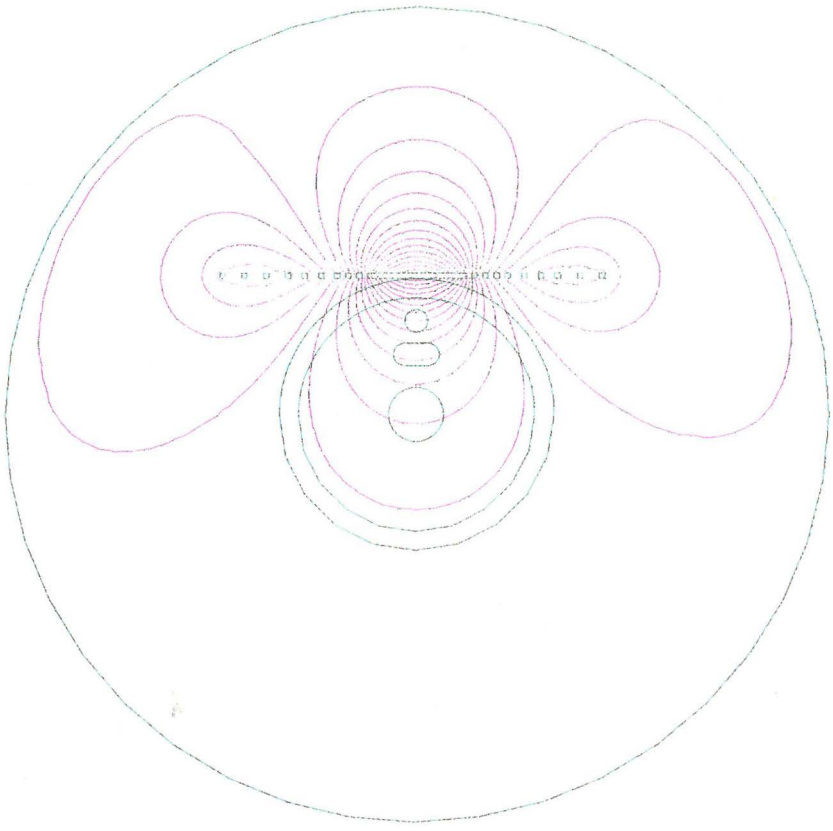

B at the centre of the nerve is =0.05089 Tesla

B at the centre of the bone is =0.095964 Tesla

Figure 3.8
The field lines for a "butterfly" coil with decentralized windings

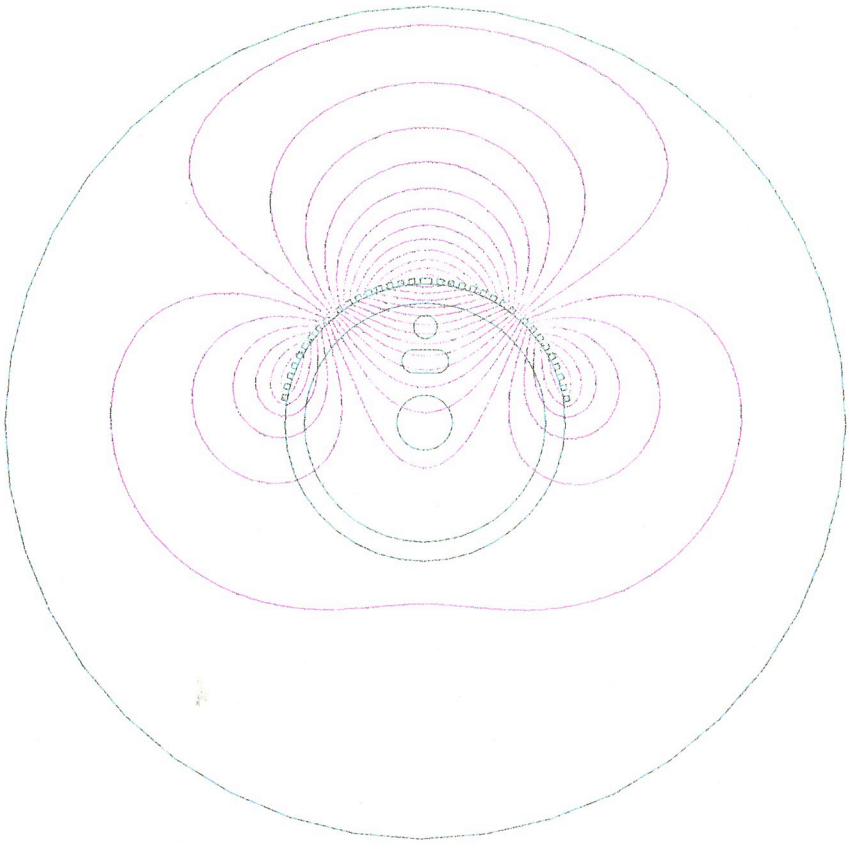

B at the center of the nerve is =0.04960 Tesla

B at the center of the bone is =0.11364 Tesla

Figure 3.9
The field lines for a "butterfly" coil with uniform distributed windings modified to accommodate the curvature of the arm

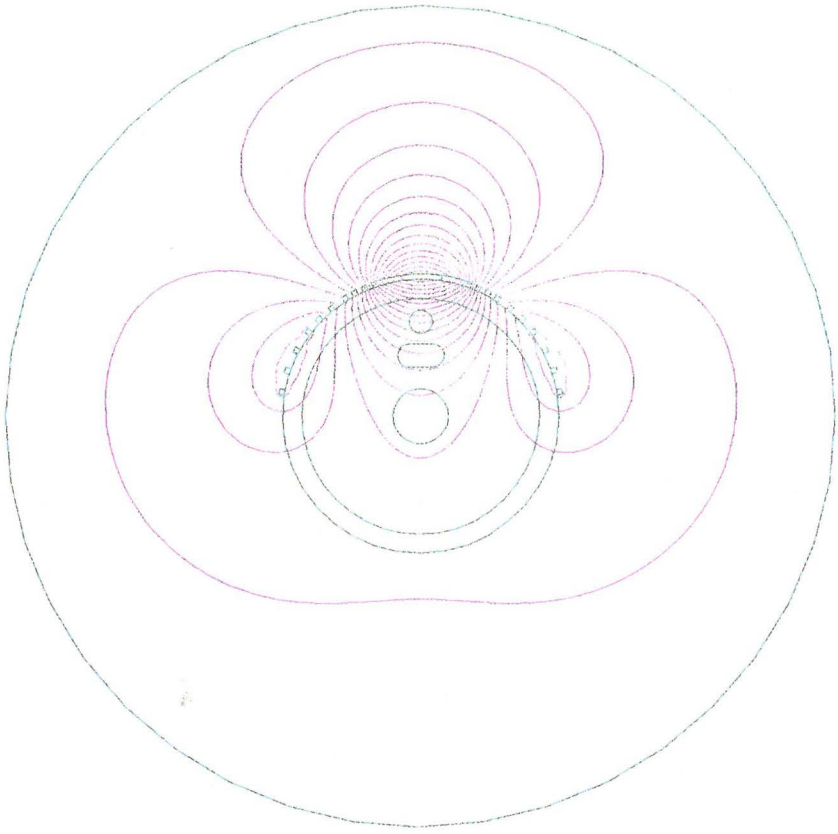

B at the center of the nerve is =0.06157 Tesla

B at the center of the bone is =0.008526 Tesla

Figure 3.10
The field lines for a "butterfly" coil with decentralized windings modified to accommodate the curvature of the arm

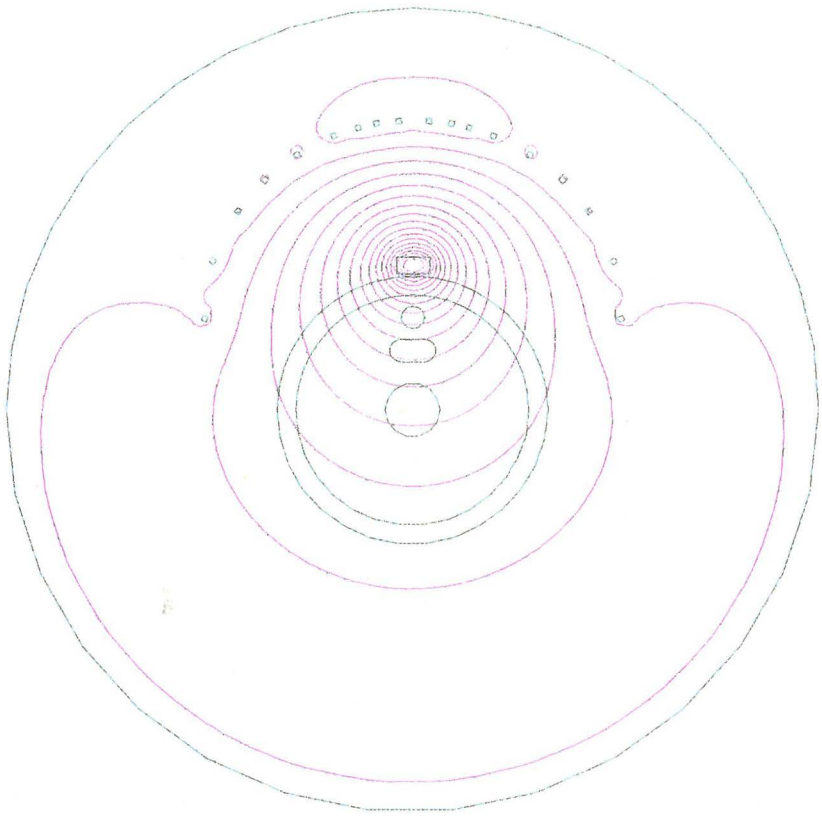

B at the center of the nerve is =0.05682 Tesla

B at the center of the bone is =0.008765Tesla

Figure #3.11
The field lines for Slinky coil with one set of winding

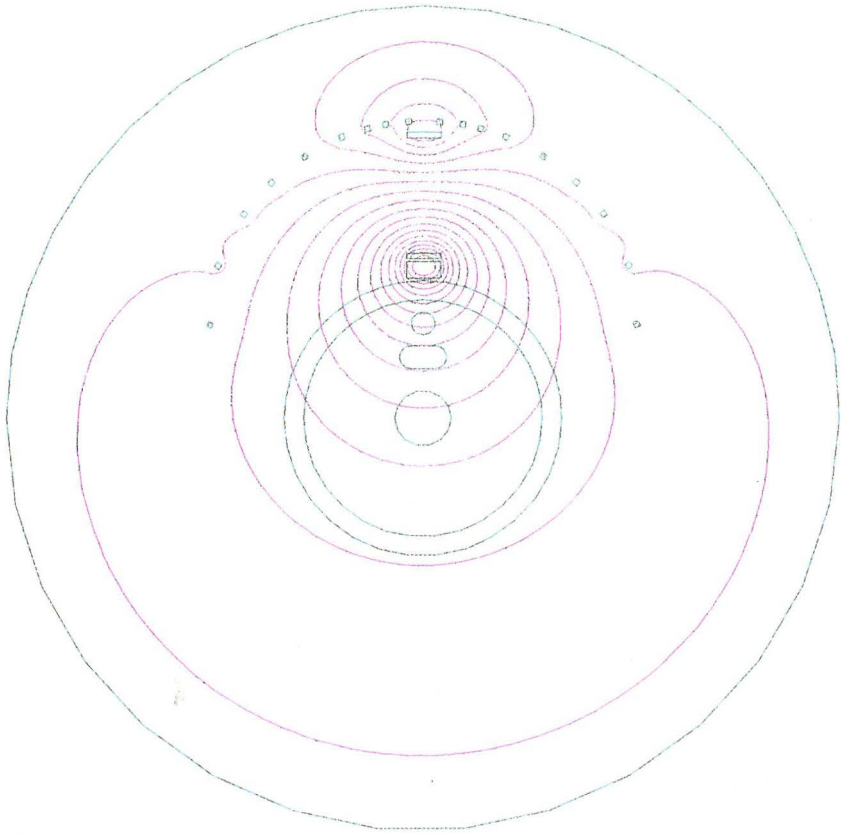

B at the center of the nerve is =0.055434 Tesla

B at the center of the bone is =0.015605 Tesla

Figure 3.12
The field lines for our air core coil with three sets of windings

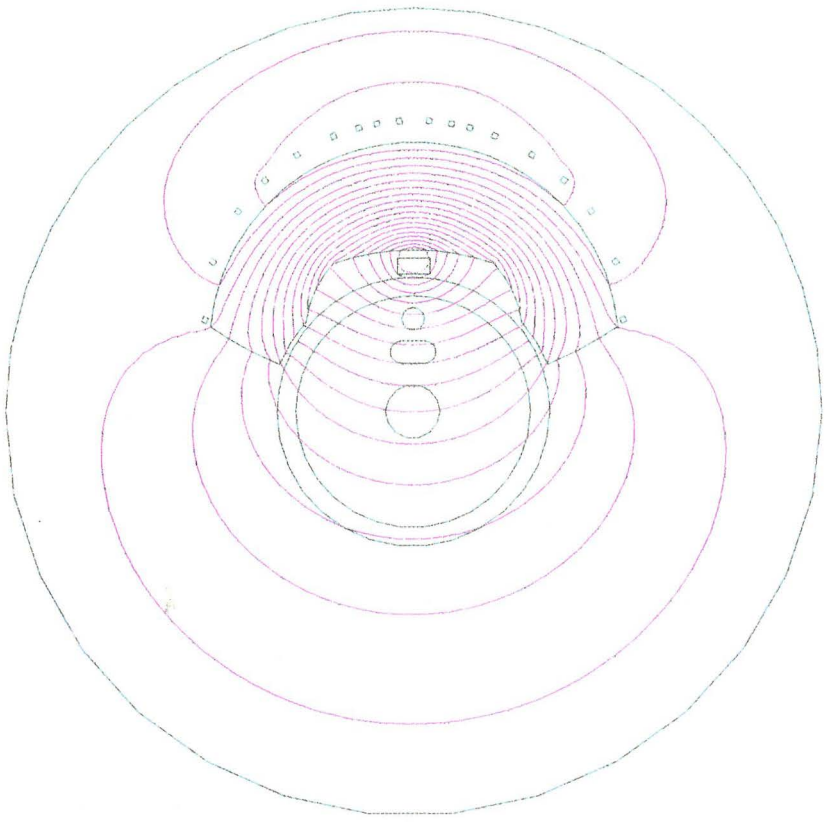

B at the center of the nerve is =0.1445 Tesla

B at the center of the bone is =0.06688 Tesla

Figure 3.13
The field lines for our ferromagnetic core coil with three sets of windings

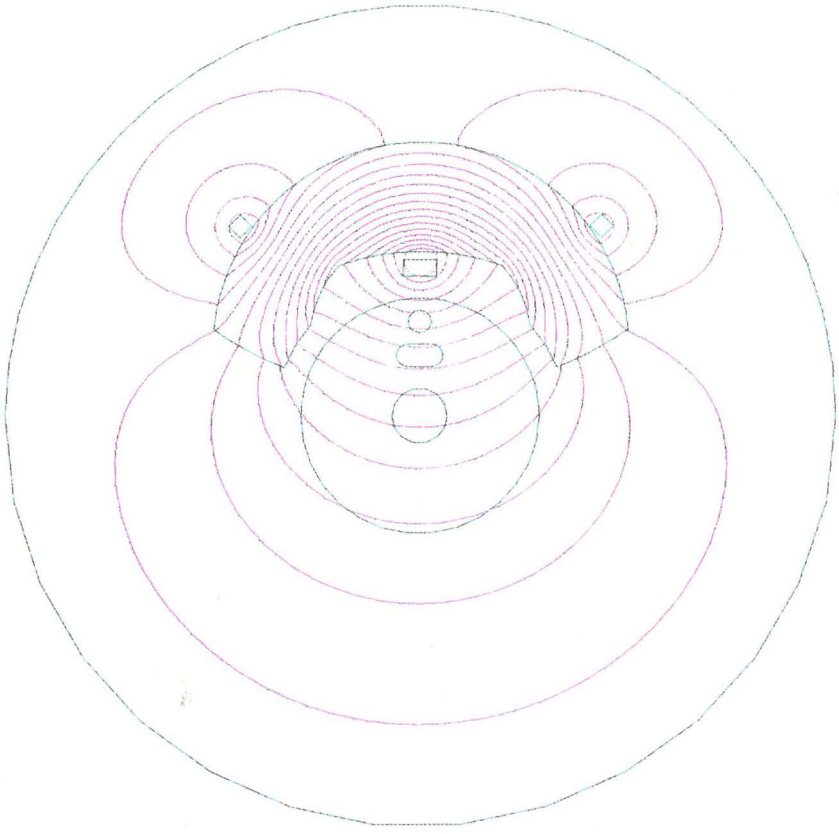

B at the center of the nerve is =0.1445 Tesla

B at the center of the bone is =0.06680 Tesla

Figure 3.14
The field lines for our magnetic core coil with two sets of concentrated windings

Chapter #4

Conclusion and Future Work

Over the last decade magnetic nerve stimulation has gained popularity as its clinical benefits became more realizable. Literature study conducted at the beginning of this work indicated that the main limitation of this technique was the lack of ability to focus the external magnetic field on the targeted nerve.

To overcome this deficiency, a novel coil design concept was proposed and investigated. Two distinctive coil designs, one with a non-magnetic core and the other with a special magnetic core, were developed for the purpose of this study.

In order to assess the technical merit of the proposed coil designs a detailed numerical analysis, based on the finite element method, has been carried out on a wide range of commercially available coil designs suggested by other researchers as well as on the proposed coil designs.

To carry out this analysis a commercial software package "Magnet" has been used. The assumptions made in connection with specifying the solution region, material properties, boundary conditions, the type of solver, and the interpretation of the results have been clearly outlined.

The main criteria used to perform a consistent comparison between the various coil designs has been developed.

Analysis of the results obtained from the numerical investigations for the various coil designs considered, clearly indicated that the coil designs proposed in this thesis provided

significant advantages in focusing the magnetic field on the targeted nerve (more specifically, the proposed coil design with Cobalt 50 core was determined to be the most attractive coil). This coil yielded a 130% better focusing than the best coil and configuration, reported in the literature, for magnetic nerve stimulation. In comparison to the figure "eight" coils, the proposed coil with a magnetic core provided 250% improvement in focusing the field on the targeted nerve.

The proposed coil design with a non-magnetic core was equivalent to the best commercial coil available for focusing the field on the targeted nerve. However, the non-magnetic core coil has 90% improvement in penetration depth. Comparing the non-magnetic core coil with the poorest commercial coil available, the field focusing in the targeted nerve was improved by 35% (see simulation results in chapter 3). Moreover, this coil design provided a mechanism to change the location of the maximum field intensity by adjusting the ratio of the current in the perpendicular coil relative to the horizontal coil. To achieve this functionality other researchers have to resort to using different coils having different degrees of physical curvature.

Based on the results of this work, it can be concluded that selection of the proposed coil with a magnetic core is obvious if cost is not a limiting parameter. In the event that the coil cost is prohibitive, the proposed coil with an non-magnetic core becomes the next best choice.

Future work

Thus far, the work in this project has been restricted to theoretical analysis, relying on computerized numerical simulations. Future work on this problem can be divided into three stages.

1. Constructing a Computer Model to solve this Problem using FEM in 3-Dimensions and for a Transient field.

   This stage has already been initiated as we have recently purchased an upgraded version of the software Magnet. This new version has the capability to handle 3-D problems and provides the option of a transient solver.

2. Testing the Proposed Coils in Clinical Applications.

   The proposed coils will be tested in Germany. We have an agreement with the University of Munich to use their testing facilities as we do not have access to such facilities in Canada.

3. Building a Stimulating Circuit that can be used to test the Proposed Coils.

   The guidelines and the main components required to build such a circuit are outlined in Appendix B.

REFERENCES

1. Jalinous, Reza, "Guide to Magnetic Stimulation", Jali Medical, Inc. 1996.

2. Weiss, Fischer Thomas, "Cellular Biophysics Electrical Properties", 1996

3. Maccabee, P.J., Amassion, V.E., Cracco, R.Q., Eberle, L.P., Rudeel, A.P., "Mechanisms of Peripheral Nervous System Stimulation Using the Magnetic Coil", Magnetic Motor Stimulation: Basic Principles and Clinical Experience (EEG Suppl. 43), Editors: W.J. Levy, R.O. Cracco, A.T. Barker, and J. Rothwell, 1991 Elsevier Science Publishers, B.V.

4. Barker, A.T., "Stimulation of Nerves and Muscles Using Large Pulsed Magnetic Fields", Department of Medical Physics and Clinical Engineering, Royal Hallamshire Hospital, Sheffield.

5. McRobbie, D., "Design and instrumentation of a magnetic nerve stimulator", The Institute of Physics, 1985.

6. Jalinous, R., Barker, A.T., Freeston, I.L., "The Design, Construction and Performance of a Magnetic Nerve Stimulator", Royal Hallamshire Hospital, Sheffield and University of Sheffield, UK.

7. Barker, A.T., Freeston, I.L., "Medical applications of electric and magnetic fields", Electronics and Power, October 1985.

8. Freeston, I.L., Barker, A.T., Jalinous, R., Polson, M.J.R., "Nerve Stimulation Using Magnetic Fields", IEEE Frontiers of Engineering and Computing in Health Care, 1984.

9. Stoehr, Hans Georg; May, Winfrid; Thoma, Herwig; "Multipurpose Implantable Nerve Stimulators", Bioengineering Laboratory, 2nd Surgical University Clinic, Vienna, Austria.

10. Barker, A.T.,and Lunt, M.J, "The Effects of Pulsed Magnetic Fields of the type used in the Simulation of Bone Fracture Healing", Clin. Phys. Physiol. Meas., 1983, 4, pp.1-27.

11. Coulton, L.A., Barker, A.T., Baldwin, J.A., Caine, M.W., "An Investigation of Some Claimed Biological Effects of Electromagnetic Fields", University of Sheffield, UK.

12. Hiwaki, O; Ueno, S; "Selective Magnetic Stimulation of the Spinal Cord", Annual International Conference of the IEEE Engineering Medicine and Biology Society, Vol 12, No 1, 1990.

13. Hosono, Akihiko; Andoh, Tomio; Goto, Tsuneaki; Kawakami, Tadashi; Okumura, Fukuichiro; Takayama, Kenichi; Takenaka, Toshifumi; Ueno, Shoogo; Yamaguchi, Masuhiro; Yamamoto, Isao, "Effective Combination of Stimulating Coils for Magnetic Heart Stimulation", Japan, Applied Physics, Vol 31, Part I, No 11, November 1992.

14. Mouchawar, GA., Nyenhuis, JA., Bourland, JD., Geddes, LA., "Guidelines for Energy-Efficient Coils: Coils Designed for Magnetic Stimulation of the Heart" Magnetic Motor Stimulation: Basic Principles and Clinical Experience (EEG Suppl. 43)

15. Maccabee, P.J.; Eberle, L; Amassian, R.Q.; Cracco, Rudel, A;, "Studies of 3-Dimensional Voltage Distributions Induced in Homogeneous Media Volume Conductors by Round and Butterfly Magnetic Coils", IEEE Engineering in Medicine and Biology Society 11th Annual International Conference, June 1989.

16. Knaulein, R; Weyh, Th.; "Minimization of Energy Stored in the Magnetic Field of Air Coils for Medical Application", Techinische Universitat, Munchen Germany, 1996.

17. Mouchawar, G.A.; Nyenhuis, J.A.; Bourland, J.D.; Geddes, L.A.; "Influence of Coil Geometry on Localization of the Induced Electric Field in Magnetic (Eddy-Current) Stimulation of Excitable Tissue", IEEE Transactions on Magnetics, Vol 26, No 5, September 1992.

18. Ren, Chunye; Tarjan, Peter; "Coil Design for Adjustable Magnetic Stimulation", IEEE, June 1994.

19. Ferguson, Stewart A.; Durand, Dominique; Dalbasti, T; "Optimization of Coil Design for Neuronal Excitation by Magnetic Stimulation", IEEE Engineering in Medicine and Biology Society 11th Annual International Conference, June 1989.

20. Cadwell, John, "Optimizing Magnetic Stimulator Design", Magnetic Motor Stimulation: Basic Principles and Clinical Experience (EEG Suppl. 43), Editors: W.J. Levy, R.O. Cracco, A.T. Barker, and J. Rothwell, 1991 Elsevier Science Publishers, B.V.

21. Amassian, Vahe E., Cracco, Roger Q., Maccabee, Paul J., Bigland-Ritchie, Brenda, Cracco, Joan B., "Matching Focal and Non-Focal Magnetic Coil Stimulation to Properties of Human Nervous System: Mapping Motor Unit Fields in Motor Cortex Contrasted with Altering Sequential Digit Movements by Premotor-SMA Stimulation", Magnetic Motor Stimulation: Basic Principles and Clincial Experience (EEG Suppl. 43)

22. Amassian, Vahe E., Cracco, Roger Q., Maccabee, Paul J., "Basic Mechanics of Magnetic Coil Excitation of Nervous System in Humans and Monkeys and their Applications", Special Symposium on Maturing Technologies and Emerging Horizons, 1988 IEEE

23. duBruin, Hilbert "Lecture Notes 4UA3", McMaster University, Hamilton Ontario, 1996.

24. Basser, PJ., Roth, BJ., "Stimulation of a myelinate nerve axon by electromagnetic induction", Medical and Biomedical Engineering & Computing, May 1991.

25. Bradley, Roth J., Basser, Peter J., "A Model of the Stimulation of a Nerve Fiber by Electromagnetic Induction", IEEE Transactions on Biomedical Engineering, Vol 37, No. 6, June 1990.

26. Roth, Bradley J., Cohen, Leonard G., Hallett, Mark., "The Electric Field Induced During Magnetic Stimulation", Magnetic Motor Stimulation: Basic Principles and Clinical Experience (EEG Suppl. 43)

27. Kraus, J.D., and Carver, K.R., "Electromagnetics", McGraw-Hill book company, New York, 1973.

28. Reilly, J.P., "Peripheral nerve stimulation by induced electric currents: exposure to time-varying magnetic fields", Medical and Biological Engineering and Computing, March 1989.

29. Xi, Weiguo; Stuchly, Maria; Gandhi, Om P.; "Induced Electric Currents in Models of Man and Rodents from 60 Hz Magnetic Fields", IEEE Transactions on Biomedical Engineering, Vol 41, No 11, November 1994.

30. Bren, Stephan P Albert, "60Hz EMF Health Effects -- A Scientific Uncertainty", IEEE Engineering in Medicine and Biology, July/August 1995.

31. Durand, Dominique, Ferguson, Stewart A; Dalbasti; "Induced Electric Fields by Magnetic Stimulation in Non-Homogeneous Conducting Media", IEEE Engineering in Medicine and Biology Society 11th Annual International Conference, 1989.

32. Davey, Kent R., Luo, Lanbo, "Calculation of Induced Electric Fields by Duality", IEEE Transactions on Magnetics, Vol. 30, No. 5, September 1994.

33. Carstensen, Edwin L, "Magnetic Fields and Cancer", IEEE Engineering in Medicine and Biology, July/August 1995.

34. Ueno, Shoogo; Harda, Koosuke; "Experimental Difficulties in Observing the Effects of Magnetic Fields on Biological and Chemical Processes", IEEE Transactions on Magnetics, Vol Mag-22, No 5, September 1996.

35. Lorenzen, H.W.; Weyh, Th.; "Practical Application of the Summation Method for3-D Static Magnetic Field Calculation of a Setup of Conductive and Ferromagnetic Material", IEEE Tranactions on Magnetics, Vol 28, No 2, March 1992.

36. Nagarajan, Srikantan S; Durand, Dominique, "Theoretical and Experimental Aspects of Magnetic Nerve Stimulation", Applied Neural Control Laboratory Department of Biomedical Engineering, Case Western Reserve University, Cleveland, OH 44106.

37. Durand, Dominique, Nagarajan, Srikantan, "Analysis of Magentic Stimulation of an Axon in a Nerve Bundle", IEEE Transactions on Biomedical Engineering, Vol 3, 1993. p. 1429 - 1430

38. Nakata, T., and Kawase, Y., "Numerical Analysis of Nonlinear Transient Magnetic Field using the Finite Element Method", Electrical Engineering in Japan, Vol 104, No. 4, 1984.

39. Mouchawar, G.A.; Nyenhuis, J.A.; Bourland, J.D.; Geddes, L.A.; Schaefer, D.L.; Riehl, M.E.; "Magnetic Stimulation of Excitable Tissue: Calculation of Induced Eddy-Currents with a Three-Dimensional Finite-Element Model", IEEE Transactions on Magnetics, Vol 29, No 6, November 1993.

40. Eaton, H.; "Electric field induced in a spherical volume conductor from arbitrary coils: application to magnetic stimulation and MEG", Medical & Biological Engineering & Computing, July 1992.

41. Wang, Weiping, Eisenberg, Solomon R., "A Three-Dimensional Finite Element Method for Computing Magnetically Induced Currents in Tissues", IEEE Transactions on Magnetics, Vol 30, No. 6, November 1994.

42. Nagarajan, Srikantan S, Durand, Dominique, "Determination of Excitation Sites During Magnetic Stimulation of Nerve Fibres", Applied Neural Control Laboratory Department of Biomedical Engineering, Case Western Reserve University, Cleveland, OH 44106.

43. Winkel, Henrik; Jennum, Poul M.D.; "Compound Motor Action Potentials generated by Repetitive Magnetic Stimulation", IEEE February 1992.

44. Reuter, Christopher, Battocletti, Joseph, Myklebust, Joel, Maiman, Dennis; "Magnetic Stimulation of Peripheral Nerves", IEEE Engineering in Medicine & Biology Society 10th Annual International Conference, 1988.

45. Babb, Christopher, Coon, David, Rechnitz, Garry, "Biomagnetic Neurosensors. 3. Noninvasive Sensors Using Magnetic Stimulation and Biomagnetic Detection", Analytical Chemistry, Vol 67, No. 4, February 15, 1995.

46. Esselle, Karu P., Stuchly, Maria A., "Cylindrical Tissue Model for Magnetic Field Stimulation of Neurons: Effects of Coil Geometry", IEEE Transactions on Biomedical Engineering, Vol 42, No. 9, September 1995.

47. Hayt, A. Jr., "Engineering Electromagnetics", Third Edition, McGraw-Hill Book Company, New York, 1974.

48. Stratton, A.J, "Electromagnetic Theory", McGraw-Hill Book Company, New York, 1941.

49. Zienkiewwicz, O.C., Kelly, D.W., and Bettess, P., "The Coupling of the Finite Element Method and Boundary Solution Procedures", International Journal for Numerical Methods in Engineering., Vol. 11, 1977.

50. Cristina, S., and DiNapoli, A., "Combination of Finite and Boundary Elements for Magnetic Field Analysis", IEEE Trans. on Magnetics, Vol MAG - 19, No. 6, Nov 1983.

51. Smith, G.D., "Numerical Solution of Partial Differential equations", Oxford University Press, 1965.

52. Dableh, Youssef Hanna, "A Novel Electromagnetic Technique for Remote Repositioning of Coolant Tube Spacers in Candu Nuclear Reactors", A Phd. Thesis, McMaster University, April 1986.

53. Silvester, P., and Ferrari, R.L., "Finite Elements of Electrical Engineers", Cambridge University Press, Cambridge, 1983.

54. Chari, M.V.K., amd Silvester, P.P., "Finite Elements in Electrical and Magnetic Field Problems", John Wiley and Sons, 1980.

55. Zienkiwwicz, O.C., "The Finite Element Method", McGraw-Hill Book Company, 1977.

56. Infolytica Corporation, "Magnet 5.1a User manual", © Copyright Infolytica Corporation, Part Number 5T0302, Revised November 4, 1994

57. Wolf, Erich W, Walker, Cedric F, "Design and Practical Consideration in the Construction of Magnetic Induction Stimulators", Annual International Conference of the IEEE Engineering in Medicine and Biology Society, Vol 13, No 2, 1991.

58. Lui, J.L., Faust, U., "Theorical Considerations on Coil Design For Magnetic Stimulation", IEEE 1993.

59. Ren, Chunye; Tarjan, Peter; Popovic, Dejan D.; "A Novel Electric Design for Electromagnetic Stimulation -- The Slinky Coil", IEEE Transactions on Biomedical Engineering, Vol 42, No 9, September 1995.

60. Agur, Anne M.R., Lee, Ming J., "Grant's Atlas of Anatomy", Ninth Edition, Williams & Wilkins, pp. 362 - 365 and pp. 441 - 442.

61. Williams, Peter L., Warwick, Roger, "Gray's Anatomy", Churchill Livingstone, 1980, pp. 702 - 706.

62. Fuks, Luiz Felipe; Cheney, Margaret; Isacson, David; Gisser, David G.; Newell, J.C.; "Detection and Imaging of Electric Conductivity and Permittivity at Low Frequency", IEEE Transactions on Biomedical Engineering, Vol 38, No 11, November 1991.

63. Cracco, Roger Q., Amassian Vahe E., Maccabee Paul J., Cracco, Joan B., "Excitatory and Inhibitory Effects of Magnetic Coil Stimulation of Human Cortex", New Trends and Advanced Techniques in Clinical Neurophysiology (EEG Auppl. 41)

64. Reilly, JP., "Magnetic field excitation of peripheral nerves and the heart: a comparision of thresholds", Medical & Biomedical Engineering & Computing, November 1991.

65. Sgro, Joseph, Stanton, Paul, Emerson, Ronald, "Theoretical and Practical Performance of Magnetic Stimulators and Coils", Magnetic Motor Stimulation: Basic Principles and Clinical Experience (EEG Suppl. 43)

66. Bozorth, M., Richard "Ferromagnetism ", 4th edition,@1951, by D. VAN NOSTRAND COMPANy, Inc. (Canada), Ltd.

67. DeMaw, "Doug", M.F., "Ferromagnetic-Core Design Application & Handbook", @1981 by Prentice-Hall, Inc., Englewood Cliffs, N.J. 07632.

68. Schmid, M., Weyh, T., Meyer, B.-U., "Development, Optimization and Testing of New Devices for Magnetomotive Nerve Fibre Stimulation", Biomed. Technik, Vol. 38, 1993, p. 317 - 324.

69. Ravazzani, P., Ruohonen, Grandori, "Magnetic stimulation of peripheral nerves: computation of the induced electric field in a cylinder-like structure", Advances in Engineering Software 22 (195) 29 - 35, 1995 Elsevier Science Limited, Printed in Great Britain, All rights reserved.

70. Chemeris, V.T., and Podol Tsev, A.D., "A Study of The Magnetic-pulse Interaction of Moving Conductive Bodies in the Presence of a Ferromagnetic Medium (MU=CONST)", TEKH Electrodin. (USSR), No. 1, Jan - Feb 1980.

71. Geddes, L.A., "Stimulation of Excitable Tissue with Time Varying Magnetic Fields", IEEE Engineering in Medicine & Biology Society 10th Annual International Conference, 1988.

72. Barker, Anthony T, Garnham, Carolyn W, Freeston, Ian L, "Magnetic Nerve Stimulation: the Effect of Waveform on Efficiency, Determination of Neural Membrane Time Constants and the Measurement of Stimulator Output", Magnetic Motor Stimulation: Basic Principles and Clinical Experience (EEG Suppl. 43), Editors: W.J. Levy, R.O. Cracco, A.T. Barker, and J. Rothwell, 1991 Elsevier Science Publishers, B.V.

73. Mullin, W.F., "ABC's of Capacitors" 3rd Edition Indianapolis: Sams, 1980.

74. Yarita, Masaru; Hosaka, Hidehiro; Ueno, Shoogo; "Reduction of Acoustic noise and Leakage fields in Magnetic stimulation by using a Coaxial cable", IEEE, June 1994.

75. Schmid, M., Weyh, T., Meyer, B.-U., "High - Performance Biopotential Amplifier for Electrophysiological Research that needs special safety requirements", Biomed Technik, Vol. 39, 1994, p. 279 - 286.

APPENDIX A

Design Considerations and Guidelines for the Proposed Coils

As stated in Chapter 1, the following design considerations and procedure are presented as a reference for future work to ensure that the constructed coils can survive the intense electromagnetic forces and stresses. Also, the magnetic saturation and losses issues have to be carefully considered in the case where a magnetic core is used. This Appendix covers the most critical design elements that have significant influences in this particular application.

A.1 Coil Conductor

A.1.1. Conductor Material

When deciding upon the material for the coil, a balance between two important factors should be considered: electrical conductivity and mechanical strength. A material with high electrical conductivity normally has poor mechanical strength, ie: copper. On the other hand, a material that has high mechanical strength normally has lower electrical conductivity, ie: steel. The ratio between the *dc* resistance of a coil made of copper relative to the same coil made of steel is approximately 1 to 10. As shown in Appendix B, maintaining low resistance is a very important factor when designing a coil.

The conductor we recommend for the coil is a solid, square copper wire (size 12) which has a low resistance (approximately 8 to 10 mΩ/m *dc* resistance). A square wire lends itself to be tightly packed into a small space with a maximum number of turns. The resultant current density at the joint using a square wire is higher than using a circular wire. As a result, the

current density in the centre of the coil will be the highest, and consequently, the amount of the induced current in the targeted nerve will be higher. The disadvantages of using a solid square wire are: the skin effect because of the circuit frequency, and the heat accumulation in the "packed" portion of the coil.

A.1.2. Conductor Layout

The conductor layout affects the magnetic field shape and distribution. It forms the field spatial pattern while its distribution contributes to the intensity of the field. Various arrangements and layouts for the conductors results in different field shapes and intensities. For magnetic nerve stimulation, we need to have an intense, focussed field that penetrates to deep nerves. This can be achieved by concentrating the coil conductors over the targeted nerve at one side, while uniformly (or non-uniformly) distributing them on the other side of the coil.

In our coil, the shape and layout for the conductors resembles a "slinky" toy. We decided to concentrate the field through a distributed coil such that the internal coil sides (next to the skin) were compressed, while the external coil sides were widely distributed. We used two sets of windings in either side. A third set of windings is positioned perpendicularly to these side coils, with one of its sides close to the joint of the others while its other side is positioned 180° from the joint (see figure 1.5).

A.1.3. Size of the Coil

The stored energy in the coil is a function of effective coil length, flux area, current and the permeability of the core material. A coil which stores more energy may be used to stimulate

large organs (heart) [13,14], whereas a coil that stores less energy can be used to stimulate small regions (nerves) [63,64]. Also, a coil with a large diameter has a more uniform field than one with a small diameter. However, a coil with a small diameter and a relatively high current creates a higher flux density that penetrates only the region close to the surface of the skin. The above discussion is also applicable to a pair of joined coils ("eight" shape or "butterfly" coils) [14,21,22,63-65].

As our coil is intended for stimulating peripheral nerves over different parts of the body, more than one coil size must be constructed for varying depths of nerve stimulation. The coil can be represented as a section of a toroid with an inner and outer diameter. The general shape for the different coil sizes remains the same. However, adjustments are needed to accommodate the required coil geometry. Varying the coil size to cover different stimulating areas is a costly venture. Nevertheless, it can be justified if effective stimulation results.

A.1.4. Number of turns and the spacing between the turns

It is crucial to keep a balance between the coil inductance and the coil current as the inductance (reactance) dominates the value of the current within the circuit. Therefore, to maintain a precise level for the magnetic field strength it is essential to choose the number of turns carefully as the field strength is proportional to the square of this number.

The space between the turns will depend on the size of the core, the number of the turns, the diameter of the coil and the wire size and shape. The total coil turns we suggest is 27 turns (9 turns for each coil). From the computer simulations this number generated the required field strength, and provided an acceptable current density distribution through the coil turns. To

maintain fixed spacing between the turns on the distributed side, grooves were etched into the circumference of the plastic casing, with each groove containing one turn.

A.2. Core of the Coil

From the research conducted, we concluded that air core coils are the predominate coils used in magnetic nerve stimulation. A high flux density (2 Tesla), and relatively high operating frequency (1.5-2.5 kHz) are needed to obtain effective stimulation. Commonly used magnetic materials saturate in the range of 1.2-1.4 Telsa and suffer sever magnetic losses as the frequency increases. In order to introduce a magnetic core, one has to resort to special purpose material that saturates at 2 Telsa or above and has acceptable losses at the operating frequency mentioned above.

Investigation of available special magnetic material led us to select a Cobalt alloy[1]. The Cobalt alloys B-H curves reach high flux densities (2 Tesla) for relatively low coercive forces (0.2 - 1 A\m). Also, when we examined the mechanical characteristics for the Cobalt alloy, we discovered that these alloys can be manufactured in extremely thin strips (as low as 12.5 μm). Consequently, this will minimize the eddy current losses tremendously.

Using a ferromagnetic core for the coil will result in an increase in the coil inductance. The higher inductance will result in a reduction for the coil current and rise time. Consequently, more energy is required to obtain effective stimulation. However, this is a small penalty considering the realized advantages in focussing the field.

---

[1]The characteristics of the selected Cobalt alloys are presented in reference [64,65] as well as manufacturer data sheets (VacuumSchumelze). These data sheets are attached at the end of this Appendix.

The proposed ferromagnetic material to be used for the coil is Cobalt 50 which is an alloy that consists of 49% Cobalt, 49% Iron and 2% Vanadium. This material can be purchased under the name of Vacoflux 50 from a company called VaccumSchumelze in Germany. The data sheets for Vacoflux 50 are shown in the attached data sheet. These sheets illustrate the material B-H curve, the relation between the material thickness versus losses, and the relation between the operating frequency versus the material losses. The data sheets for the Vacoflux 50 indicate the reason for choosing such a material as a core for the coil. For instant, the flux density in the linear region reaches 1.95 Tesla., and its losses are acceptable relative to our circuit operating frequency.

This material was the first proposed choice for the core, however, after contacting VacuumSchumelze we discovered that they manufacture two other materials that are superior to Vacoflux 50 in terms of their characteristics relative to the core requirements. These materials are Vacoflux 48 and Vacoflux Z, the data sheets for these materials are attached to this Appendix.

The characteristics for Vacoflux 48 are better than Vacoflux 50 regarding the coercive forces (lower) which results in lower losses for the same volume. Vacoflux Z has the lowest coercive forces of the three materials for the same magnetic flux density which makes its losses the lowest of all three materials. The other fascinating feature about Vacoflux Z is that the hysteresis losses are in a sharp rectangular shape (refer to the data sheets). This makes the switching of this material fast enough to accommodate high frequency applications.[2]

---

[2] The manufacturer was able to achieve the low losses (narrow, sharp hysteresis loop) by applying a magnetic field during the heat treatment of Vacoflux Z.

The obstacle in using these materials is their cost ($300.00 per pound for Vacoflux 48 and 50) which means the raw material for our core will cost approximately $1,500.00. Additional costs are incurred for the slicing, machining, and heat treatment of the core to complete the fabrication process. On the other hand, Vacoflux Z costs approximately 5 times that of the other two materials depending on the complexity of the core. This increased cost is attributed to the sophisticated procedure needed to manufacture a core which can only be done by material manufacturer (VacuumSchumelze).

A.2.1. Core Shape and Geometry

To achieve effective stimulation the targeted nerve should be enclosed within the path of the magnetic lines. This path is defined by the conductor layout and core geometry. When using an air core coil the field distribution is defined only by the geometrical layout of the conductors, however, when using a ferromagnetic core coil, the shape of the core contributes to the field distribution as well. This provides more flexibility and control in defining the shape of the required field. The shape of the core determines the path for the field spatial distribution. Therefore, the geometry of the core plays an important role in determining the effectiveness of stimulation.

In determining the geometry for the coil core, the simulation results generated by the software Magnet were used. The simulations showed that our proposed core shape provides the required path for the field which is needed to effectively penetrate the tissue and enclose the targeted nerve.

A.2.2 Core Fabrication

The core fabrication is a process of constructing the required shape and size for the core. This process involves slicing, laminating, heat treating, machining, and assembling the material (which can come in various forms) supplied by the manufacturer.

After considering the type of material for the core, we must then decide on the dimensions of the material. From the geometry and shape of the core we decide the material length and width while the thickness is determined according to the operating frequency in our circuit. The thickness of the material represents the primary factor affecting the core losses and the fabrication procedure. For materials with a thickness less than 200 μm, high precision tools are needed to obtain the required shape.

Lamination is the next step in fabrication. This requires 'dipping" the slices into a pool of Mgo (Magnesium oxide). The Mgo coating increases the resistivity of the slices which reduces the path of the circulating eddy currents within the core. In other words, lamination will help in reducing the core losses.

The following step depends on the method chosen to construct the core. If we chose to construct the core from a "toroid" shape, then the slices must be rolled to form a "toroid". If we chose to construct the core by "layering" the slices, then we use the punching technique where the slices are punched through a "die" and the resulting pieces will be laid out together. As the air gap in our coil is large, it is not feasible to construct the core from a toroid because of high eddy current losses. The alternative is to use the punching technique. Regardless of the cutting method, the structure of the core must be firm and solid before sending it for heat treatment.

The heat treatment is a very delicate and important procedure as it represents the step to

restore the magnetic characteristics of the material[3]. The core must be cooled immediately after the heat treatment. The cooling factor, which is the rate of cooling over a certain period of time (C°/s) will effect the core losses.

The assembly stage is the most important part of the core fabrication. This is a very delicate step which requires the use of precision tools along with machining experience with such materials. Depending on the core shape, this procedure might include different steps in machining, cutting, etching and polishing. Using an exotic magnetic material like the Cobalt 50 means we are dealing with a material which is very sensitive to mechanical stresses. Any mechanical stresses applied can result in permanent damage to the core.

In this study Vacoflux 50 was used (we would have used Vacoflux 48 because of its low losses however, it was not available in the thickness we needed). The sheet thickness was 100 μm. The first step in the core fabrication is to determine the dimensions of the core. According to our simulation, we decided the dimensions of our core to be 15 cm length, 10 cm width and a thickness of 2.5 cm. Consequently, the material we ordered was 110 mm tape to minimize the slicing cost and wastage Figure A.1 shows a projection for the final shape of the coil core. It shows that the dimensions result in minimum waste to achieve the required core.

The laminating process can be done by dipping the pieces (after dicing) into a pool of Mgo. This step adds a coat with a thickness of 10 μm to each piece. Considering the additional thickness and the stack factor (see the data sheets) for the coil, the final stack factor will be 0.9. This value depends on how tightly the pieces are compressed.

---

[3]The fabrication rules outlined by the core manufacturer were followed precisely, these rules can be found in the material manufacturer data sheet.

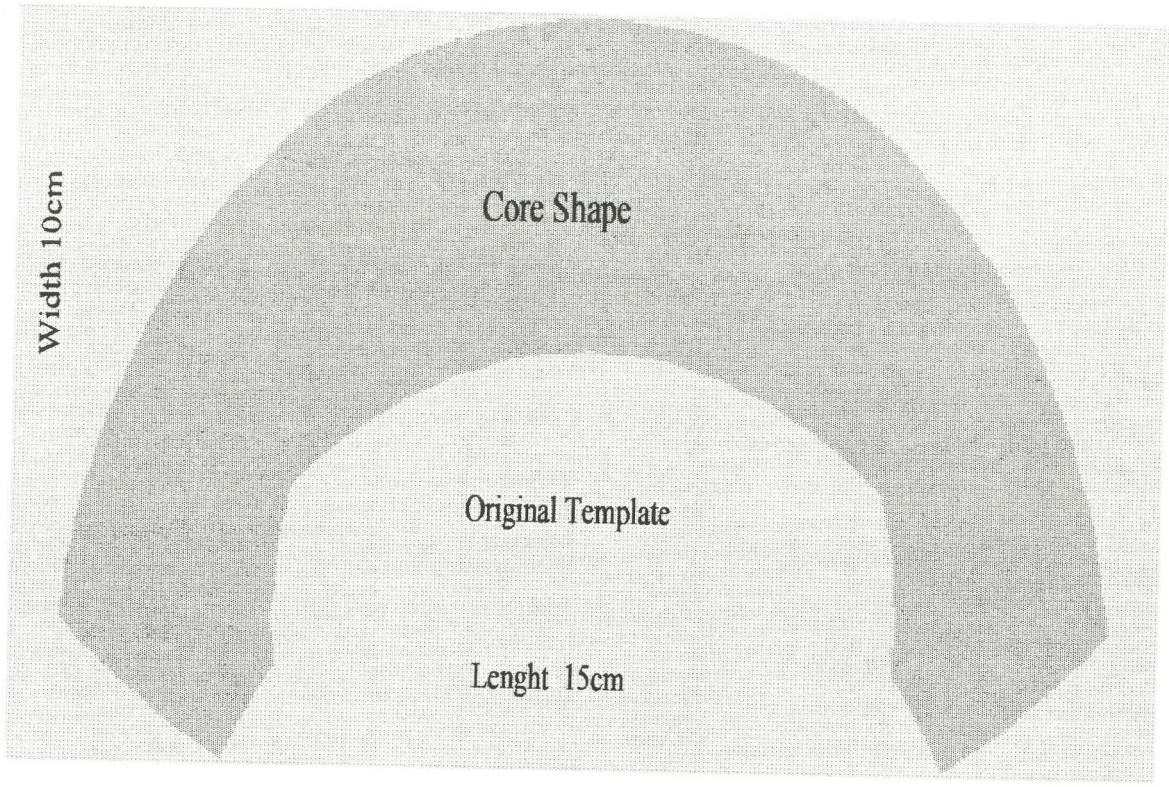

Figure A.1
A projection for the final shape of the coil core.

The heat treatment and the cooling processes were followed according to the manufacturer data sheets. [4]

The final stage of our coil fabrication is the assembly procedure. This step involves carving the plastic casing according to the core shape, and then embedding the core into the casing. This completes the coil fabrication procedure.

---

[4]The laminating, heat treating, cooling, and cutting procedures were done locally at BCL Company in Burlington, Ontario. As BCL Company is interested in this topic, they provided these services complementary.

A.3. Safety Issues

The safety issue for magnetic stimulation for both operator and patient is a very important concept as this application operates with a high power level. As the coil is in direct contact with the patient, safety is a primary issue to address when designing the coil. Design criteria are required to meet maximum electrical safety standards to prevent electrical shocks.

Mechanical safety is important to minimize any hazards in case of coil failure or capacitor malfunctioning. Other important safety issues have been documented by John Cadwell[20].

To cover both mechanical and electrical safety aspects for our coil design, it is recommended to consider the following procedure.

A Teflon tape was wrapped around the conductor to increase the insulation and absorb the mechanical vibrations. These vibrations result from the forces that occur between the windings because of the high currents passing through them over a short period of time.

Once the coil was wound, it was dipped into a pool of varnish. This is a corrective measure to restore the conductor insulation as cracks can form due to the mechanical stresses during the winding procedure. The dipping process fills the existing cracks and prevents the possibility of current leakage.

After the insulation has cured, high voltage tests were run on the windings to determine the integrity of the insulator. The testing voltage was four times the intended operating voltage. This test provided assurance for the integrity of the coil insulation.

A.4. Other Considerations

A.4.1. Mechanical Considerations

As magnetic stimulating coils provide rapidly changing magnetic fields, the coil conductors may be subjected to enormous forces for the duration of the current pulse [52]. A high discharge current over a very short period of time results in a force that may be strong enough to cause permanent damage to the coil or even destroy it. A proper coil design must ensure that these forces do not compromised the mechanical integrity of the coil. This can be accomplished by limiting the generated magnetic field so that the exerted stress is less than the yield strength of the conducting material or by providing a support structure that can withstand the forces. In practice, the Lorentz forces exerted on the conductors limit the maximal pulse that can be generated.

In a multi-turn coil, the total force exerted on each turn consists of two components; the first is the self-induced force and the second arises from the magnetic field generated by the other turns. Geddes et al., [14] have a detailed outline for calculating the forces exerted on the coil turn for different types of coils.

The primary indicator of the mechanical forces are cracks on the conductor insulation. The impact of these forces depends on the number of times the coil is used, and on the peak value of the pulsating currents. Special consideration should be given to the type of insulation applied to the conductor. The insulation should be able to withstand these stresses to ensure the coil longevity.

We have considered the effect of the mechanical forces and created grooves in the casing to embed the windings so that they can withstand these forces. Also, to further reduce the effect

of the mechanical forces, we have tightly wound the coil conductors to limit their movement (as a result of vibration).

A.4.2. Electrical Insulations

The conductor insulation material must be selected carefully as it should provide high electrical insulation and high thermal conductivity. When considering an insulator for the conductors we should choose the kind of insulator that can withstand the high rate of change in current and voltage. It should also withstand the heat build up especially when the conductors are close to each other. For these reasons, a special insulated tape is suggested. This kind of tape has a guard electrode around it which will conduct and detect when a breakdown in the insulation occurs. This detection will prevent exposing the patient or the operator to electric shock hazards. We did not use this tape however, the type of insulator we used for our coil conductor is B type. This insulator can withstand the required performance expected from the coil.

A.4.3. Thermal Considerations

In general, the pulses used in magnetic stimulation are for a short period of time which generates a minimum amount of heat. The discharged energy from the capacitors results in heat accumulation within the coil windings. This heat will accumulate based on the number of times that we repeat the stimulation. This is one of the limitations in using a repetitive procedure in magnetic stimulation. Therefore, thermal considerations are important in the design of the coil. The heat accumulation is also dependent on the coil resistance, the spacing between the

windings, the thermal conductivity of the insulator, and the peak value of the coil current. One approach to reduce the temperature can be achieved with the use of an epoxy resin mixed with a heat sink compound. This mix will improve the coil thermal conductivity and enhance the heat transfer from the coils' surface to the surrounding space. An interesting method to reduce the heat accumulation problem was accomplished by Schmidt et al [68]. They designed a coil that can be used for repetitive stimulation at a high rate. It was achieved by introducing a conductor for the coil in the form of "tape". This increased the coil surface area which resulted in an increase in the heat dissipation.

To monitor the heat accumulation, a thermal sensor should be built into the coil. This sensor will shut down the coil if the coil temperature exceeds the specified limits.

For our coil, we did not stress all the above issues for thermal considerations, as we will not use the coil for repetitive stimulation. However, for the purpose of developing a standard coil, we embedded thermal sensors in different spots to collect the variation in temperature for the windings throughout the experimental process.

A.4.4. The Coil Leads

The coil leads represent the interface between the coil ends and the stimulating circuit. The leads are an integral part of the coil which should have the same dimensions as the coil conductors on one end and the circuit conductors on the other end. In order to maintain low resistance for our circuit special considerations should be taken in the design of the leads that interface between the coil ends and the circuit. The leads should have a reliable mechanical structure, provide easy access to change coils and add a minimum amount of resistance to the

circuit. By applying leads with the above characteristics, welding the coil to the circuit is not necessary, instead we can mechanically attach it to the circuit.

The leads that we used for our coil were made of copper insulated with Teflon. The leads were constructed from a 7 cm long plate of copper with a width of 2 cm and a thickness of ½ cm. On one end there is a square groove in the centre of the lead and on the other end there is a circular groove in the centre of the lead. Figure A.2 illustrates the shape and construction of the leads for our coil.

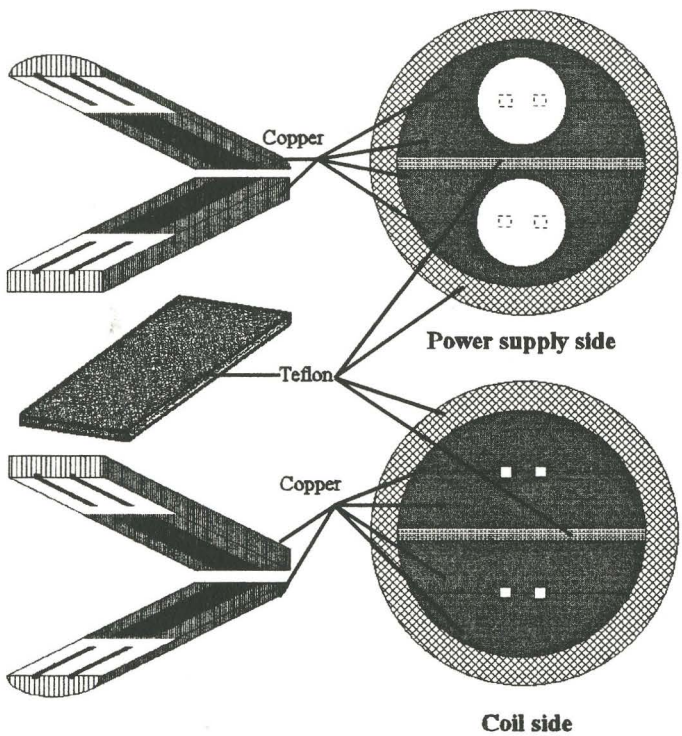

Figure A.2
The coil leads

A.4.5. Coil Position and Orientation

One other parameter that determines the effectiveness of the coil performance is the coil orientation relative to the targeted nerve. The coil position is a very important factor in the stimulation process. In general, we desire the coil to produce the largest charge injection for a certain pulse width. The factors that affect the total charge relative to the coil position are:

1. The distance between the coil and the excited nerve.
2. The angular position of the coil relative to the nerve.
3. The position of the nerve relative to the closed path of the magnetic field generated by the coil.
4. The orientation of the coil relative to the nerve ie: whether it is along side or transverse.

Thorough research has been conducted regarding the coil position and orientation relative to the nerve [17,21,22,69]. The conclusion of these researches is by adjusting the coil orientation and displacement angle, different types of nerve stimulation can be achieved. We have considered this aspect in the design of our coil, specifically by adding the third coil and varying the supply currents between the three coils.

4. Magnetic Properties

The typical magnetic properties of VACOFLUX after optimum final annealing are given in Table 2. Figs. 1 to 3 show the initial magnetization curves and the core losses versus excitation. The core losses were measured with flux density being almost sinusoidal. Fig. 4 shows the temperature dependence of the saturation polarization.

Table 2 **Typical Properties of VACOFLUX 50, VACOFLUX 48 and VACOFLUX Z after Optimum Final Annealing**

Property		VACOFLUX 50		VACOFLUX 48	VACOFLUX Z
		(material not reworked)	(material reworked)		
Coercivity H_c	A/cm	1.6	1	0.3	0.2
Permeability μ_4		1000	1000	1200	
Permeability $\mu_{max.}$		8000	12000	20000	40000
Flux density at: $H = 3$ A/cm	T	1.6	1.8	2.0	2.1
$H = 10$ A/cm	T	2.0	2.05	2.1	2.2
Saturation polarization J_s	T	2.35			
Curie temperature T_c	°C	950			
Magnetostriction λ_s	10^{-6}	+70			

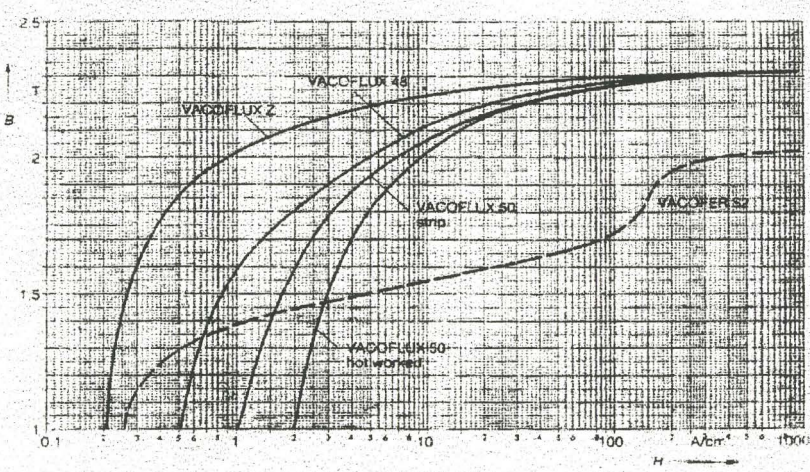

Fig. 1 Typical Magnetization Curves of VACOFLUX. Pure iron (VACOFER® S2) for comparison.

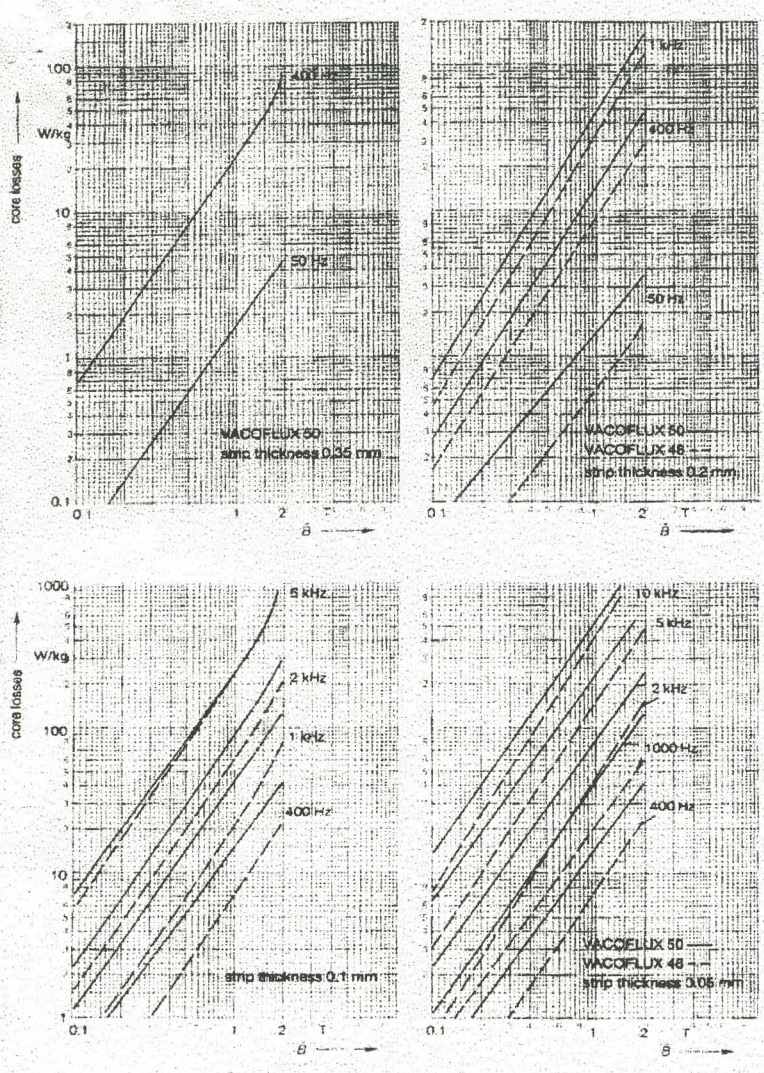

Fig. 2 Core losses of VACOFLUX, different strip thicknesses.

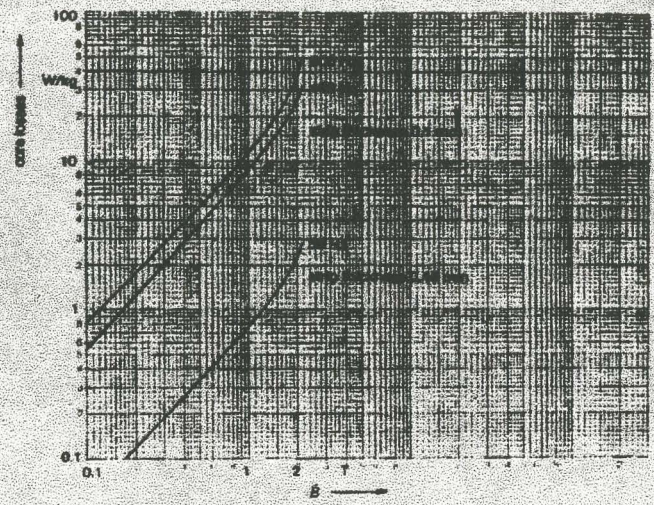

Fig. 3 Core losses of VACOFLUX 2.

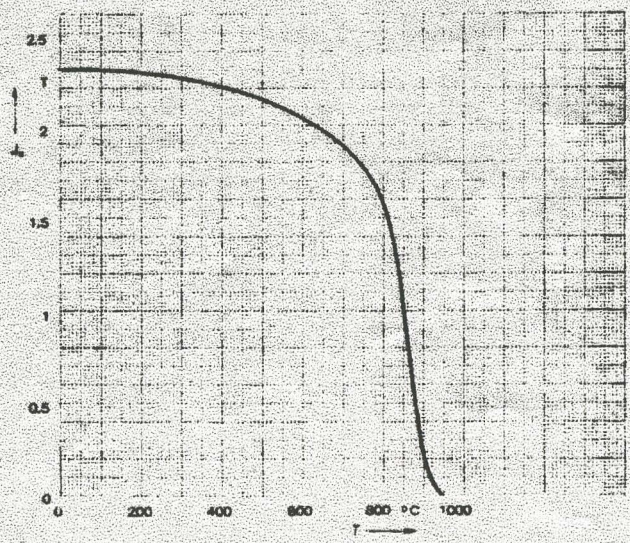

Fig. 4 Temperature dependence of saturation polarization J_s of VACOFLUX.

Physical Properties of VACOFLUX 50 and VACOFLUX 48 (guidance values)

Density		g/cm³	8.15	8.15	8.15
Hardness	*HV*	hard annealed *)	270 250	350 220	300 200
Yield strength	$R_{p\,0.2}$	hard annealed *)	N/mm² N/mm²	250 300	1000 300	600 200
Tensile strength	R_m	hard annealed *)	N/mm² N/mm²	300 400	1000 500	900 300
Elongation	A_{L50}	hard annealed *)	% %	0.5 1	1 4	2 6
Young's modulus		hard annealed *)	kN/mm² kN/mm²	– 200	220 200	210 200
Coefficient of expansion (20–200 °C)			1/K	$9.5\ 10^{-6}$		
Thermal conductivity			W/K m	30		

*) magnetically field annealed

Table 4 Magnetic Qualities of VACOFLUX 50, VACOFLUX 48 and VACOFLUX Z (standard quality)

Material	Form of Supply		Test Values
VACOFLUX 50	Strip 0.05–1.5 mm	V-050	$H_c \leq 1.6$ A/cm $B \geq 1.7$ T ($H = 3$ A/cm) ≥ 2.0 T ($H = 10$ A/cm)
	Telephone diaphragms	V-051	$\hat{B} \geq 1.5$ T ($f = 50$ Hz, $\hat{H} = 4$ A/cm) $HV = 200–250$
	Telephone diaphragms	V-052	$HV = 250–350$ or $HV = 350–410$
	Bulk material	V-090	$H_c \leq 2.4$ A/cm $B \geq 1.95$ T ($H = 10$ A/cm)
VACOFLUX 48	Strip 0.05–0.3 mm	V-055	$H_c \leq 0.4$ A/cm (0.1–0.3 mm) $H_c \leq 0.6$ A/cm (< 0.1 mm)
	EK cores	V-065	A_L values for glued cores
	EK cores	V-075	P (2 T / 50 Hz) ≤ 5 W/kg P (1.8 T / 400 Hz) ≤ 50 W/kg
VACOFLUX Z	Toroidal strip-wound cores	VZ-001	$\hat{B} = 2$ T at $\hat{H} \leq 0.76$ A/cm; $f = 50$ Hz strip thickness: 0.05–0.15 mm $\hat{B} = 2$ T at $\hat{H} \leq 1.4$ A/cm; $f = 50$ Hz strip thickness: 0.03 mm
VACOFLUX 48 S	Moulded sintered parts	VS-090	$H_c \leq 1.2$ A/cm

APPENDIX B

Circuit Design Considerations

The circuit current waveform is the most crucial parameter that should be taken into consideration when designing a stimulating circuit. This is because the current induced in an excitable tissue is linearly proportional to the first time derivative of the flux produced by the current in the excitation coil. The shape of the current in the coil depends on the relation between the inductance (L) of the coil, the capacitance (C) and the total resistance (R) of the discharged circuit.When designing a stimulating circuit there are many factors that must be taken into account. Some of these factors are summarized as follows.

B.1 The effect of R, C, L on the pulsating current magnitude and frequency

The basic concept of nerve excitation is to initiate and sustain a current through a stimulating coil located close to a nerve. This current should have sufficient magnitude and be within a certain frequency range to achieve the required stimulation. The current magnitude is limited by the stimulating circuit components, while its frequency is defined by the nerve depolarization time [1]. The peak value of the current is determined mainly by the capacitor initial voltage and the coil inductance. The duration of the current is determined by the inductance of the coil and the capacitor bank, while the damping rate is determined by the coil inductance and the equivalent circuit resistance.

---

[1]The depolarization time for peripheral nerve is between 100 μsec-1msec.[28] Therefore, the circuit frequency, which is the inverse of time, is 1kHz - 10 kHz.

Of the three components, L_c (coil inductance) can not be changed as its value is predetermined by the coil design. The value of the coil inductance determines the peak value of the pulsating current and the amount of energy stored within the coil. An extremely large inductance reduces the coil current which results in an insufficient induced current within the nerve. On the other hand, an extremely small inductance (despite the high pulsating current passing through it) will not stimulate a nerve as its stored energy is inefficient for triggering. Therefore, we should balance the value of the coil inductance as a part of the circuit design to achieve the required stimulation.

The equivalent circuit resistance (R) is the combination of resistance for the coil, connectors, switching devices and the cables that link the capacitor bank to the coil. In order for the circuit to generate the desired high pulsating current, the equivalent resistance should be maintained low which results in minimum losses and less heat generated within the circuit.

To maintain a low equivalent resistance we will analyze the effect of the resistance for the coil and the stimulating circuit separately. The coil resistance (which includes the wires and the leads) has a fixed value defined by the coil design. Therefore, to reduce the circuit resistance we should focus on the other elements (which includes connectors, capacitors, switching devices, and cables) that comprise the total resistance. The connectors should be made of copper which is the most practical material with the lowest resistance. The capacitor should have a low internal resistance which in turn adds a negligible amount to the circuit resistance. The type of switching device and its mode of connection could have an important role in minimizing the total resistance. For example, if a sharp current decay for the stimulating circuit is desired, then an ignitron crowbar should be used instead of a semiconductor crowbar because its resistance is

very low. To further reduce the resistance, more than one switching device should be used in parallel as this combination generates a lower resistance than a single device. Finally, the main component that adds resistance to the circuit is the cables. Coaxial cables should be used instead of conventional parallel cables as their resistance is lower. (More details regarding the co-axial cables will be discussed later.)

The charging capacitor is the most important component in the circuit design as its value is the main parameter that can be used to vary the pulsating frequency. Furthermore, the capacitor value and voltage determine the amount of energy that is supplied by the stimulating circuit to the exciting coil. If the capacitor value is increased then, the pulsating frequency will decrease. This decreases the rate of flux change in the stimulating coil to a point where it may not be able to excite the nerve. Conversely, decreasing the capacitor value increases the pulsating frequency to a point where the excitation field is faster than the time needed by the neuron to be triggered. In other words, the value of the capacitor combined with a fixed coil inductance is bounded with upper and lower time boundaries. For the lower limit, the duration time of the current pulse must not be less than 40 μs or it will not be able to fire the neurons. For the upper limit, the duration time of the current pulse must not be higher than 1 ms or it will result in muscle contraction and fatigue because of nerve saturation.

While examining the circuit current, we must also address the skin effect which is governed by the commonly used formula:

$$\delta = \frac{1}{\sqrt{\pi f \mu \sigma}} \qquad \text{(B.1)}$$

where δ is the electrical skin depth, f is the circuit operating frequency, μ is the tissue magnetic permeability and σ is the tissue conductivity.

A typical frequency spectrum for magnetic stimulation is about 1-10kHz. The permeability of tissue is close to that of free-space (μ_o), therefore we will assume that its relative permeability, $\mu_r = 1$, which results in tissue magnetic permeability $\mu = 4\pi \times 10^{-7}$ H/m. We consider the electrical conductivity of the tissue to be homogenous with $\sigma = .5$ S/m. This assumption is justified as the average value for tissue conductivities is within this range [27,62,70]. Table 3.1 in Chapter 3 shows the conductivity of different tissues. By substituting the above values in equation (B.1) we find that the skin depth in tissue is

$$\delta_{tissue} = \frac{1}{\sqrt{(\pi)(10^4)(4\pi \cdot 10^{-7})(.5)}} = 7.11m \qquad \text{(B.2)}$$

Typically, the distance between the coil and the target nerve is a few centimetres, which is much less than δ_{tissue}. Consequently, we can conclude that the skin effect is not evident. Therefore, the stimulating field will easily penetrate the human body and the current density is relatively constant across the tissue.

B.2 Type of waveform

The stimulating circuit governs the current pulse form where the pulse width determines which group of nerves will be excited, the frequency indicates how deep and effective the stimulation will be, and the rate of repetition (the number of times we repeat the stimulation) dictates the induced current in the nerve.The stimulating circuit can generate three types of

current waveforms.[2] Figure B.1 and B.2 illustrate the different types of induced waveforms associated with magnetic stimulation: under damped, and over damped. It also shows the threshold values for currents needed to achieve effective stimulation.

Notice that when the condition is under damped, the induced current waveform is poly-phasic, while for the over damped condition it is bi-phasic. The difference between the two conditions is outlined below.

CASE1: when $(\frac{R}{2L})^2 > \frac{1}{LC}$ Overdamped

In this case, the stimulating circuit supplies a mono-phasic pulse (where one pulse goes from 0 to positive and back to 0 again). As the main parameter of induced current in a nerve is the rate of change of the current in the coil, I will focus on the coil current rate of change. From the section B.8, di/dt for this case will be[3]:

$$\frac{di_{COIL}}{dt} = \frac{V_C(0)}{2\omega L} e^{-\Upsilon t} \left(\Upsilon \left(e^{-\omega t} - e^{\omega t}\right) + \left(e^{-\omega t} + e^{\omega t}\right)\right) \qquad \text{(B.3)}$$

CASE2: when $(\frac{R}{2L})^2 < \frac{1}{LC}$ Underdamped

In this case, the stimulating circuit supplies a bi-phasic pulse (where the pulse will vary from 0 to positive and then to a negative value and back again to 0). Also from section B.8, di/dt for this case will be:

---

[2]A detailed waveform analysis is illustrated at the end of this Appendix (section B.8).

[3]The parameters for equation B.3 and B.4 are defined in section B.8.

$$\frac{di_{COIL}}{dt} = \frac{V_C(0)}{\omega_o L} e^{-\Upsilon t}[\frac{(\omega^2 - \beta^2)}{\omega}\sin(\omega t + \beta) + 2\,\Upsilon\cos(\omega t + \beta)] \qquad (B.4)$$

From figure B.1, B.2 we notice that the current rate of change (slope) for the under damped condition is higher than for the over damped condition as the pulse moves from a positive peak to a negative peak, resulting in a higher induced voltage. Unfortunately, with all the damping techniques available, we can not completely suppress the current waveform in an over damped case after it passes its negative peak. This results in induced current in the reverse direction or nerve re-polarization. This explains why researchers recommend applying nerve stimulation using a pulse in one direction (mono-phasic). The other disadvantage of the bi-phasic pulse is the increase of the supplied threshold voltage above that required for a mono-phasic pulse. This increase means more stored energy is needed to achieve the required stimulation.

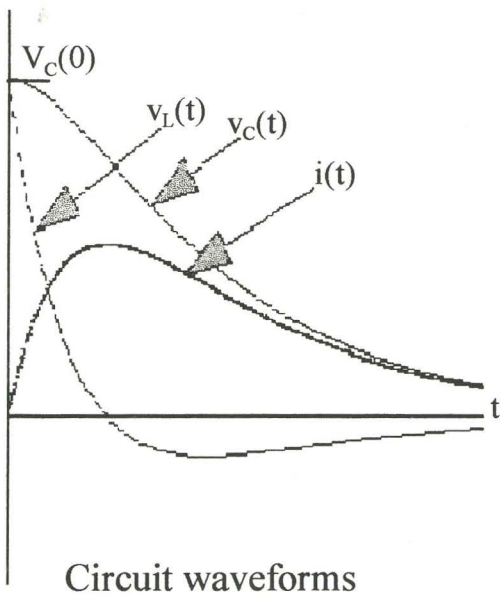

Figure B.1
The waveforms for an overdamped circuit

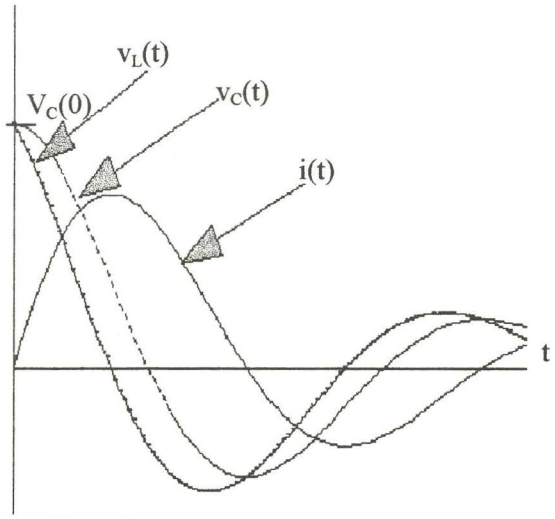

Figure B.2
The waveforms for an underdamped circuit

Figure B.3 shows the relation between the required threshold voltage for mono-phasic and bi-phasic pulses (adopted from [71]) .

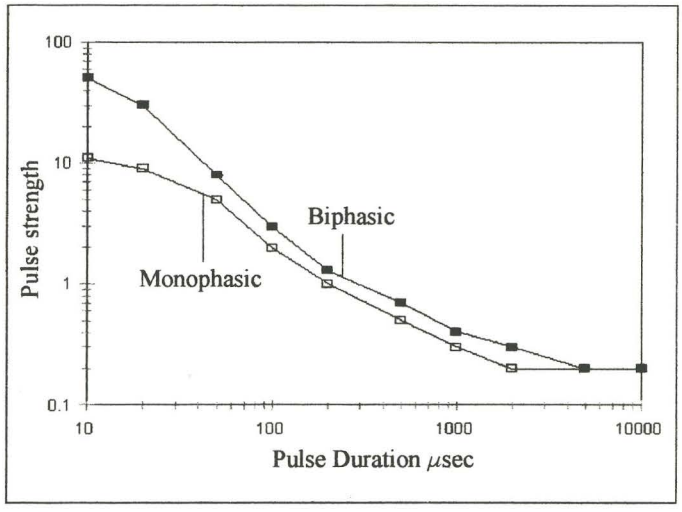

Figure B.3
Pulse strength vs. Pulse duration (after [71])

B.3 The Pulse Duration and Strength (S-D)

In general, regardless of the type used for stimulation (mono-phasic or bi-phasic) it is important to notice that there are two parameters that govern the induced current pulse. They are: its peak value and its effective duration (the period from the onset until it first crosses the 0 amplitude axis). As the effective duration of the first phase for the circuit current decreases, the intensity of the nerve induced current increases. This is conveyed by the fundamental law of excitation [71] embodied in the strength - duration curve (S-D curve).

An S-D curve represents the relationship between the threshold amplitude of a stimulus and the first phase duration for which that stimulus must be applied to elicit a response from a nerve. From the S-D curve we can obtain the rise time of the pulse needed to stimulate a specific tissue in conjunction with the peak value of the current required. These two values will be the constraints for the stimulating circuit design.

The S-D curve is applicable for a single neuron, for which the response is a binary phenomenon. Thus, it is easy to judge if a certain strength and duration of a stimulus is adequate to trigger a response (action potential) of a single neuron. Also, it is important to know that the duration time of the induced current needed depends on the type of tissues. For example, the pulse needed to stimulate a cardiac muscle has a higher peak current and is longer in duration time than a pulse needed to stimulate a peripheral nerve.

Figure B.4 presents a typical strength-duration curve for mammalian motor nerve and a cardiac muscle (adopted from [71]). From the figure it is clear that the strength and the duration of the pulse needed for a cardiac muscle is higher than that for a motor nerve. Also we notice that with decreasing the pulse duration the peak current required for stimulation increases.

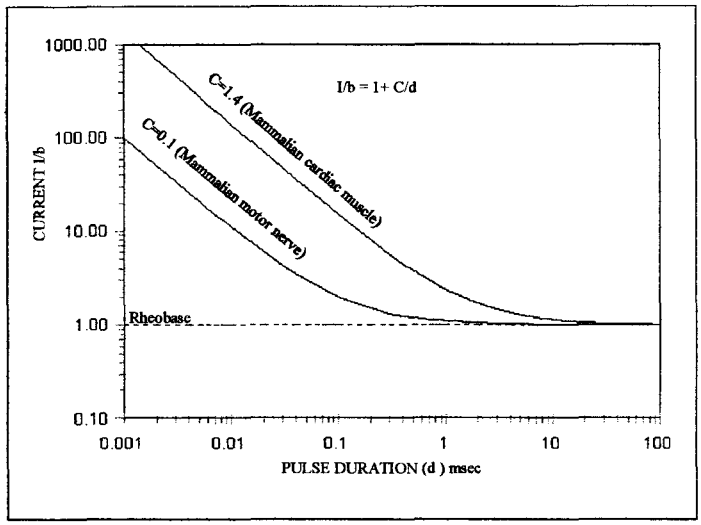

Figure B.4
Excitable current vs. the pulse duration (after [71])

B.4 Efficiency and Performance

The efficiency of a magnetic stimulator depends on the amount of transferred energy from the circuit to the targeted nerve. The poorest transferred energy occurs at the interface between the coil and the nerve, therefore, to improve the circuit performance it is important to increase the transfer of energy especially in that region. Also, Geddes and Barker [71,72] showed that the charge required to stimulate a nerve decreases as the pulse duration decreases. This means to improve the stimulating circuit efficiency, the threshold charge must be transferred over the shortest period of time and be supplied by the minimum possible stored energy. This can be achieved by decreasing the rise time or a combination of decreasing the rise time and increasing the charged voltage.

The circuit rise time can be decreased by 1 of 2 methods, both relying on the fact that the rise time or the circuit frequency is proportional to $(LC)^{½}$. In the first method the system

capacitance can be decreased, which will require an increase in operating voltage to maintain the stored energy constant. In the second method, the coil inductance can be decreased while the capacitor and its operating voltage are kept constant. By decreasing the coil inductance, the mutual inductance between the coil and the nerve will be decreased. Consequently, the transferred energy from the coil to the nerve is reduced (despite the increase in the coil current as it is proportional to $1/(L)^{3/2}$ (See section B.8).

Of the two approaches, it is clear that the reduction of the capacitor value is preferable. This approach will compensate for the reduced energy by increasing the capacitor charged voltage as the energy is proportional to the square of the voltage.

To express the impact of the rise time reduction mathematically, we will consider a square current pulse driving a parallel RC circuit (simple equivalent circuit for a membrane). It can be shown that the charge Q required to achieve a particular threshold voltage V_T (which represents an action potential) across the capacitor is given by [72]:

$$Q = \frac{C_n V_T \tau_d}{1 - e^{-\tau_d}} \quad where \quad \tau_d = \frac{T_p}{C_n R_n} \qquad (B.5)$$

where τ_d (unitless) is the ratio of the current pulse duration, (T_p) to the circuit time constant (C_nR_n.). As τ_d tends to zero (i.e. $T_p \ll C_nR_n$) this expression reduces to:

$$Q = C_nV_T \qquad (B.6)$$

Thus, all the applied charge is stored in the capacitor. As τ_d tends to infinity (i.e. $T_p \gg C_nR_n$) the total charge Q equation (B.5) reduces to:

$$Q = C_n V_T \tau_d = \frac{V_T}{R_n} T_p \qquad \text{(B.7)}$$

From equation (B.7) it is obvious that we can reduce the charge needed for stimulating the nerve by reducing the time period for the pulse (T_P) [72]. However, the charge required to achieve stimulation is constrained by a time boundary which is defined by the nerve physical characteristics. It also shows the concept of losses in the induced current as it travels through the nerve due to the nerve leakage properties.

Having covered the reduction of the rise time, let us now analyse the impact of increasing the operating voltage on the system performance. If the charged voltage is increased while the other elements remain constant, then the induced current in the nerve will increase.[4] This means that the charge required to activate the nerve will be attained in a shorter period of time (figure B.4). This has been confirmed through an experiments conducted by Reilly, Barker [64,72] in which they varied the discharge voltage in steps and calculated the threshold charge required to stimulate the nerve in each step. They discovered that by increasing the discharged voltage, the threshold charge required to achieve the same level of stimulation was reduced.

Another benefit of increasing the operating voltage is that a wide range of stored energy becomes available which helps to obtain a suitable pulse strength for stimulation.

---

[4] For both cases (over and under damped) the peak current (I_{peak}) value is proportional to the applied voltage (V), and inversely proportional to both the angular frequency(ω) and the inductance (L), ($I_{peak} \propto V/\omega L$).

B.5 Advantage of Reducing the Pulse Duration

Efficiency improvement is not the only advantage of reducing the pulse duration. By reducing the pulse duration the energy required to achieve effective stimulation will be less. Consequently, the stored energy in the circuit will be reduced, resulting in the possibility of using smaller capacitors. Also, there will be less coil heating due to the shorter time scale of the current pulse and its lower amplitude. This allows for faster repetition rates for a given coil design before thermal limits are reached.[72] Furthermore, less peak energy in the coil improves the longevity of the coil and makes it less hazardous in the event of coil failure. Finally, decreasing the exposure of the patient to a magnetic field remains preferable (although there is no evidence that the magnetic fields are hazardous). Exposure decrease can be achieved by reducing the pulse width, which in turn reduces the peak value of the magnetic flux and its duration time.

B.6 The Guidelines and the Main Components for the Stimulating Circuit

The guidelines and the main components required to build the stimulating circuit can be summarized as follows:

B.6.1 Power Supply

The power supply for a proposed stimulating circuit consists of a step-up transformer, bridge rectifier, and switching circuit. The transformer provides a variable high output voltage for the system, (i.e 0 - 5 k V_{pp}) which will be rectified by the bridge rectifier. The output voltage from the bridge will be directed to the capacitor bank through a switching circuit. This

switching circuit can be comprised of an SCR or a set of transistors. These transistors can be a combination of drivers and a switching power transistor (BJT).

B.6.2 Capacitor Bank

The circuit should have a variable capacitor bank which will allow us to control both the rise time and the stored energy. For both cases (over and damped and under damped) we can approximate the frequency for the stimulating circuit by the following equation (assuming the equivalent circuit resistance (R) is small).

$$f = \frac{1}{2\pi}\sqrt{\frac{1}{LC}} = \frac{1}{T} \qquad \text{(B.8)}$$

where T is the period of one complete cycle. For a frequency range 1-5 kHz, considering our coil inductance (8.5 μH for an air core coil and 16 μH for the ferromagnetic core) a capacitor bank range between 50-1250 μF is needed. The limitations associated with this range are the capacitor size and weight. For practical purposes the range will be reduced to 50-600 μF . This will make the frequency range approximately from 1.5-5kHz. This capacitor range can be achieved by using several capacitors with different values, (ie: 100 μF, 200 μF, etc.) connected in a combination of parallel and series. The minimum rated voltage for each capacitor should be 1.5 kV. If the capacitors are connected in parallel (C = 600 μF), then the system will be at its minimum operating voltage;1.5 kV. If the capacitors are connected in series (C = 50 μF), then the operating voltage will be higher (3 kV) which is preferable.

The major obstacle when using a capacitor bank is the time needed to recharge the

capacitors, however, if the need for repetition is low or not applicable then this obstacle can be over looked.

Finally, a very important parameter to be considered when selecting the capacitor is its internal resistance [73]. This resistance should be extremely low to minimize the circuit equivalent resistance and subsequently the circuit losses.

B.6.3 Switching Devices for discharging the Capacitor

The switching device suitable for the circuit is an SCR (silicon controlled rectifier) as it is practical and economical. The effective cost of this device is less than the alternative (the Ignitron) especially when the transferred energy is low relative to the ignitron capabilities. To further reduce the cost of the switching device, it is recommended to have several SCRs connected in parallel instead of having a single device to accommodate the total circuit current. To ensure the longevity of the switching device a "pilot" SCR can be added to trigger the main SCRs.

B.6.4 Circuit Cable

The cables that supply the coil have an important role in the circuit performance as they add unwanted resistance and inductance to the circuit. There are two possible choices of cables, either a pair of parallel cables or co-axial cables.

A conventional pair of parallel cables have many disadvantages when they are used to transfer energy in magnetic nerve stimulation. The main disadvantage of these cables is their large inductance which increases the total inductance of the circuit and hence, reduces the

circuit efficiency. Also, the acoustic noise associated with these cables is large enough to invoke auditory potentials. Finally, a large leaky magnetic field is generated around these cables. This field may trigger undesirable operations in the surrounding apparatus.

The cable inductance for a pair of parallel cables per unit length (d) is given by Krause [27] as:

$$\frac{L}{d} = \frac{2}{5} \mu_r \ln \frac{D}{a} \qquad \text{(B.9)}$$

where μ_r is the relative permeability of the medium between the two cables, D is the distance between the centres of the cables, a is the radius of the cable. Krause [27] also gives the inductance per unit length (d) for co-axial cables as:

$$\frac{L}{d} = \frac{1}{5} \mu_r \ln \frac{b}{a} \qquad \text{(B.10)}$$

where μ_r is the relative permeability of the medium inside the co-axial cable, b is the inside radius of outer conductor, a is the outside radius of the inner conductor.

From the two equations, it can be seen that using a pair of cables (each having a radius a) results in higher equivalent inductance than using a co-axial cable (having an inner conductor radius of a). The ratio between these two inductances will be 3:1. Therefore, in order to maintain a higher efficiency for the stimulating circuit, a co-axial cable is preferred. In fact, Uneo et al. proved that using co-axial cables resulted in a higher system performance [74]

B.6.5 Measurement Devices

Special measurement and detecting devices are needed for the experiment set-up. The properties of these devices must be very specific as the circuit operates on high voltage and current [75]. As the circuit variables (inductance, and resistance) are very low and sensitive, high precision equipment is needed for measurement. The measurements should be confirmed through the calculations of the circuit waveforms.

There are two methods used to capture the waveforms. The first method involves using a storage oscilloscope with high voltage props, while the second method involves using A/D card with isolated operational amplifiers. A Gaussmeter will aid in the pre-measurements of the flux density. However, this device does not give an accurate measurement of the field as the reading are highly dependent upon the probe position.

B.6.6 Circuit Safety

It is paramount to consider the safety of the patient and operator first as this circuit operates with very high voltage. The secondary safety consideration is protecting the circuit components from any damage to ensure the longevity of the apparatus.

In magnetic stimulation the risks facing both the patient and the operator fall into two categories. The first area of concern involves coil failure, while the second involves malfunctioning of the stimulating circuit. The issues involving the circuit safety are isolating the circuit from its surroundings physically and electrically. Isolating the circuit physically can be achieved by containing it in a well secured metal box. Isolating the circuit electrically involves three aspects. Firstly, a fast response switch must be embedded in the circuit to

automatically turn it off should any failure occur. This switch must also safely discharge all the stored energy from the capacitor and the power supply. Secondly, a transformer or a photo switch should be used to isolate the control circuit from the discharging circuit to prevent any high currents or voltage to reach the control circuit. Thirdly, it is recommended to embed extra breakers and sensors to prevent the possibility of damage in case of the main sensors or breakers failure.

Finally, special consideration should be given to the limitations of the circuit components. The operating variable for the circuit should always be lower than the rated values for any of its components. For example, the amount of energy stored in the capacitor should be less than the maximum energy of the capacitors. Maintaining this rule will extend the life of the components and minimize the risk for any circuit failure.

B.7 The Proposed Circuit

Figure B.5 shows a schematic representation for a possible stimulating circuit.

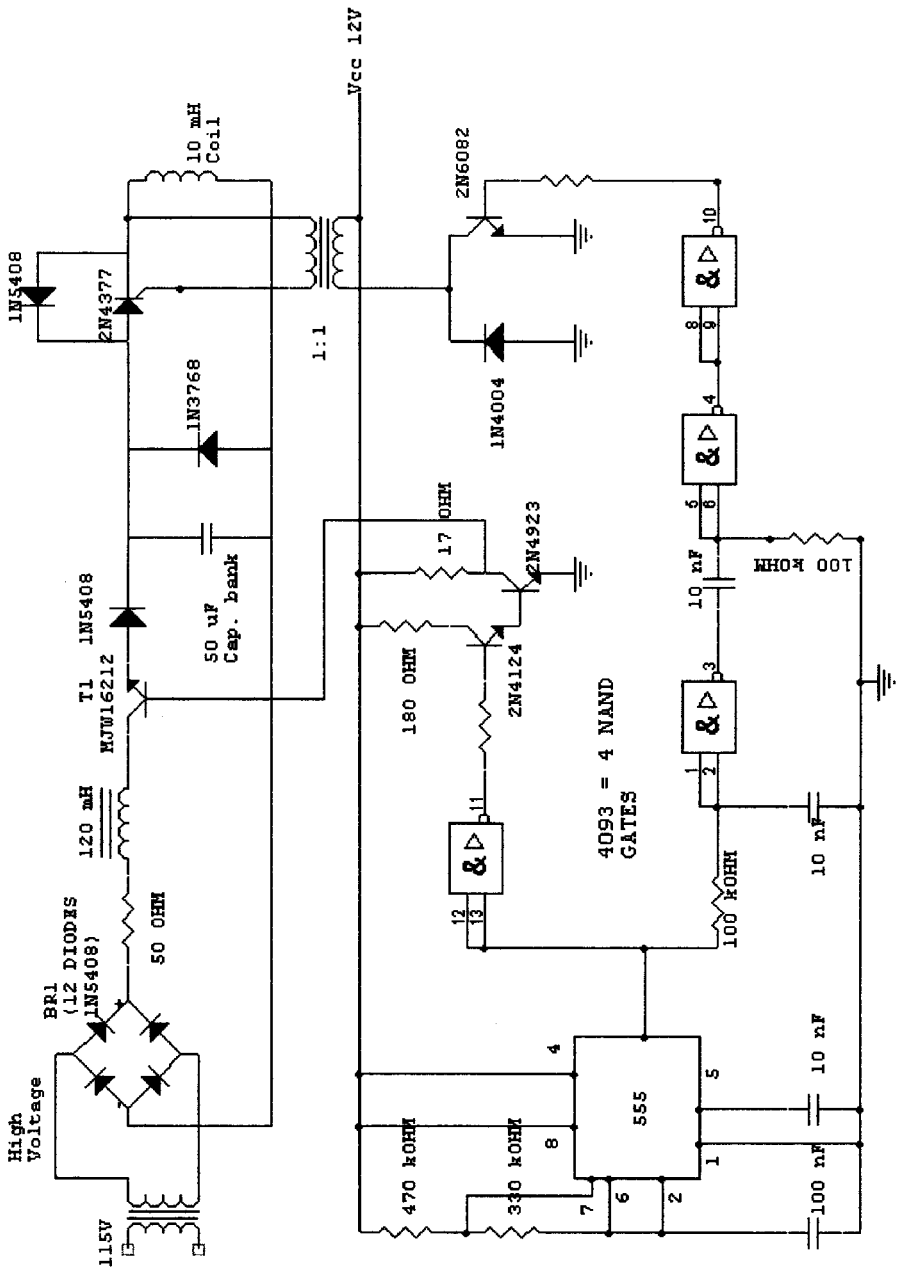

Figure B.5

Schematic representation for a stimulating circuit.

From figure B.5 the transformer high voltage output is rectified by the bridge rectifier BR1 which consists of twelve diodes (1N5408), 3 diodes for each arm of the bridge. This combination of diodes is more economical and effective than a single bridge rectifier. A high power resistor (200 W) R_1 connected in series with an inductor L_1 to shape the waveform for the charging current and minimizing the resultant losses for charging the capacitor. The high voltage transistor T_1 presents the switch to charge the capacitor from the power supply. D_1, the diode which connects T_1 to the capacitor bank C_1, prevents the discharging of the capacitor through the controlling and charging circuitry. The thyristor SCR_1 can be implemented through two different combinations. The first combination uses four SCRs (50RIA120) in parallel with four diodes (IN5408). The second combination uses 1 SCR (ST230S12PO) in conjunction with a pilot SCR (16RIA120). Either combination will perform adequately for this circuit. For this circuit the first combination will be used. Figure b.7 shows the schematic diagram of the SCR combination.

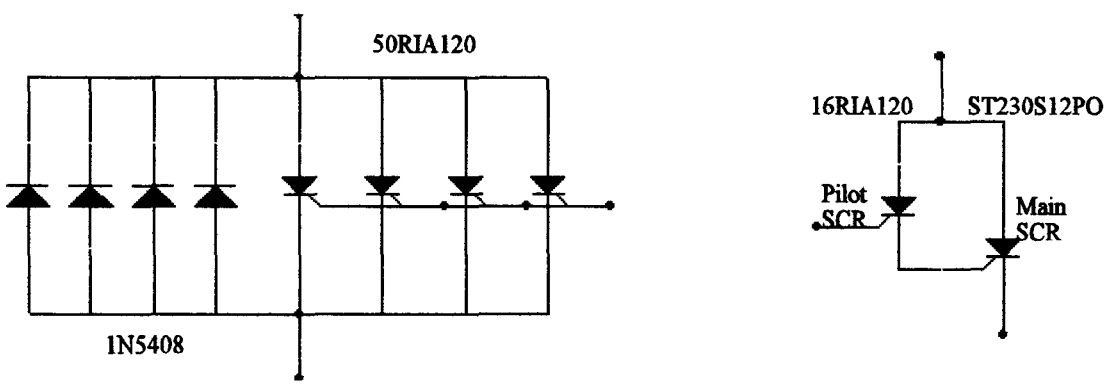

Figure B.6
Schematic diagram of the SCR combination

The multi-vibrator for the circuit is built around the timer integrated circuit (555), while the timing pulses are produced by four Schmitt triggered NAND Gates (4093). The transistor T_2 is responsible for boosting the pulse power to a level sufficient to drive the transistor and the thyristors. To isolate the control circuit from the discharging circuit, a pulse transformer with a turn ratio of 2:1 for triggering the thyristors will be used. The capacitor and resistor combination $(R_2\ C_2)$, $(R_3\ C_3)$, control the charging time for the capacitor bank C_1 and the discharging of the capacitor bank into the coil respectively.

From the previous circuit the charge time for the capacitor bank (600 μF /1500 V) is approximately 5 minutes while charge time for the capacitor bank (50 μF /3000 V) is approximately 25 seconds. The stored energy in the first case is 675 joule, the ætored energy in the second case is 225 joule, the rise time for a 600 μF /20 μH coil is 166 μsec, while the rise time for a 50 μF/20 μH coil is 50 μsec. This is an excellent range as the practical range is 100-150usec for peripheral nerve stimulation. If the coil inductance is reduced to 10 μH then the frequency range for the same capacitor bank will be approximately 2kHz- 7kHz. This means that the rise time is for a 600 μF /10 μH coil will be 125 μsec, while the rise time for 50 μF/ 10 μH coil will be 35 μsec . Once again the frequency range is acceptable with caution in the upper limit.

Finally, to measure the response of magnetic stimulation is complicated because of the high noise level during stimulation due to the high flux density. Weyh et al. [75] documented a procedure for building a special amplifier used to detect nerve stimulation.

B.8 Analysis for the Stimulating Circuit Waveforms

To analyse the stimulating circuit we will simplified it to a series RLC . The figure below shows a simple equivalent circuit for the stimulating circuit.

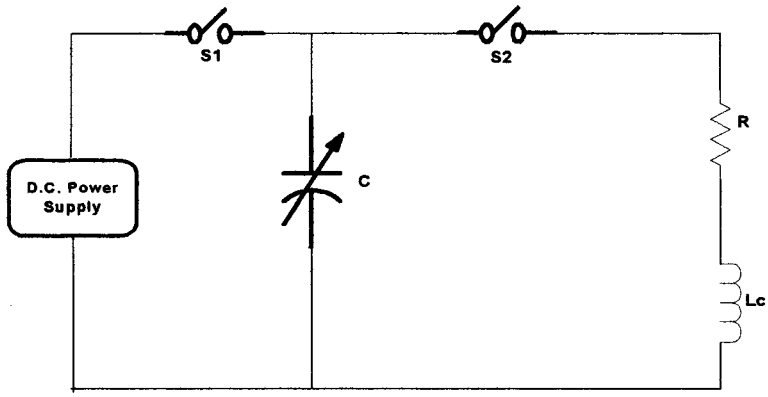

Figure B.7
The equivalent circuit for the stimulating circuit.

We will assume that S_1 was closed for a long period of time (enough to charge the capacitor) while S_2 is open. After we have the capacitor charged we will open S_1 and have S_2 closed. In this case we will have a series *RLC* circuit . By applying Kirschoff's Voltage Law around the circuit for any instant of time after switch two is closed we will have:

$$v_R + v_L - v_C = 0 \qquad \text{(B.11)}$$

Substituting the parameters $i = -C(dv_C/dt)$, $v_R = Ri = -R\,(Cdv_C/dt)$, $v_L = Ldi/dt = -LC\,(d^2 v_C/dt^2)$ and rearranging the above equation we will get:

$$LC\frac{d^2v_c}{dt^2} + RC\frac{dv_c}{dt} + v_c = 0 \qquad \text{(B.12)}$$

The solution for the above equation can be represented in the form $v_C = V_C e^{st}$

which, when substituted into the previous equation, results in:

$$LCs^2 + RCs + 1 = 0 \qquad \text{(B.13)}$$

There will be two values (roots)for s that will satisfy the above equation and they will be:

$$s_1 , s_2 = -\frac{R}{2L} \pm \sqrt{(\frac{R}{2L})^2 - \frac{1}{LC}} \qquad \text{(B.14)}$$

Substituting the values for s_1, s_2 will allow us to represent $v_c(t)$ as

$$v_c = A_1 e^{s_1 t} + A_2 e^{s_2 t} \qquad \text{(B.15)}$$

In order to solve this equation we will consider two cases.

Case 1: when t = 0, then $v_C(0_+) = v_C(0_-) = V_C(0)$, where $V_C(0)$ is the initial voltage of the capacitor before we turned switch two on. Substituting this in the above equation:

$$A_1 + A_2 = V_C(0) \qquad \text{(B.16)}$$

Case 2: when t = 0, as $dv_C/dt = 0$, then $i_C(0_+) = i_C(0_-) = 0$ which means that

$$s_1 A_1 + s_2 A_2 = 0 \qquad \text{(B.17)}$$

After solving the above two equations we will get:

$$A_1 = \frac{s_2\, V_C(0)}{s_2 - s_1} \quad ; \quad A_2 = \frac{-s_1\, V_C(0)}{s_2 - s_1} \qquad \text{(B.18)}$$

There are three possible outcomes from the RLC circuit depending on the value of R,L,C. Which are as follows:

1. $(\frac{R}{2L})^2 > \frac{1}{LC}$ This is an overdamped circuit
2. $(\frac{R}{2L})^2 < \frac{1}{LC}$ This is an underdamped circuit
3. $(\frac{R}{2L})^2 = \frac{1}{LC}$ This is a critical circuit

In our problem, we will be interested in the overdamped circuit performance if the kind of stimulation we are looking for is mono-phasic pulse stimulation The underdamped circuit will be of interest if we are looking for a bi-phasic pulse stimulation.

Case 1: When

$$(\frac{R}{2L})^2 > \frac{1}{LC}$$

Substituting the values for A_1, A_2, the general form for the capacitor voltage will be

$$v_C = \frac{V_C(0)}{s_2 - s_1}(s_2\, e^{s_1 t} - s_1\, e^{s_2 t}) \qquad \text{(B.19)}$$

While the general form for the circuit current is

$$i = -C\frac{dv_C}{dt} = -\frac{V_C(0)}{L(s_2 - s_1)}\,(e^{s_1 t} - e^{s_2 t}) \qquad \text{(B.20)}$$

The value for *di/dt* for the coil can be represented as :

$$\frac{di_{COIL}}{dt} = \frac{V_C(0)}{2\omega L}\, e^{-\Upsilon t}\,(\Upsilon\,(e^{-\omega t} - e^{\omega t}) + (e^{-\omega t} + e^{\omega t})) \qquad \text{(B.21)}$$

As our main object is to find the value for the induced voltage in the coil, then

$$v_{COIL} = L\,\frac{di_{coil}}{dt} = -\frac{V_C(0)}{(s_2 - s_1)}\,(s_1 e^{s_1 t} - s_2 e^{s_2 t}) \qquad \text{(B.22)}$$

We can modify the above equation by substituting s_1, s_2 by the formula shown below :

$$s_1\,,\ s_2 = -\Upsilon \pm \omega \qquad \left(\text{ when } \quad (\frac{R}{2L})^2 > \frac{1}{LC}\right)$$

where

$$\Upsilon = -\frac{R}{2L}\ ,\quad \omega = \sqrt{(\frac{R}{2L})^2 - \frac{1}{LC}} \qquad \text{(B.23)}$$

and the result will be

$$v_{COIL} = \frac{V_C(0)}{2}\, e^{-\Upsilon t}\,(\frac{\Upsilon}{\omega}\,(e^{-\omega t} - e^{\omega t}) + (e^{-\omega t} + e^{\omega t})) \qquad \text{(B.24)}$$

The figure below shows the wave forms for this circuit:

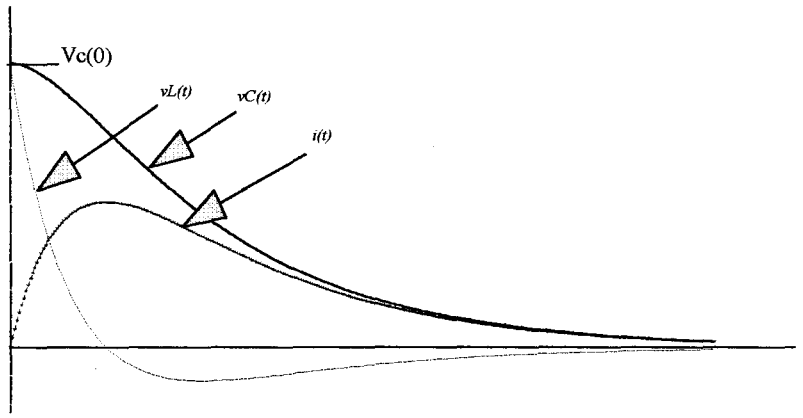

Figure B.8
Waveforms for overdamped circuit

Case 2: When

$$(\frac{R}{2L})^2 < \frac{1}{LC}$$

In this case we will have complex roots for s_1 and s_2.. Before we proceed with the analysis of this circuit we will define some important variables that will help us when we substitute the values for s_1 and s_2. We can also represent s_1, s_2 as shown below:

$$s_1 , s_2 = -\Upsilon \pm j\omega \qquad (\text{ when } \quad (\frac{R}{2L})^2 < \frac{1}{LC})$$

where

$$\Upsilon = -\frac{R}{2L} \qquad \omega = \sqrt{(\frac{R}{2L})^2 - \frac{1}{LC}} \qquad \text{(B.25)}$$

Other values that needed to be defined are ω_o and β, where :

$$\omega_o = \frac{1}{\sqrt{L\,C}} \qquad \beta = \sin^{-1}(\frac{\omega}{\omega_o}) \qquad \text{(B.26)}$$

The figure below shows the relation between those variables

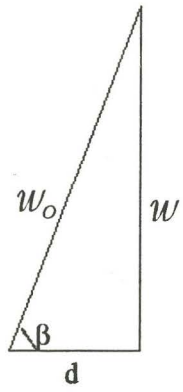

Substituting the values of s_1, s_2 in the values for v_c, i_c, v_L will give

$$v_c = \frac{\omega_o}{\omega} V_C(0)\, e^{-\Upsilon t} \sin(\omega t + \beta) \qquad \text{(B.27)}$$

$$i_c = \frac{\omega_o}{\omega} CV_C(0)\, e^{-\Upsilon t}\, \delta \sin(\omega t + \beta) - \omega_o C V_o\, e^{-\Upsilon t} \cos(\omega t + \beta) \qquad \text{(B.28)}$$

$$\frac{di_{COIL}}{dt} = \frac{V_C(0)}{\omega_o L}\, e^{-\Upsilon t}[\frac{(\omega^2 - \beta^2)}{\omega} \sin(\omega t + \beta) + 2\,\Upsilon \cos(\omega t + \beta)] \qquad \text{(B.29)}$$

$$v_L = L\left(\frac{di_c}{dt}\right) = \frac{V_C(0)}{\omega_o} e^{-\Upsilon t}\left[\frac{(\omega^2 - \beta^2)}{\omega}\sin(\omega t + \beta) + 2\,\Upsilon\cos(\omega t + \beta)\right] \qquad \text{(B.30)}$$

The next figure shows the wave forms for this circuit:

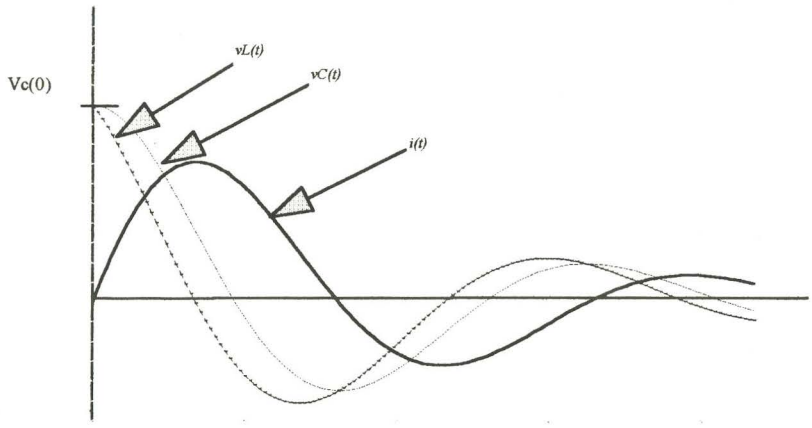

Figure B.9
Waveforms for underdamped circuit

APPENDIX C

C.1 Calculating the Inductance of a Wire

As I outlined in Chapter 2, the inductance of the nerve can be represented as a self inductance of a thin wire. In order to calculate this inductance we have to separate the region that is laying outside the wire from the region laying inside it. The contribution of the latter to the inductance is frequently negligible (this can be justified as the radius of the wire is too small compared with the dimensions of its surroundings). We may assume that the field outside is the same as if the current was concentrated at the axis of the wire. Therefore, the lines of forces (near the surface) surrounding the axis of the wire are circles. The flux outside wire will link the axial filament with any line drawn parallel to it on the surface of the wire. To calculate the self inductance we need to find the mutual inductance between two parallel curvilinear circuits spaced at a distance equal to the radius of the wire. Inside the wire, the flux density around any circle of radius r can be represented as

$$B = \frac{\mu I_i}{2 \pi r} = \frac{\mu_o \mu_n r I_T}{2 \pi a^2}$$

where μ_o is the space permeability ($4\pi \times 10^{-7}$ H.m^{-1}), μ_n is the relative permeability for the wire (the nerve) and it is equal to 1, I_T is the total current running through the wire (the nerve), I_i is the enclosed current for radius r and a is the radius of the wire. The above equation can be expressed as:

$$B = \frac{\mu_o \, r \, I_T}{2\pi a^2}$$

The energy inside the wire can be expressed as [27]:

$$W_i = \frac{1}{2} \int_v B \cdot H \, dv = \frac{1}{2 \, \mu_o} \int_v B^2 dv$$

Substituting B in the above equation results in:

$$W_i = \frac{\mu_o \, I_T^2 \, \ell}{8 \, \pi^2 a^4} \int_0^a r^2 2\pi r dr = \frac{\mu_o \, I_T^2 \ell}{16 \, \pi}$$

However, the energy stored in this wire can be expressed as:

$$W_i = \frac{1}{2} L_n \, I_T^2$$

which implies that the nerve inductance L_n can be represented as:

$$L_n = \frac{\mu_o \, \ell}{8 \, \pi}$$

where L_n is the inductance of the wire (nerve), ℓ is the wire (nerve) length, and μ_o is the permeability of free space. To calculate the inductance of the coil we will apply the following equation [27]:

$$NI = H_{(air)} \cdot g + H_{(core)} \cdot d$$

To calculate the value of the flux density (B) we will consider the coil's magnetic circuit where the total ampere turns for the coil can be expressed as:

$$NI = \frac{K_2 B g}{\mu_o} + \frac{B d}{\mu_o \mu_c}$$

where N is the number of turns for our coil, I is the coil current, $H_{(air)}$ is the magnetic field into the air gap, g is the air gap length, $H_{(core)}$ is the magnetic field in the core and d is core length. Use of the above equation is permitted for the case when $\mu_c = 1$ or μ_c is piece wise linear. In this application the air gap is relatively large which precludes saturation of the magnetic material for the level of the current used. Considering that the flux density into the air is proportional to the flux density in the core with a factor K_2 (which is less than or equal to 1), we can express the above equation as:

$$B = \frac{NI\mu_o\mu_c}{K_2\, g\mu_c + d}$$

The final equation can be modified to present the value of B as follows:

$$L_c = \frac{\Lambda}{I} = \frac{N\psi_m}{I} = \frac{NBA}{I}$$

Substituting the flux density shown above to calculate the inductance of the coil will result in:

$$L_c = \frac{\mu_o \mu_c N^2 A}{d + K_2\, g \mu_c}$$